Report on the R&D of Uranium Carbide targets by the PLOG collaboration at PNPI-Gatchina

A.E. Barzakh, D.V. Fedorov, A.M. Ionan, V.S. Ivanov, M.P. Levchenko, K.A. Mezilev, F.V. Moroz, S.Yu. Orlov, V.N. Panteleev, Yu.M. Volkov,

PNPI , Leningrad district, 18850 Gatchina, Russia

O. Alyakrinskiy, A. Andrighetto**,** A. Lanchais, G. Lhersonneau[*], V. Rizzi, L. Stroe[#], L.B. Tecchio,

INFN-LNL, viale dell'Universita` 2, 35020 Legnaro (PD), Italy

O. Bajeat, M. Cheikh Mhamed, S. Essabaa, C. Lau, B. Roussière,

IPNO, bat-106, F-91406 Orsay, France

M. Dubois, C. Eléon, G. Gaubert, P. Jardin, N. Lecesne, R. Leroy, J.Y. Pacquet, M. -G. Saint Laurent, A.C.C. Villari.

GANIL (IN2P3/CNRS – DSM/CNRS), BP 55027, 14076 Caen CEDEX 5, France

* now at GANIL,
[#] and NIPNE, POB MG-6, 077125 Bucharest, Romania.

Abstract

The aim of this report is to summarize the experimental results of the R&D program on Uranium Carbide targets for Radioactive Ion Beam (RIB) production performed at the Petersburg Nuclear Physics Institute (PNPI) of Gatchina (Russia). The targets have been irradiated with 1 GeV protons delivered by the Synchrocyclotron and the measurements were carried out at the IRIS isotope separator on-line. Different compositions of Uranium Carbide targets as well as different kinds of ion sources have been tested in order to evaluate efficiency and release times of the reaction products. The report includes the results of experiments performed in the period of time going from November 2001 up to March 2006. This R&D program was performed in the framework of the collaboration with the EURISOL, SPES and SPIRAL-2 projects and ISTC program.

Foreword

This report has been motivated by the need of the PLOG collaboration to obtain an overview of the numerous experiments performed at PNPI-Gatchina about the properties of high-density targets with the aim to learn about the feasibility of a massive target containing about 1 kg of natural or depleted uranium. The acronym PLOG stands for P(NPI)-L(NL)-(IPN)O-G(ANIL), institute members of the collaboration. Our insight and understanding varied steadily over the years, thus resulting in occasional differences in the treatment of data. Accordingly, the section devoted to the methods and analysis reflects our present view of the matter, while examples extracted from early publications could occasionally appear to show some inconsistencies. We apologize to the reader for this, but it had not been possible to repeat the whole analysis within causing unnecessary delay. It must be stressed that if some deduced values may change somewhat, there should be in no case another conclusion about the evaluation of a target than the one then presented.

The decision about writing a report stems from a discussion after a proposition during an experiment at Gatchina on early 2006. The LNL group accepted the task and generated a draft at Legnaro before the summer vacations. It contained an up-to-date description of the analysis method and a summary of experiments on fission products published up to that time by the collaboration. The report was improved in September when very promising results on Francium isotopes and a few other elements were implemented. The resulting text was submitted to the members of the collaboration in October. A discussion meeting including all participating institutions was held at GANIL on November 30th/ December 1^{frst} in order to agree on the contents of the final text. In addition to web diffusion a formal publication of this work is envisaged at the next EMIS conference, to be held at Deauville, France 2007.

at GANIL, May 2007

List of contents

I. INTRODUCTION

During the latest thirty years at the ISOL (Isotope Separation On-Line) facilities there has been a steady trend of developing fast uranium-carbide targets for on-line production of rare nuclides. Growing interest in the development of uranium-carbide targets has been stimulated by the study of exotic neutron-rich nuclei far from stability. In addition, these targets enable the production of a wide region of neutron-deficient heavy nuclei by means of fragmentation reactions with energetic charged particles.

Presently, an increasing demand for targets containing large amounts of ^{238}U has been additionally enhanced by the new projects concerning ISOL facilities of the next generation [1-3], where two-step reactions [4] will be used to produce intense neutron-rich ion beams. As the driver beams of these next-generation ISOL facilities will be about two-to-three orders of magnitude more intense than those at the presently working installations, a serious problem arises for the replacement of the highly radioactive target assembly after its possible breakdown. Therefore the new target units must be able to work efficiently for several months without failures. It is very important to know whether the target keeps its working characteristics (yields and release efficiency for the produced species) during a long heating period or not.

For a more efficient use of the secondary neutron beam, the density of the target material containing ^{238}U should be as high as possible. Our targets are made of special high-density uranium carbide, with a density that is very close to the theoretical mono-crystal value. In order to measure their characteristics, long-term tests of these high-density UC targets have been carried out at the IRIS facility in the framework of the PNPI – LNL - IPN Orsay - GANIL (PLOG) collaboration.

The yields and delay times, in function of target temperatures, obtained in testing different targets are here reported to demonstrate the reproducibility of the relevant values. In particular, yields and release curves for Rb and Cs isotopes are reported for comparison with results published in literature. These alkaline elements can be easily ionized owing to their low ionisation potential, which has the advantage of simplicity of the ion-source construction and reproducibility of its performance. Occasionally data about In are shown since this element is also obtainable, though with lower efficiency, from such sources. In addition, we added a chapter about separation of the more challenging Ag and Sn isotopes, especially because of the importance of Sn due to the doubly-magic character of its isotope 132 which is expected to be among the favorite beams for reaction studies. Very encouraging data on Fr are also shown. This element is not a fission product but is generated by spallation owing to the high proton energy at PNPI. It is of huge interest as a probe for fundamental physical properties via atom trapping and shall be one of the key elements to be investigated at EURISOL.

II. EXPERIMENTAL

II.1 The IRIS facility at PNPI

The IRIS (Investigation of Radioactive Isotopes at Synchrocyclotron) on-line isotope separator facility and the layout of the experimental area [5] are depicted in Fig. 1.

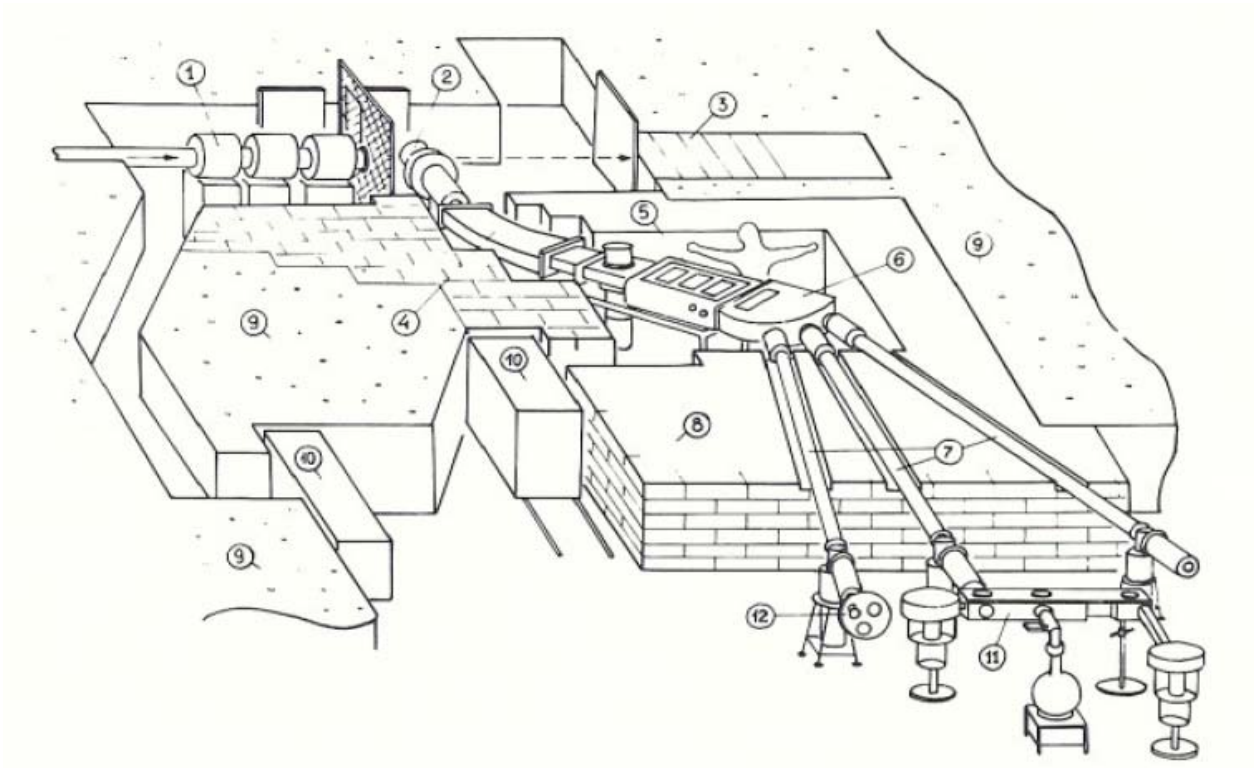

Fig. 1: Experimental set-up: 1) proton beam line; 2) target-source chamber; 3) beam dump; 4) mass separator magnet; 5) collector chamber; 6*)* switchyard; 7) transport tubes; 8) iron shield; 9) concrete wall; 10) concrete sliding doors; 11) tape transport system.

The heart of IRIS is the mass-separator on-line with the PNPI synchrocyclotron. Nuclei far from stability are formed as a result of interaction of 1 GeV protons with the uranium target. The typical energy loss of protons in our targets (about 10 g/cm^2 thick) is 4 MeV. Proton currents are somewhat below 0.1 μA so that the heating power (< 0.4 W) is too low to keep the targets at a suitable temperature to allow for migration of atoms out of them. The number of fissions in such targets (with density 10 g/cm^2 of uranium, fission cross-section σ_F = 1 barn, and I = 0.1 μA) is 1.6 10^{10}/s, which adds only 0.5 W of heating. Targets are thus heated externally with an added power of typically 1.8 kW. The difference of scale is favourable for safety as well as in the context of working with beam pulsing, since thermal conditions are not affected by switching the beam on or off. The dimension of the beam spot at the target is about 10 mm, corresponding to the diameter of the targets. The target material is therefore irradiated in a more or less uniform way, comparable to irradiation by neutron fluxes generated by converters.

The atoms of the produced radioactive nuclei are thermally released from the target, ionized in the ion-source, mass-separated and then implanted on a movable tape. Identification of the mass-separated nuclides and counting of their activities are performed by standard decay spectroscopy techniques. A tape transport system, working in the 'start-stop' mode transports the collected activity in front of α, β and γ-radiation detectors. Yield measurements are carried out with constant proton current to allow for equilibrium to be reached in the target. In contrast, delays between production and delivery onto the tape (release times) are obtained from the analysis of the so-called release curves, i.e. by collecting the radioactive beam during a series of short time intervals after switching off the proton beam and bringing the collected sources one-by-one in front of the detector. Gamma-spectroscopy is normally used to calculate the number of incoming ions. In addition, beta-counting is used for the shortest-lived activities, too weakly produced to be studied by γ-spectroscopy. In this case, the detector is placed close to the implantation station.

II.2 Targets and ion sources

2a Target construction

Different kinds of target ion-source assemblies were adopted during experiments, as explained below. In principle, the target holder is similar for all the experimental set ups, but the ion source is different depending on the ion species to be investigated. A schematic view of the target ion-source assembly is shown in Fig. 2. One of the essential issues of the target construction is the use of a tungsten container (0.2 – 0.3 mm thick) in which a graphite container, with the target material, is housed. Employment of the most temperature resistant material, such as tungsten with melting point at 3422°C, allows keeping the target temperature as high as it needed to ensure a fast release of the reaction products from the target material and from the target container volume [5]. The graphite container preserves the tungsten container from the very aggressive chemical corrosion of uranium. Both, target and ion source are operated in the temperature interval of (1900 – 2300)°C by Ohmic-heating independently.

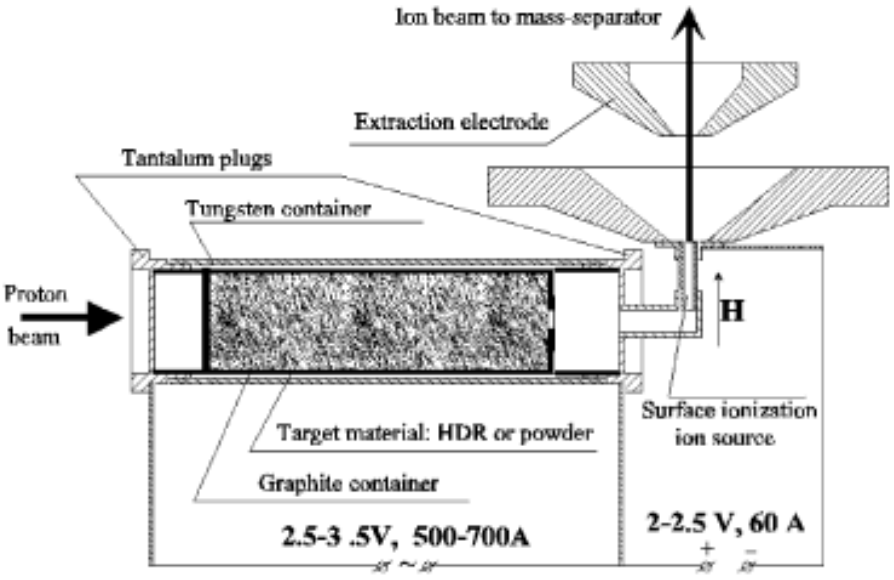

Fig. 2: Schematic drawing of the target assembly coupled with a high-temperature surface ionization source.

In order to ensure good working conditions of the ion sources, it is important to keep the pressure below 10^{-4} Torr. This requires high purity of the materials used in the entire assembly. Furthermore, an out-gassing procedure which lasts for more than 150 hours at temperature of about 2000°C is applied. This is normally done at an off-line target pump stand, which is identical to the one of the on-line separator. The temperature calibration of the target container and ion source as a function of the applied heating power is performed with an optical pyrometer through a glass window in the vacuum chamber.

2b Ion sources

Conventional surface-ionisation ion sources were employed to ionize alkali elements, like Rb, Cs, while electron-bombardment ion sources were used for elements with higher ionisation potential, like Ag and Sn. Both kinds of ion sources are tested off-line before experiments to define their ionisation efficiency. The surface-ionisation source efficiencies have been measured off-line using the well-known implantation technique [6]. They are ranging from 30 to 90% for Rb and Cs and 1 - 3% for In. The work function ϕ of a pure tungsten surface (4.53 eV) sharply decreases at a temperature of about 2300^{o}C due to the interaction with carbon vapour and subsequent formation of a thermally very stable carbide of tungsten on the target and ion-source inner surface. This process decreases the ionisation efficiency even for elements with low ionisation potentials such as Rb and Cs. In that case the efficiency can be restored by using rhenium for the target-ion source unit, as Re does not form carbides.

In Fig. 3 a schematic view of a High Temperature Electron Bombardment Ion Source (HTEBIS) coupled with a UC_x target is shown [7, 8]. An essential feature of this ion source is the absence of insulators close to the source volume. It allows the target to maintain a temperature of about 2600°C. Off-line tests have shown that all elements of the Periodic Table can be ionized with an efficiency of 0.2 – 5 %. The same values have been obtained for Mn, Ag, Cd, In and Sn neutron-rich isotopes in on-line separation. An efficiency ionisation increase for easily volatile elements can be achieved by closing the cathode-anode gap by an insulator ring.

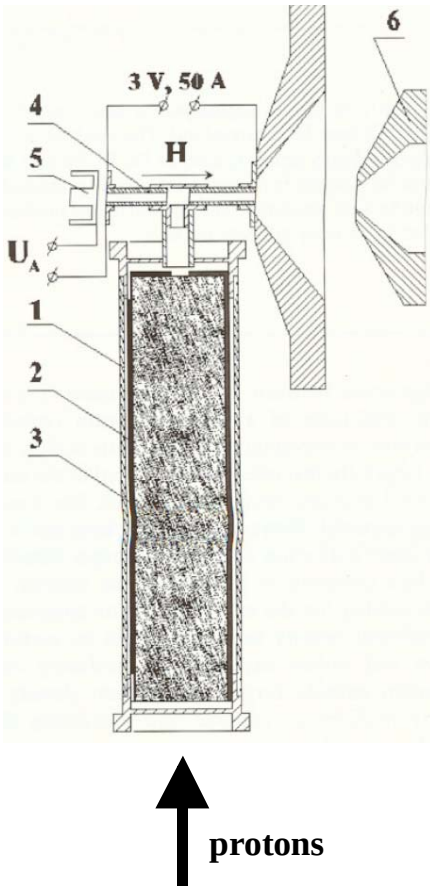

Fig. 3: Uranium carbide **(**UCx) target coupled to the high-temperature electron-bombardment ion source: (1) tungsten container, (2) graphite container, (3) uranium carbide, (4) ion source anode tube, (5) cathode, (6) extraction electrode.

2c Uranium-carbide target material

Essentially, four kinds of target materials have been tested: two types of low-density UC_x and a high-density UC in two physical forms. The low-density UC_x was tested under form of powder (LDP - density 1.5 g/cm^3) and of pellets (LDT) like those used both at CERN-ISOLDE and at PARRNe at IPN-Orsay (density 3.5 g/cm^3, uranium density 2.32 g/cm^3). The high-density target was either a rod (HDR) or manufactured as pellets (HDP). A high-density powder obtained by smashing the HDR material has been investigated as well. Fig. 4 shows the three kinds of uranium-carbide materials used

in our experiments and their main characteristics. All have a diameter of 11 mm. The high-density pellet target has been first used during 2006. Preliminary results establish fast release in spite of the low temperature (1700°C) at which the tests have been performed.

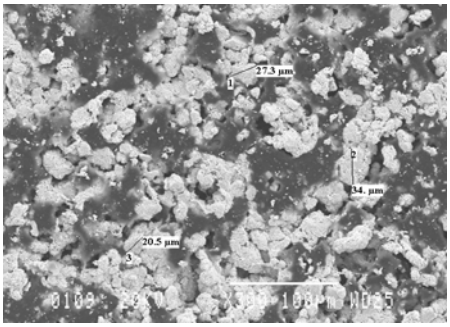

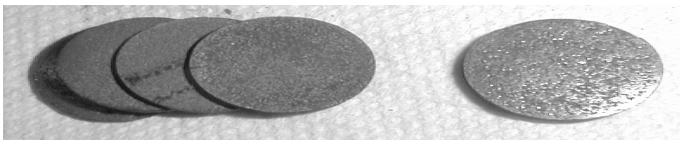

Low density target (LDT): thickness 1 mm, density 3.5 g/cm^3, grain size 25–35 μm, prepared according to the procedure used at ISOLDE and PARRNe.

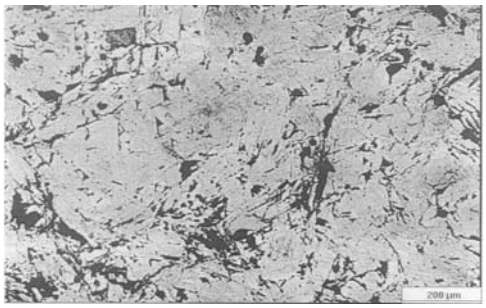

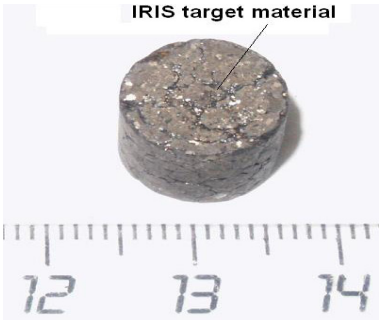

High-density rod (HDR): UC, uranium density 11 g/cm^3, grain size about 200 μm, used in the early tests, occasionally as a powder.

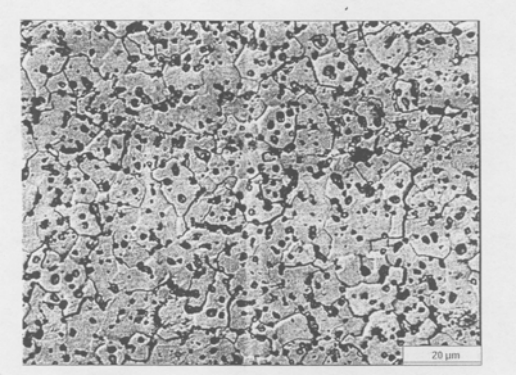

High density pellet (HDP): thickness 2 mm, UC, uranium density 12 g/cm^3, grain size about 20 μm. This is the new target material with promising properties introduced in 2006.

Fig. 4: The different kinds of uranium carbides used in experiments and their main characteristics.

III. METHODS OF ANALYSIS

III.1 Definitions

Observables that establish the performance of a target + ion-source unit are the efficiency of separation and release time of products. Efficiency is defined as the ratio of the number of ions leaving the source per time unit to the rate of corresponding nuclei created in the target. Release is described by a distribution. In a loose way, the release time is the time span during which a pre-defined fraction of the stable atoms created at time t = 0 in the target have left it. In several models this distribution can be characterized by a single constant. Actually it can be different. It is a problem to find a set of parameters to accurately reproduce this distribution. There have been several methods designed in the past to measure yields and release times. This chapter describes the basics and presents our attempts to match analysis methods and experimental conditions specific to our experiments

III.2 Yield measurements

Yields are the number of ions delivered per time unit, and in fact usually they mean the ion current collected and available for experiments. The yield of the target and ion source is attenuated by the efficiency for beam transport in the separator magnet and further beam line. This factor is absorbed in the overall efficiency. For ease of comparison, all yield values quoted in this report are corrected for the actual transmission in the beam transport system and thus represent the yield at the exit of the ion source. In following tables or figures presented yields are often the so-called normalised yields, i.e. scaled for a target thickness of $1 g/cm^2$ and a proton beam current of 0.1 μA, in order to facilitate comparison between various targets. These reference values are close to our experimental conditions (currents delivered by the PNPI synchrocyclotron are of 0.05 - 0.07 μA).

The yield is measured in a steady state when the accelerator beam has been on target for a time long enough to reach saturation. Saturation means the output of the target is constant. Mathematically it is a consequence of the exponential functions $\exp(-\lambda t)$ and $\exp(-\mu t)$ entering the description of radioactivity and release (they become negligible against constants when the time t is large enough). Accelerator current and performance of the target + ion source must be stable during the measurement cycles. This requirement is normally satisfied since the measurement can be carried out within few minutes, at least for the strongly produced activities. The ions are collected on a tape during the collection time t_c, then transported with the tape (t_t) and counted by γ (or sometimes α) spectroscopy during another time interval equal to t_c, during which a new sample is collected. This scheme is depicted in Fig. [5]. As it was already mentioned, β-counting is used for the shortest-lived nuclei with a shorter transport distance and time in order to avoid prohibitive decay losses. The method is somewhat different to allow for separation of the various activities on the basis of their lifetimes. Thus, during these measurements the whole decay curve for the collected radioactive source is measured.

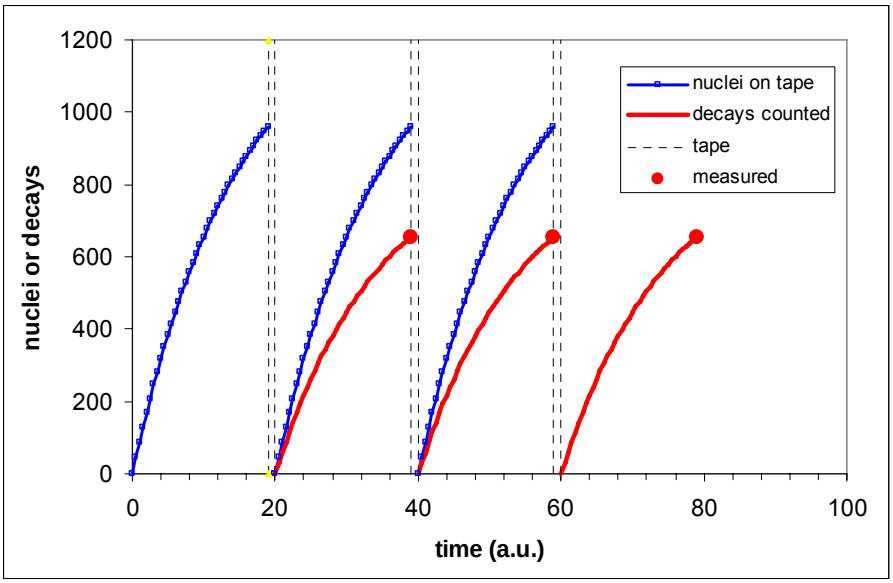

Fig. 5: Yield measurement. The proton beam is always on target so that the mass-separated ion beam collected on tape is constant. The number of nuclei (blue, line with small circles) grows during a preset time interval (here 19 arbitrary time units) followed by a transport (here 1 time unit). The decays are counted while a new sample is collected. The smooth line (red) shows the growing of the summed up decays, proportional to the observed peak area, whose final value is marked by a circle. This example is for 100 ions/a.u. produced in the target, $T_{1/2}$ = 10 a.u. and a simple exponential release function with T_R = 1 arbitrary unit. The measurement of release curves differs in that the tape is moved at short intervals and that a release cycle consists of a succession of transport cycles first with, and then without, proton beam. The effect of short intervals is to differentiate the curve, i.e. to show the ion current modulated by radioactivity, which is more direct, but the price is a loss of statistics.

The transport time t_t has been 1.36 s and presently is 1.25 s, but a newly constructed tape transport system close to become operational at Gatchina shall strongly decrease this time (to 0.25 s) so that short-lived species shall be counted more efficiently. The alternative method is to count directly during collection. In that case one can indeed access very short-lived activities. This method was applied for Fr isotopes with half-lives of a few milliseconds. Unfortunately, there is a risk of implanting part of the ions next to the tape. Accumulation of long-lived background can disturb β and γ- measurements. The new transport system is also being improved in that respect by having a wider tape.

In the most simple case the nucleus of interest has no isomer and its β-decay parent is short-lived (the opposite is very rare). Decays in the target have reached saturation. One thus measures a current corresponding to the sum of productions cumulated over all the more neutron-rich isobars. Yet, there is a chance that the mother nucleus shall escape from the target before its beta decay, which reduces the extra contribution. This complicates the evaluation of the number of nuclei in the target and, consequently, of the efficiency. We shall come back to this issue later.

2a Yields by gamma spectroscopy

First we review the simple and, fortunately most common, case of a nucleus having no isomer before we extend to more complex cases. The simple formula found in many papers, also those published by our collaboration, can be used:

$A = \varepsilon(\gamma)\, b(\gamma)\, p\, f(\lambda, t_c, t_t)$ with

A the peak area for a γ-ray, scaled for a measurement cycle,
ε(γ) the efficiency to detect the peak associated with the gamma ray,
b(γ) the probability of the γ-ray to be emitted in a decay of the nucleus (also called branching),
p the production rate of nuclei, i.e. the ion current to the tape, and
$f = (1/\lambda)\,(1-\exp(-\lambda\, t_c))^2\, \exp(-\lambda\, t_t)$ a function only dictated by time constants of cycle and half-life.

The function f results from solving the simple equation for the number of nuclei present on the tape:

$dn/dt = p - \lambda\, n$
with $p > 0$, $n(t = 0) = 0$ during collection and
$p = 0$, $n(t = 0) = n(\text{collection}, t = t_c)$ during counting.

The number of decays is $N_{dec} = \int \lambda\, n\, dt$.

The detector is a Ge crystal of 160 cm^3. Its front face is placed at about 1.5 cm from the tape in the off-beam position. The energy range covered is typically from 100 keV to 2 MeV. The peak efficiency in the counting position has been carefully measured by the Gatchina group and is known to an accuracy better than 5% (ε = 1.2% at 1.3 MeV). The data points on Fig. 6 are empirically reproduced by the simple function:

$$\varepsilon(E_\gamma) = \exp(2.29 - 0.90\, u) \quad \text{for } u = \ln(E_\gamma/180) > 0,$$
$$= \exp(2.29 - 0.90\, u - 1.79\, u^2) \quad \text{for } u < 0,$$

where the efficiency ε is in % and the γ-energy is in keV.

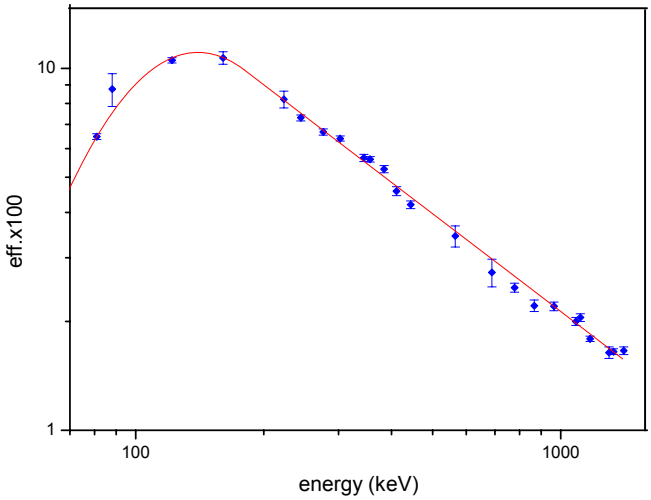

Fig. 6: Peak efficiency of the Ge-detector in the measurement position versus energy. The solid line represents a fit with an empirical formula shown in the text.

Nuclear decay lifetimes are usually well known and their errors even if fairly large have little impact on the final error. Gamma-ray branchings (probability of a γ–ray to be emitted per decay) are supposed to be well known quantities tabulated in compilations [9]. Unfortunately, for exotic nuclei they become less trustable or even are not quoted in literature. Yield measurements are in fact very sensitive to wrong γ-branchings. In the context of cross-section measurements for production or neutron-rich nuclei by neutron-induced fission, this problematic was investigated during 2 series of measurements carried out at the Jyväskylä IGISOL [10, 11]. In Gatchina we concentrate our efforts to alkaline elements (Rb and Cs isotopes). For these nuclei too there happens to be severe mistakes even for nuclei quite close to stability. For instance the normalisation for branchings of γ-rays in ^{92}Rb decay listed in ENDSF is too high by an order of magnitude. We discuss our branching measurement of ^{92}Rb decay [12] and others in a later section. There is a suspicion that many other values could be possibly wrong by factors of 2-3 times. This is an issue we wish to investigate in the future. It is especially of interest in connection with the seemingly odd-even effects in the population of isotopes of a certain element and indirect measurements of release times via efficiency. The branching problem does not exist with β-counting, except for the very exotic nuclei emitting β-delayed neutrons (which seldom have a large neutron branching) or the later mentioned isomers causing electron transitions. The problem in these measurements is a lack of selectivity, but progress has been made very recently.

Yield measurements are not always as simple as depicted above. In case the nucleus of interest has an isomer the γ-rays usually cannot be classified as belonging to one or the other decay uniquely. Instead they are populated with different probabilities in each decay mode. One also needs to consider that during collection and measurement the isomer may decay to the ground state. Observed peak areas are a superposition of 2 contributions. Accordingly, at least two γ-peaks are needed to solve a system of 2 equations with the 2 unknown production rates, but it is recommended to use more peaks and apply the χ^2 method. This is the method we have implemented recently [13]. It naturally contains the case without isomer, in which case the solution of the matrix equation reduces to the simple formula for the function f. The calculation should be expanded to a ground state and 2 isomers, leading to a 3 by 3 system. The occurrence of 2 isomers in a nucleus is quite rare, but some indium isotopes which we

have measured must be treated this way and there are many other cases near Sn isotopes of special physical interest for RIB facilities. The solution for dimension up to 3 has been worked out and is detailed in appendix A1. It is probably not necessary to go beyond since a higher-dimension problem can be decoupled in sub-systems of smaller dimension owing to decay selection rules.

2b Yields by beta counting

For the most exotic isotopes the γ-measurement fails due to possibly unknown γ-branchings and/or the low efficiency of Ge detectors, and the decreasing peak-to-background ratio. The alternative is beta counting. The β-branching is 100% in the absence of isomers. This avoids the problems caused by the often inaccurate γ-ray branchings. We use a 1 mm thick Si(Li) detector placed next to the collection position to avoid the delay due to transport. Its intrinsic efficiency has been measured by coincidences with a total γ-absorption spectrometer at Gatchina. Fig. 7 shows that for the decays of nuclei of interest which have β end-point energies of several MeV it is close to 100%, independently of the details of the decay schemes. The efficiency in the measurement position is 20(3)%, which represents the fraction of 4 π solid angle covered by the detector. Unfortunately, the energy signals of continuous β spectra do not contain a direct signature of the decaying nuclei. The detector triggers also on β-particles from daughter decays (isobars and, although weakly, of A-1 daughters if there is β-delayed neutron emission) as well as occasionally from unwanted molecular ions and long-lived activities being daughters of nuclei collected beside the tape during previous measurements. The measurement method shown in Fig. 5 is accordingly modified. After a short beam pulse the decay of the collected activity is followed as function of time without moving the tape. The different half-lives of the collected species allow to extract the number of beta-particles of interest that have decayed and to compute back their production rate. The tape is moved only at the end of the cycle to remove long-lived activities and to keep the background low. The β method is obviously best suited when the half-lives of isobars are very different. The method of analysis has been very recently revisited (communicated by A. Barzakh at the December 2006 PLOG meeting).

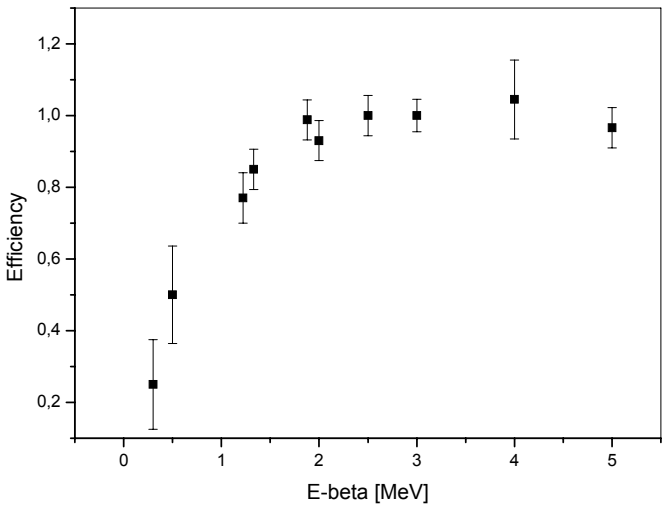

Fig. 7: Intrinsic efficiency of the Si-detector versus β-end-point energy.

2c Efficiency of separation

The concept of efficiency implies that the number of nuclei produced per time unit in the target is known. For 1 GeV protons the targets of about 10 g/cm^2 can be regarded as being thin and the concept of cross-section can be used to a reasonable approximation. In first order, the cross-sections for production of neutron-rich isotopes by 1 GeV proton-induced fission of ^{238}U can be employed. They are known owing to systematic work at the fragment separator at GSI using inverse kinematics [14]. It is thus straightforward to compute the number of nuclei produced per time unit:

$p = n\ \sigma(Z,A)\ I_p$

with
n the number of uranium nuclei per surface unit [/cm^2] = 6.022 10^{23} density [g/cm^2]/A[g],
$\sigma(Z, A)$ the production cross-section, (1 mb = 1.0 10^{-27} cm^2) ,
I_p the particle current on target = I/e (1 nA of protons corresponds to 0.624 10^{10} protons/s).

Since nuclei spend a time inside the target, the effective σ for the nucleus of interest must include contributions from the more exotic isobars because of their possible β-decay. This effect is difficult to estimate. Close to stability, most elements would be released in times shorter or comparable with their half-lives and therefore only a small fraction of their (however large) cross-sections has to be added. Very far from stability, almost all nuclei would decay in the target before being released, whereas their cross-sections are smaller. In some of our reports we have explored both limiting assumptions. It is more realistic to assume a release function for the parent nuclei in order to calculate the fraction that decays in the target and has to be added to $\sigma(Z,A)$ as taken from Ref. [14]. That measurement yields cross-sections without contribution of - long-lived with respect to flight time - precursors, unlike in our measurements. The presence of isomers is a further complication. They can either be separated and observed as such or remain in the target and contribute to feeding of the ground state. The corresponding probabilities are governed once more by the interplay of half-life and release time. Development of a code based on these considerations and extended to up to 3 states (ground state and 2 isomers in parent and nucleus of interest) is in progress.

The use of a cross-section is a useful simplification. However, for targets of a certain thickness there is a non- negligible probability that neutrons generated by fission or spallation could induce secondary fissions. This should cause an enhancement of the 'normalised' yield (per mass unit of target), which indeed has been seen and is reported later. The in-target production can be estimated by Monte Carlo Methods to correct for this effect.

2d Release-time efficiency

The experimental efficiency can be split into several factors, first the in-target efficiency and ion-source efficiency, then transport through the beam line. The ionisation efficiency is measured off-line by putting a controlled amount of an element and looking at how much of it is collected during a time sufficiently long to observe the ion current has vanished [6].

The target efficiency depends on chemistry of the element, i.e. its willingness to form compounds with the target and surrounding materials, and its diffusion and effusion behaviour. If these processes are too

slow with respect to the nuclear lifetime decay losses may become prohibitive and prevent observation of the nucleus of interest. The evolution of efficiency with nuclear lifetime thus gives a hint about release times and, possibly, about which mechanism is at work. This issue is addressed in a following section.

2e Measurement of gamma branchings

Comparison of yields deduced from γ-peak areas and from β-counts is one of the methods to measure absolute transition intensities per decay. According to our most recent data hardly any of the investigated branchings of Cs isotopes reported in literature seems to be correct within 40%. This method has a big potential to provide reliable decay data.

Another method to measure gamma-ray branchings is based on the comparison of γ-peaks in several isobars. It works if the ion source is selective and if the γ-branchings are well known in at least one of the isobars, in which case the number of produced nuclei and decays can be calculated back. In this case, the reference transition replaces the number of β-particles of the β-γ method.

Such measurements can also be done without using conservation of the number of nuclei during decay by decomposing the decay curves to separate the feeding modes. This procedure, however, requires high statistics. It is more reliable to have a selective ion source so that no ions of daughters, grand-daughters, etc. are collected. For our measurement of ^{92}Rb [12] we achieved this goal by lowering the temperature of the ionizing surface to about 1700^{o}C.

III.3 Release-time measurements

3a Definitions

The release function represents the probability that an atom created at time t = 0 shall leave the target at time t. One identifies t with the time of arrival of the ion on the collecting tape since flight through the separator magnet and beam line is fast on the scale of release processes. The release function would be the observable if a short (δ-function like) beam pulse of sufficient intensity would be available and the huge rate at the beginning of counting could be processed by the acquisition system. In practice, in order to get better counting statistics one performs an irradiation, followed by a decay period without accelerator beam. This integrates the release function, which becomes the so-called release curve. It is safer to concentrate the analysis on the decay part, since beam fluctuations could affect the measurement during the irradiation. The irradiation is normally chosen long enough to reach saturation of the ion current. This simplifies the calculations and decreases the impact of beam fluctuations.

Diffusion is the migration inside the target grain (200 μm diameter for the oldest targets to 25-35 μm for the PARRNe target tested at Gatchina and 20 μm the most recent pellet targets used in March and June 2006). For spherical grains the following formula [15, 16] gives the probability that stable ions filling uniformly the sphere at time t = 0 shall cross the grain boundary at time t:

$D(t) = (6/\pi^2)\, \mu_0 \sum_k \exp(-k^2\, \mu_0\, t)$ with k= 1,2 ,3 …

The diffusion parameter μ_0 is related to the Arrhenius coefficients via:

$\mu_0 = \pi^2 D / R^2$, with $D = D_0 \exp(-E_a / k T)$

in which D_0 is a diffusion coefficient [cm^2/s], E_a the activation energy [eV],
k T is the thermal energy [eV], and R the grain radius.
In practice, the generally large experimental errors on μ_0 prevent to draw definite conclusions about D_0 and E_a. The grain radius is a more critical parameter than the temperature dependence of D. It is clear that diffusion is favoured by a small grain size.

One loosely defines a diffusion time $T_D = \ln(2)/ \mu_0$. Integration of D(t) shows that half of the atoms have diffused out at a time t of about 0.44 T_D. The factor is smaller than 1 because D(t) is a series of terms with increasingly faster components versus k. This fact should be kept in mind when one tries to approximate the above diffusion formula with an exponential.

We have noticed that this formula does not apply too well to describe our release curves. Better fits can be obtained by a superposition of two exponentials with free adjustable amplitudes and time constants. In any case, the diffusion probability is conveniently written as:

$D(t) = \sum_k a_k \mu_k \exp(- \mu_k t)$, with $\sum a_k = 1$ to ensure normalisation of the integral of D(t) to 1.

Effusion, that is the process of moving and sticking with the target material and target container inner surface during the random walk of the atoms in the space between grains and in the target container volume towards the ion source, is described by a single exponential with parameter ν, i.e.:

$E(t) = \nu \exp(-\nu t)$.

For sequential diffusion and effusion the release function is a convolution:

$$R(t) = \int_0^t D(t')E(t-t')dt'$$

Indeed, D(t') dt' atoms produced at t = 0 cross the boundary of the grain at t' and have a time (t-t') left for effusion. After substituting the functions D and E the general case reads:

$$R(t) = \sum_k a_k \nu \mu_k \frac{e^{-\mu_k t} - e^{-\nu t}}{\nu - \mu_k}$$

One sees that if $\mu_k >> \nu$ the limit of the k^{th} term is

$$lim\ R_k(t) = a_k \nu e^{-\nu t}$$

The expansion of R(t) is thus numerically truncated by finite effusion time at a certain k_{max} when $t_{\mu k} = \ln(2)/\mu_k$ becomes a few times shorter than ln(2)/ν.

Finally, one accounts for nuclear decay by a $e^{-\lambda t}$ factor. The ion current is:

$$i(t) \;=\; \varepsilon\ \phi(t)$$

with ε collecting the product of time-independent efficiency factors and ϕ(t) being the flux probability, i.e. the release function modulated by radioactivity and integrated over the irradiation time:

$$\phi(t) \;= \int p(t')\, R(t-t')\, e^{-\lambda t}\, dt'$$

where p(t') is the production rate of nuclei in the target being
p(t') = p > 0 during irradiation of duration t_i, t ∈ [-t_i, 0]
p(t') = 0 after irradiation, t > 0

Note that in appendix A1 we use the symbol *p* for the constant ion currents leaving the ion source after equilibrium has been reached in a long-lasting irradiation (i.e. that p is the limit of *i(t=0)* for large t_i), whereas here *p* is the in-target production rate. After carrying out the integration the flux of atoms leaving the target is:

$$\begin{aligned}
\phi(t<0) &= p\sum_k h_k\,(\frac{1-e^{-u_k(t+t_i)}}{u_k} - \frac{1-e^{-v(t+t_i)}}{v}) \\
\phi(t>0) &= p\sum_k h_k\,(\frac{1-e^{-u_k t_i}}{u_k}\,e^{-u_k t} - \frac{1-e^{-vt_i}}{v}\,e^{-vt}) \\
h_k &= a_k\frac{\nu\,\mu_k}{\nu-\mu_k} \\
u_k &= \mu_k+\lambda \\
v &= \nu+\lambda
\end{aligned}$$

The preferred experimental condition is to seek for saturation during irradiation and to measure only the decay part (t > 0), in which case one gets:

$$\begin{aligned}
\phi_R(sat,t>0) &= p\sum_k h_k\,(\frac{e^{-u_k t}}{u_k} - \frac{e^{-vt}}{v}) \\
\phi_D(sat,t>0) &= p\sum_k a_k\,\frac{\mu_k\,e^{-u_k t}}{u_k} \\
\phi_E(sat,t>0) &= p\,\frac{\nu\,e^{-vt}}{v}
\end{aligned}$$

The ”diffusion” or “effusion” release curves are obtained from the general form by letting the other process to be very fast (ν or μ_k going to ∞). It is also useful to note the standard diffusion formula for spherical grains.

$$\phi(sat, t > 0) \;=\; \frac{6\mu_0}{\pi^2} \sum_k \frac{e^{-(k^2\mu_0+\lambda)t}}{k^2\mu_0+\lambda}$$

The measurable parameters are $u_k = \mu_k + \lambda$ and $\nu = \nu + \lambda$ rather than the release parameters μ_k and ν. Only if λ is small, thus the nucleus is long-lived, one can extract the release parameters with accuracy. Since formula involve exponentials, integration does not change the time constants in R(t) but the partial amplitudes of the various components are modified. Integration is a filter that suppresses components with short time constants (large μ_k, or high-order k-terms in the expansion).

3b Release times from direct measurement

The ion current impinging on the tape represents the flux except for a scaling factor. It is measured indirectly by γ *or* β-spectroscopy. Cycles as they have been described for yield measurements, Fig. 5, are performed but with a much shorter collection time t_c and with a different beam structure. Here, short means t_c is much less than lifetime and release time constants to be measured, which ensures that the ion current can be regarded as constant during collection. A number of these short 'tape cycles' is recorded with accelerator beam on and then is followed by other 'tape cycles' without beam. Together they form a measurement cycle that is repeated until enough statistics is collected. In order to reach saturation, the irradiation must have been long enough, i.e. has been a few times the time constant roughly defined by the sum $\lambda + \mu_R$ with μ_R a rough estimate of the unknown release constant:

$T_{irrad} > 3 / (1 / T_R + 1 / T_{1/2})$.

The mechanical transport prevents the use of the method if the relevant times are much under the second. There has been (unfortunately) so far no such short release times measured with our targets. However, there are many advantages in this method. The activity curve measured and displayed during the acquisition very closely follows the ion current modulated by the decay factor $e^{-\lambda t}$. It can be interpreted during the measurement, and if needed, the settings of the cycle can be modified for better sensitivity. The counting rate remains low owing to the short collection time. Long-lived nuclei can be used to scan a long range of the release time axis without overloading the acquisition system.

The widespread and alternative method used at CERN-ISOLDE and PARRNe consists of collecting nuclei on a standing tape during a cycle with an irradiation and a decay part. It allows to measure curves for very short-lived nuclei. This is an advantage since the more exotic isobars have low production cross-sections and do not perturb the activity curve too much. A drawback is that the counts represent the integral of the disintegrations of collected nuclei, i.e. are the fold of the integral of the ion current with radioactivity. The release constants are determined by fits based on the deviation of the activity curve with respect to the simple behaviour resulting from the nuclear lifetime (with all release time constants being zero, i.e. μ parameters are infinite). This is far less interactive and transparent. Details can be seen in various publications of the IPN-Orsay group, e.g. Ref [16]. Another limitation is that the use of short-lived activities prevents access to the long tails of the release functions, which means that only the fast part of the total function is observable.

As a final remark about the release curves measured at Gatchina, we comment on the often-discussed symmetry of the rise and fall. If the irradiation time is long with respect to the release times the

formulae shown above imply symmetry in the rise of the release curve and its fall after the beam is switched off. With $t > 0$ it is expressed as:

$$lim\ \ \phi(0) - \phi(-t_i + t) \ = \ \phi(t)$$

This result is valid for any shape of the release function R(t), as can be shown using the following identities:

$$\begin{aligned} \phi(0) &= \int_{-t_i}^{0} R(-t')dt' &&= \int_{0}^{t_i} R(t')dt' \\ \phi(-t_i + t) &= \int_{-t_i}^{-t_i+t} R(-t_i + t - t')dt' &&= \int_{0}^{t} R(t')dt' \\ \phi(t) &= \int_{-t_i}^{0} R(t - t')dt' &&= \int_{t}^{t_i+t} R(t')dt' \end{aligned}$$

3c Release times from efficiency

The efficiency in a steady state of long irradiation is obtained from the above shown formula (see 3a) by taking the flux value in saturation (long irradiation limit) at the time t = 0 at the end of irradiation and dividing by the in-target production *p*. For the general analytic form of D(t) the efficiency is:

$\varepsilon(D) = \sum_k a_k \mu_k / (\mu_k + \lambda)$

The standard diffusion formula out of grains is a particular case with $a_k = 6 / (\pi^2 k^2)$, $\mu_k = k^2 \mu_0$. Consequently:

$\varepsilon(D) = (6/\pi^2) \mu_0 \sum_k 1/ (k^2 \mu_0 + \lambda) = 3 (a \coth(a)-1) /a^2$ with the dimensionless $a = \pi (\lambda / \mu_0)^{1/2}$

For effusion it reads:

$\varepsilon(E) = \nu / (\nu + \lambda)$

If both processes are of importance the resulting efficiency is the product $\varepsilon(R) = \varepsilon(D)\ \varepsilon(E)$.

The variation of efficiency for the isotopes of an element versus the nuclear lifetime thus gives a handle on the diffusion parameters μ_k and the effusion ν. Unfortunately, there is no large difference in behaviour of these functions as long as nuclear lifetimes are not very short, see Fig. 8. Only in the asymptotic region of very short half-lives the slope of the curve $\varepsilon(T_{1/2})$ differs according to the process; $(T_{1/2})^{1/2}$ for diffusion out of spherical grains, $T_{1/2}$ for effusion and their product $T_{1/2}^{3/2}$ if both are of importance. This indeed allows a conclusion about the dominating process, as it has been shown by experiments at PARRNe [16]. We seldom can measure the yields of nuclei that are short-lived enough to cover this region, at least when using gamma spectroscopy after transport of the activity. However, recent developments in the analysis of β-spectra let us hope soon to access these very neutron-rich nuclei and without facing the problems caused by questionable spectroscopic input data. Our analysis

of release efficiency shall thus become more sensitive to the model parameters.

In short and to summarize, exploiting the variation of efficiency with radioactive lifetime is a crude method when compared to measurements of release curves. Its interest resides in its simplicity and the fact that it gives a direct view of the performance of the target, which makes it a valuable and straightforward tool to compare the evolution of release properties with temperature or the performances of different targets.

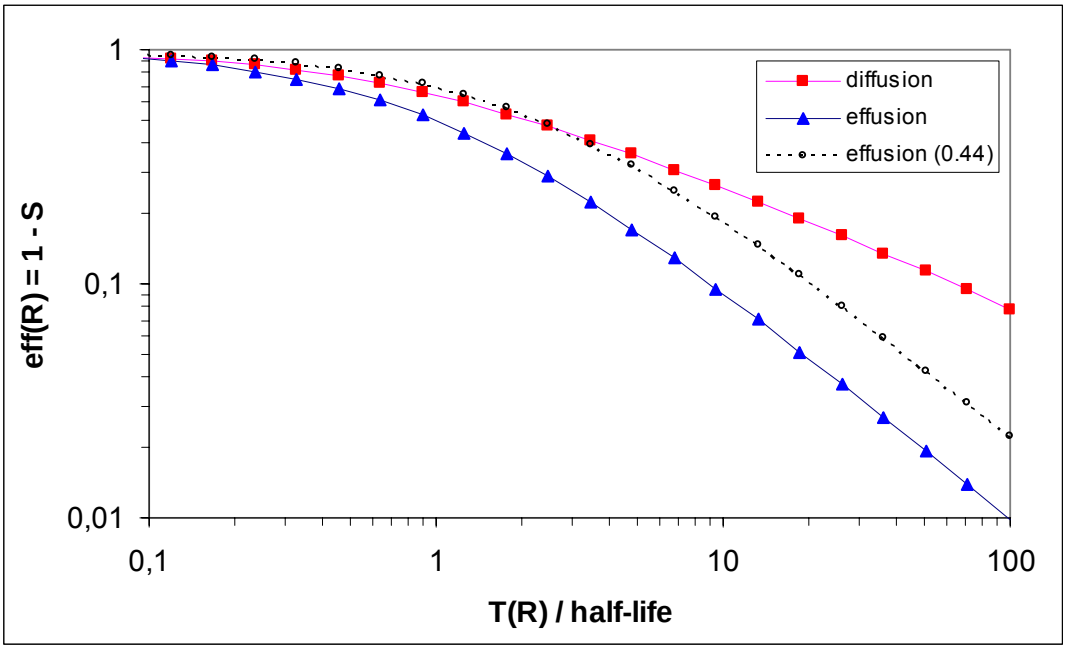

Fig. 8: Release efficiency for diffusion out of spherical grains (solid line with squares) and effusion (solid line with triangles) for the same value of the parameters μ_0 (diffusion) or ν (effusion). As long as no measurements are available for half-lives at least less than one tenth of the release time there is ambiguity in the determination of the process, as shown by the near overlap of the diffusion curve and an effusion curve calculated for a shorter effusion time $T_E = 0.44\ T_D$ (dashed line). The factor S in the ordinate is the probability for decay in the target.

III.4 Decay in target

This section contains original work, still in progress, born from the necessity to match more closely the models with the experimental conditions. We consider here that β-decay of the parent nucleus in the target is an extra channel for production of the nucleus of interest. First we outline a calculation of an effective cross-section. It could be used for calculating the in-target production and obtain more trustable efficiencies. Then we describe shortly the effect of delayed decay production on the measured release curves about which details can be found in Ref. [17].

4a Cross-section

Yield measurements are performed with proton beam continuously on target. This ensures that equilibrium has been reached and that production rates can be simply expressed by using conservation of the number of nuclei. The parent nucleus is of course itself the daughter of a more exotic isobar so that this calculation could extend very far. In practice, the corresponding cross-sections become smaller and it is acceptable to absorb their extra contribution by renormalizing the parent cross-section. Thus, by definition, all parent states are populated by fission, but not by beta-decay, which gives contributions:

$< \sigma (i=1) > \; = \; \sigma \quad f(i=1)$ for the highest level $i = 1$

$< \sigma (i) > \; = \; \sigma \quad f(i) \; + \; < \sigma (i-1) > \quad S(i-1) \; b(IT, i-1)$ $i > 1$

with,
$< \sigma(i) >$ and $\sigma(i)$ the effective and independent cross-sections for the state (i), respectively,
σ the independent cross-section for the nucleus,
f(i) the fraction of σ leading to population of the level of index (i) in fission,
S (i-1) the fraction to be summed of the effective cross-section of the higher level of index (i-1),
b(IT, i-1) the branching-ratio of the isomeric transition from level (i-1) to level (i).

Similar expressions are valid for the nucleus of interest. In addition, each level can be reached via β-decay of the parent nucleus. This gives new extra terms with similar structure as those above. Now the index (j) refers to a state in the parent nucleus instead of the upper level of index (i-1). The branching term is written as β (j, i) the β- branching from parent state (j) to daughter state (i). This factor can be calculated from the decay schemes compiled in the literature. The sum is carried over all states of the parent nucleus (j) able to decay to the daughter state (i).

$< \sigma_{\beta} (i) > \; = \; \Sigma \quad < \sigma_{-1} (j) > \quad S_{-1}(j) \; \beta (j, i)$

Starting from the highest level in the parent one can calculate all effective cross-sections by successive substitutions. Independent σ values are available for 1 GeV protons from Ref. [14]. However, there are two experimentally unknown factors which limit the accuracy of the calculation.

The fractional distribution f(i) must be estimated. A simple model is to assume a distribution of spins of the highly excited levels in the fission fragment and to divide the probability of populating low-lying levels, i.e. ground state and isomer, according to the integral of the distribution in ad-hoc defined integration bins. This approach was introduced in Ref. [18]. In spite of reasonable success at low and intermediate energy fission this procedure must carry some uncertainty.

The survival of atoms in the target with their nucleus in state (j or i-1) is unknown. It must be estimated as well for the parent (j) as for the nucleus of interest (i-1) by making some assumptions about their release properties. If one uses the general form of release function and follows the calculation of number of nuclei in the target outlined in Ref. [17] one gets in the long irradiation limit:

$$S = \Sigma\ a_k \quad \lambda\ /\ (\ \mu_k + \lambda\ )$$

This expression confirms the intuitive results that S = 0 (contribution of parent or higher-lying isomer is not added) if the parent state is very quickly released and S = 1 (in which case the cross-section of the parent is fully added) if release is very slow. The interest of this approach is thus to correct cross-sections by an amount varying with the half-life of the parent and based on physically meaningful assumptions rather than brute force. We note that

$S + \varepsilon = 1$, i.e. the nucleus either is released as such or is lost by decay in the target.

An application is the measurement of release properties based on the variation of efficiency versus half-life of isotopes of mass A. The experimental yield is expressed as (with obvious symbols):

$$p(A) = \varepsilon\ (\text{scale})\ \ n(U)\ \ I(p)\ \ <\sigma(A)>\ \ \varepsilon_R\ (A)\ .$$

For series of isotopes the scale factor is the same but ε_R (release) varies with the lifetime of the isotope. With a trial release function $R(\mu_k, \nu, t)$ one can express analytically the efficiency $\varepsilon_R\ (\mu_k, \nu, \lambda)$ and occasionally implement the correction into the effective cross-section $< \sigma >$ in case the nucleus has isomer(s). Contribution to $< \sigma >$ by decay of the parent in the target requires at least a crude assumption for the release function of the parent element. Then one fits the set of experimental p(A) yields by iterations of the release parameters (μ_k, ν) while ε (scale) is automatically adjusted at each iteration. Consistency of the approach can be tested by comparing the calculated ε_R values with the 'experimental' values, i.e.

$$\varepsilon_R\ (\mu_k, \nu, \lambda) \ = \ \varepsilon_R\ (A) = p\ /\ \ (\varepsilon\ (\text{scale})\ n(U)\ \ I(p)\ \ <\sigma(A, \mu_k, \nu, \lambda\ )>\ )$$

As long as the nuclei do not have an isomer the procedure reduces to the conventional method in which σ(A)'s are fixed input independent of the unknown release parameters. Release efficiency curves presented in this report did not include any correction for the effective σ, for which the independent values from Ref. [14] were instead employed. The interest of the extension to nuclei with isomeric states is that it allows including states of different lifetimes measured in the same experimental conditions of beam and target.

4b Release curves

The formulae shown previously for the flux of atoms leaving the target suppose the nucleus is produced at a time evenly probable during irradiation, p(t') = p constant. Production is synchronised with the beam and corresponds to the reaction, here fission, wherefrom the index F for fission shall be appended to $\phi(t)$. If the nucleus is produced by β–decay in the target, there is another distribution $p(t') = \lambda\, n(t')$, where λ is the decay constant of the mother nucleus and n(t') the number of mother nuclei in the target. The time t' is the creation time of the daughter by β-decay. Thus n(t') depends on the half-life and on the (μ_k, ν) release parameters of the mother. The calculation of this effect is quite tedious. The formalism is presented in a recently published paper [17] and in various LNL annual reports. Figure 9 shows the different time structure of the contributions by the beam and beta decay. It is quite clear that the survival of parent nuclei in the target after the beam has been switched off shall make the apparent release to be slower. Moreover, the perturbation can be seen to be minimised if either the parent half-life or release time is very short, as then the distribution of nuclei in the target moves closer to the rectangle representing the beam profile. This helps to select cases with little perturbation.

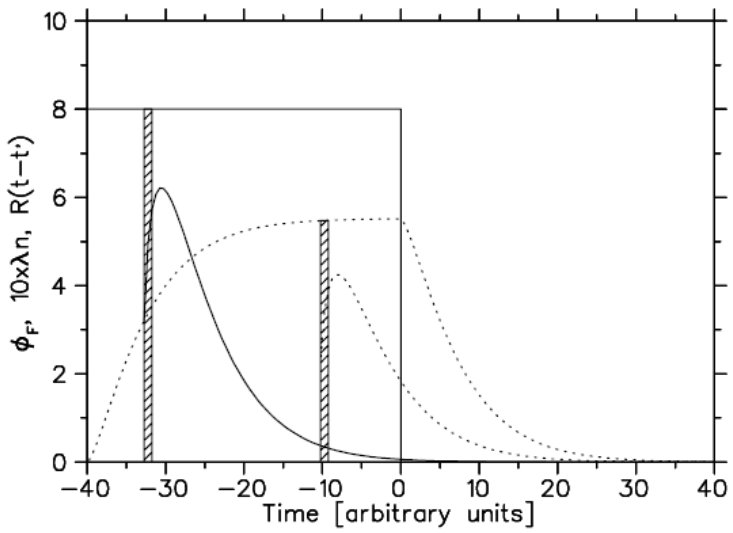

Fig. 9: Principle of calculation of the effect of beam duration and decay in the target on the experimental release curves. Each time slice [t', t'+dt'] contributes with a different time shift relative to the time of observation *t* of the ions. The square (solid line) represents the constant beam intensity. The growing and falling dotted curve is the number of parent nuclei in the target contributing to a production with a different profile given by $p(t') = \lambda\, n(t')$.

In a first version presented at the PLOG meeting in December 2004 held at Gatchina, the model used a single 'black box'. There was a single release constant for the mother nucleus and an expansion of exponentials for the daughter (= nucleus of interest). This simple model improved the consistency of data but could not reproduce a number of peculiar release curves of rubidium isotopes recorded for 'very slow' targets. The difficulty was removed by considering explicitly that β-decay occurs during either diffusion or effusion. This led to the 'two-boxes' model shown in Fig. 10. Two further flux functions, $\phi_{D\beta}(t)$ and $\phi_{E\beta}(t)$, are introduced according to where the decay takes place. The observed

release curve is thus the sum of three different flux functions with the in-target production rates (*d* for daughter, the nucleus of interest, *m* for its mother) now written explicitly.

$$\phi(t) \;=\; p(d)\,\phi_F(d,t) \;+\; p(m)\,(\phi_{D\beta}(m,t) + \phi_{E\beta}(m,t))$$

The ratio *p(m) / p(d)* can be taken from the ratio of experimental cross-sections [14] and is thus fixed. The minimum number of extra parameters is two, one for diffusion and another for effusion of the mother nucleus. Even so, it is quite impossible to extract all the parameters by fitting a single release curve. One must work with series of isotopes. This varies the experimental (u_k and ν) parameters in a controlled way through λ, while the release parameters (μ_k and ν) remain the same. Nevertheless, given the complexity of the complete function it is desirable, whenever possible, to chose transitions coming from a state not reached by β–decay. Such states are for instance high-spin isomers in odd-odd nuclei.

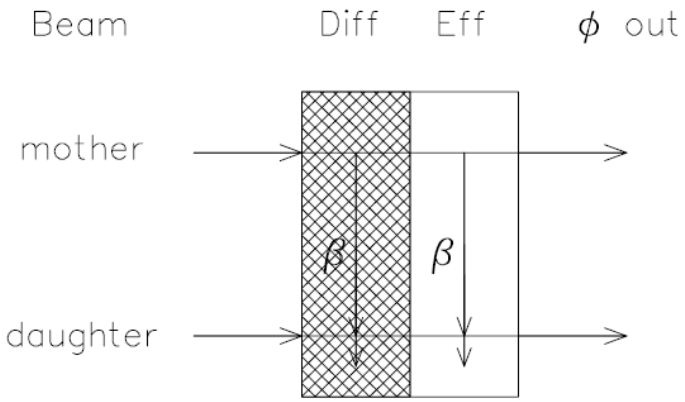

Fig. 10: Principle of the calculation of the influence of decay in the target with possibility of decay during diffusion and effusion. The horizontal axis is a time: creation by beam (left vertical line), exit from the grain and end of diffusion (middle vertical line), exit of target and end of effusion (right vertical line).

The model has been tested by comparing the release curves for the pairs of isotopes ($^{86}Rb^{m}$, ^{91}Rb) and ($^{130}Cs^{m}$, ^{139}Cs). In each pair the isomer is populated only by fission and its release curve is therefore not perturbed. The analysis provides the parameters relevant for that element. The other isotopes (^{91}Rb and ^{139}Cs) have β-decay precursors. Their release curves have been successfully fitted with realistic parameters entering $\phi_{D\beta}$ and $\phi_{E\beta}$ for the respective mother elements Kr and Xe. As one can judge so far the model seems to contain the physically relevant ingredients.

IV. EXPERIMENTS AND RESULTS

IV.1 Comparison of proton and neutron-induced fission

These measurements have been performed with a proton beam of current 0.05 μA. The proton beam is, alternatively, impinging directly on the UC_2 target or after being deflected by a magnet on a tantalum converter to generate fast neutrons [19]. A sketch of the target set up is depicted in Fig. 11.

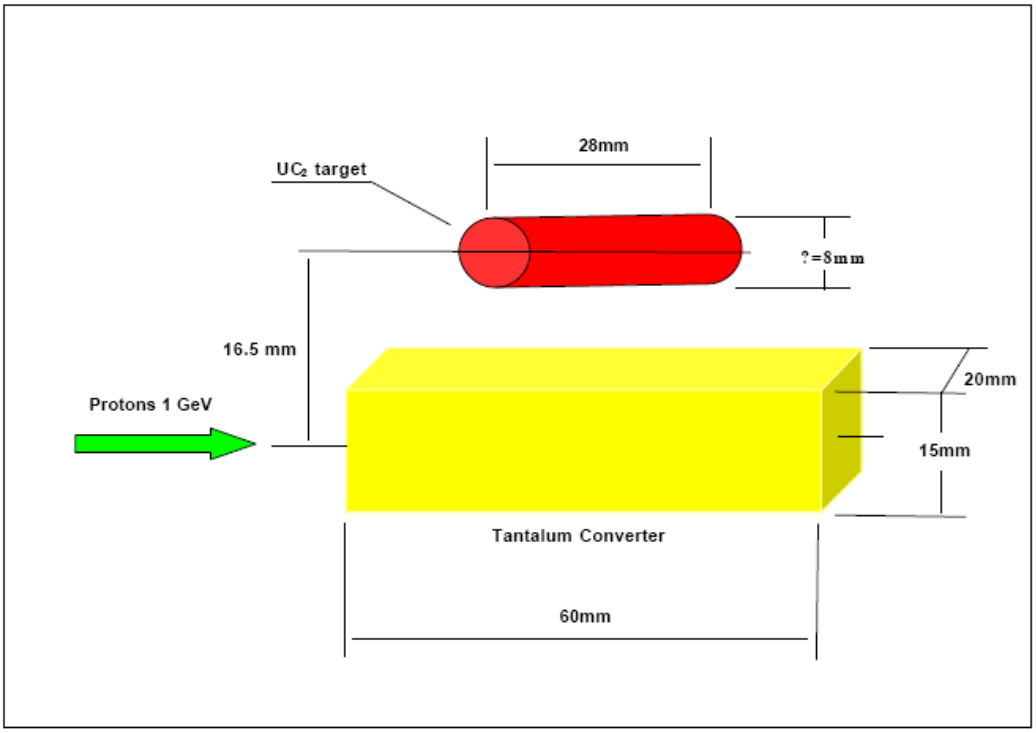

Fig. 11: Sketch of the experimental target set up. The proton beam can be switched to impinge directly onto the UC -target or onto the tantalum converter.

The target material was a High-Density-Powder (HDP) uranium carbide, obtained from the fragmentation of a high-density rod (HDR) uranium carbide (of density 11 gcm^{-3} and average grain size about 200 μm.). The HDP target has a volume of 1.4 cm^3 and contains about 10.3 grams of uranium with an effective density of 7.36 g/cm^3 (corresponding to a thickness of 19.8 g/cm^2). A surface-ionisation ion source made in tungsten (see Fig. 2) was employed. The ion-source operation has been tested using an off-line mass separator. At 2100°C ionisation efficiencies of 30 – 35% for Rb and Cs and 1 – 3% for In have been measured using the implantation technique [6]. During the on-line measurements the UC-target and the ion source were both operated at the same temperature of 2100°C.

1a Yields

The yields of neutron-rich rubidium, indium and caesium isotopes at the exit of the ion source are presented in Figs. 12 – 14. They have been scaled up to give the number of ions per μC of protons. The observed number of ions per second was thus about 15 – 20 times less than the reading on the ordinate. For comparison the in-target production, calculated with the MCNPx code [20] is also shown.

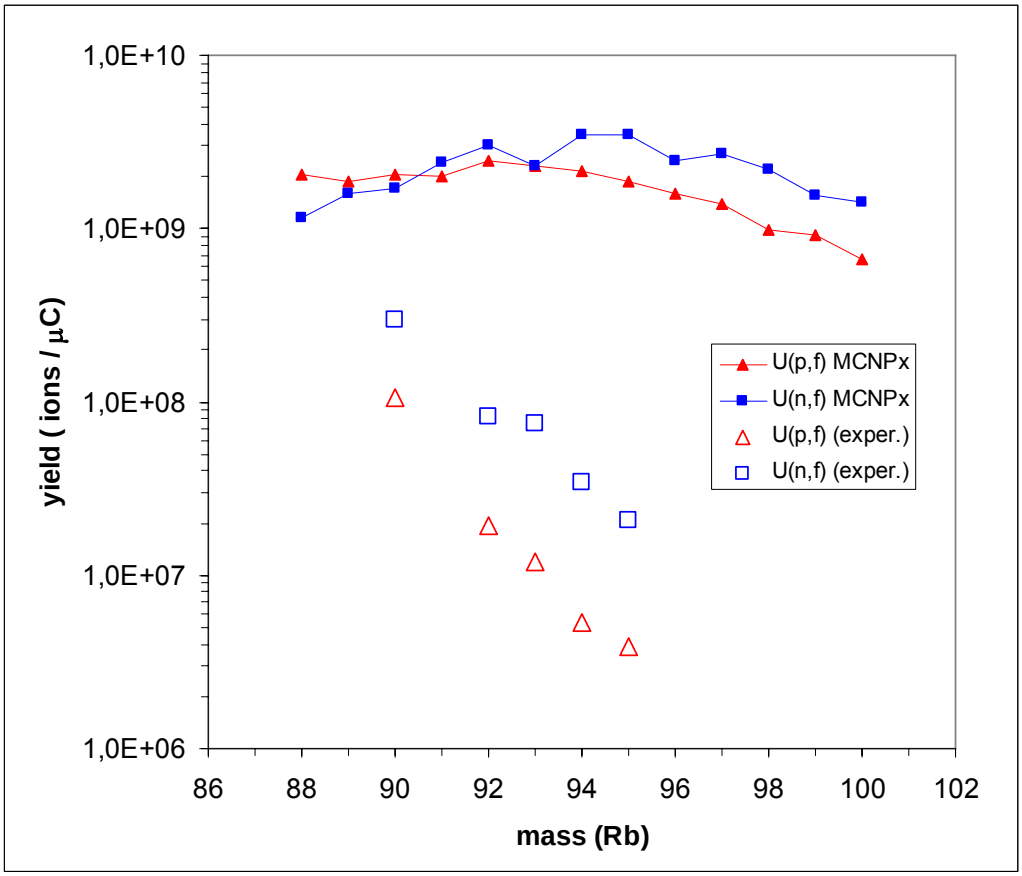

Fig. 12: Yields of neutron-rich Rb isotopes scaled for a collected proton charge of 1 μC. The target is a high-density powder (7.63 g/cm^3 of uranium) with a thickness of 19.8 g/cm^2. Solid symbols connected by solid lines are the result of a Monte-Carlo simulation for this target. Open symbols are experimental yields (ions/s), scaled to the corresponding reference current. The target temperature was 2100^{o}C.

Figures 12- 14 compare the experimental production yields for 'direct' fission by the proton beam and for fission induced by neutrons generated in the tantalum block, both on the same UC_2 high-density powder target. The neutron-induced fission yields have been scaled for the total number of neutrons generated in the converter for the reference current of 1 μA and for the fraction of them hitting the target. The MCNPx Monte Carlo code [20] predicts that the number of neutrons emitted in 4π is 5.1 times the number of incident protons and that, in the actual geometry of the set-up, 4% of them impinge onto the target.

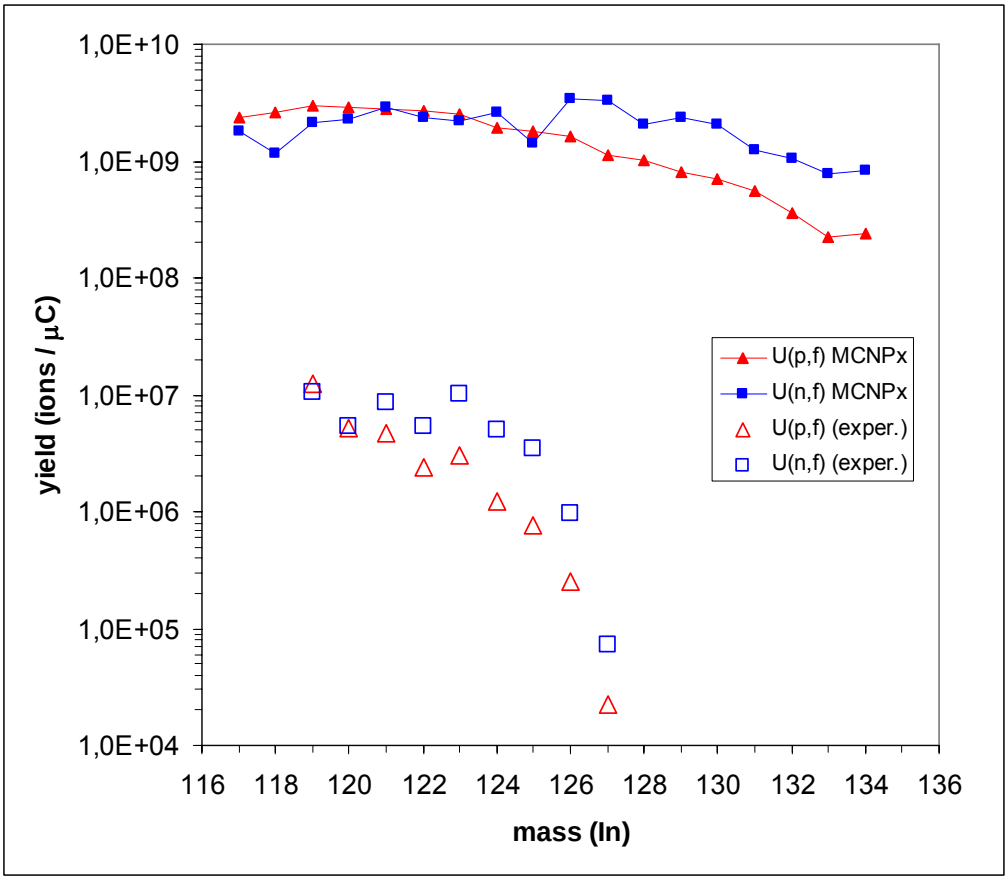

Fig. 13: Experimental yields and calculated in-target production of neutron-rich indium isotopes. See text and caption of Fig. 13 for details.

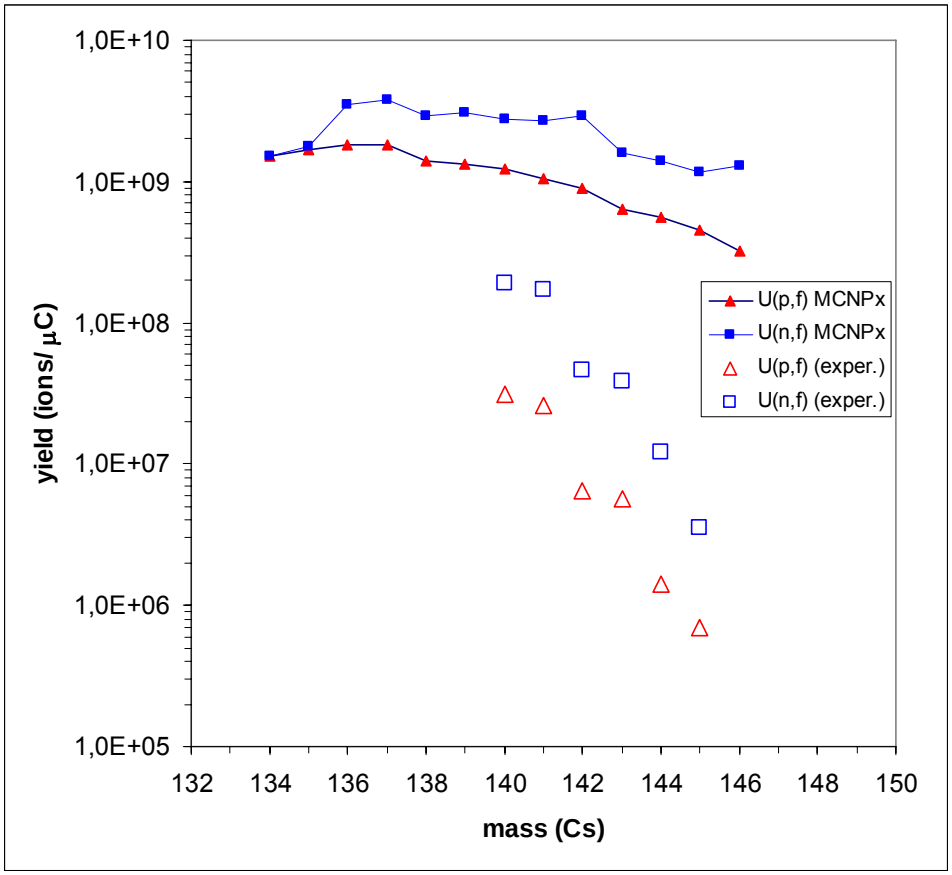

Fig. 14: Experimental yields and calculated in-target production of neutron-rich Cs isotopes. See text and caption of Fig. 12 for details.

We note that the isotopic distributions of indium and caesium show some odd-even structure, with the formation of even-neutron isotopes (odd-A) being favoured. This effect shows no apparent dependence on the production method (1 GeV protons or low-energy neutrons). The staggering is possibly artificially produced by the analysis, due to inaccurate γ-ray branchings for decays of some Cs isotopes, i.e. a systematic error on odd or even-A decay data. However, it has been observed also in β-counting at ISOLDE, which tends to suggest a physical origin. We hope that our new developments on analysis of β-spectra will shed light on this phenomenon. It is worth to stress that this odd-even effect is irrelevant for comparison of the n and p-induced fission yield curves.

In fission induced by neutrons, the production of neutron-rich isotopes far from stability is enhanced, this being a probable consequence of the lower average excitation energy and of larger N/Z ratio of the fissioning nucleus. This is well known at intermediate energies [10, 11] and is predicted by the MCNPx simulation also at 1 GeV proton energy as shown in Figs. 12, 13 and 14. Confirmation for such an effect is clear, see Fig. 15, when the ratio of experimental yields is plotted versus the difference of the actual mass minus the nearest A-value calculated from an empirical line of stability. We note that, as a consequence of a possible wrong scaling of the neutron data, the absolute values of the ratios are probably too high, while what really matters is the up-going trend versus neutron excess of the fission product. If one would force the efficiency for both experiments to be the same, the neutron data should be decreased (or the MCNPx-calculated spectrum increased) by factors of 3.3 (Rb), 2.0 (In) and 2.7 (Cs). In that case, the vertical scale in Fig. 15 is compressed, while the scattering of the points is reduced.

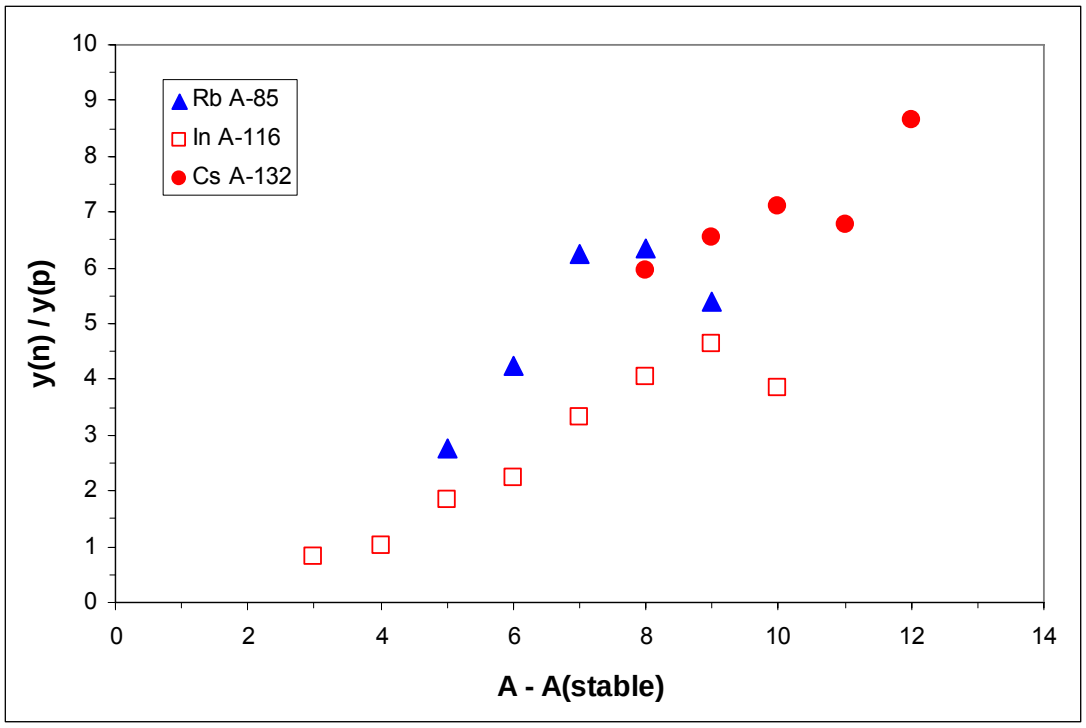

Fig. 15: Ratio of yields per projectile (n or p) for neutron-induced fission to proton-induced fission versus the distance from the line of stability for neutron-rich isotopes of rubidium, indium and caesium. The up-going trend is clear despite the scattering of the individual points.

1b Some properties of the high-density powder target

The main processes whereby radioactive species are lost between initial formation and measurement are associated with diffusion, adsorption, and ion-source efficiencies for forming beams of the species. The delay time between production and removal of the ionized fission products from the source becomes shorter when increasing the temperature of the target, with the consequent increase of the total efficiency. In fact, release properties can be determined by measuring the overall absolute efficiency [21]. The overall efficiencies measured for ^{89}Rb and ^{139}Cs obtained by dividing the experimental and calculated yields are about 20% and thus are about twice less than the off-line ionisation efficiencies at the same temperature of 2100°C. These isotopes have a half-life of a few minutes or longer and are not much affected by decay losses.

The variation of efficiency with radioactive half-life is shown in Fig. 16. The trends on the p and n-induced fission data are in fair agreement. However, there is an excess of efficiency for the n-induced fission data. It can be due to an erroneous estimate of the number of neutrons generated by the converter implying a too high up-scaling factor. The parallel evolution with λ means that the release efficiency is the same in both experiments.

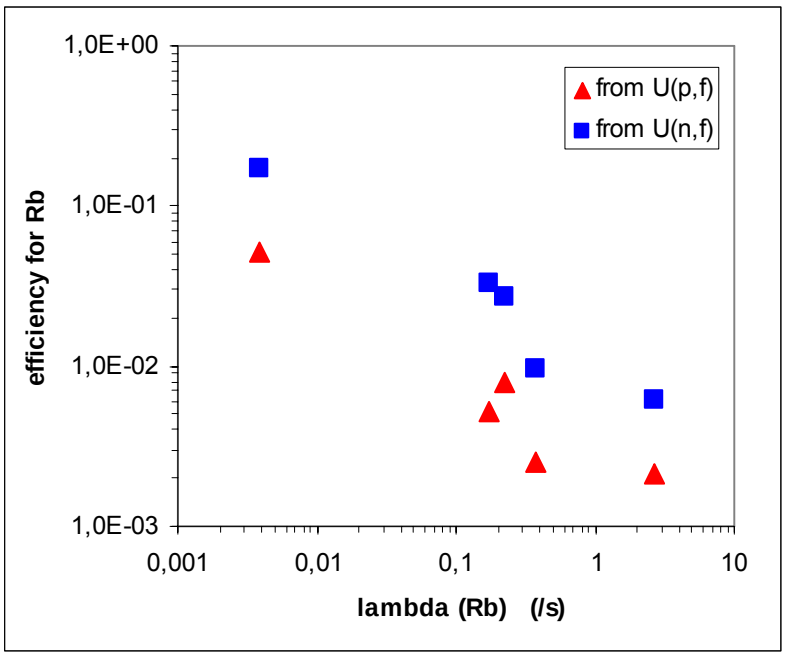

Fig. 16a: Overall efficiency of the HD powder target for various neutron-rich Rb isotopes. In spite of a discrepancy of scaling, the evolution with half-life is very similar for proton and neutron-induced fission.

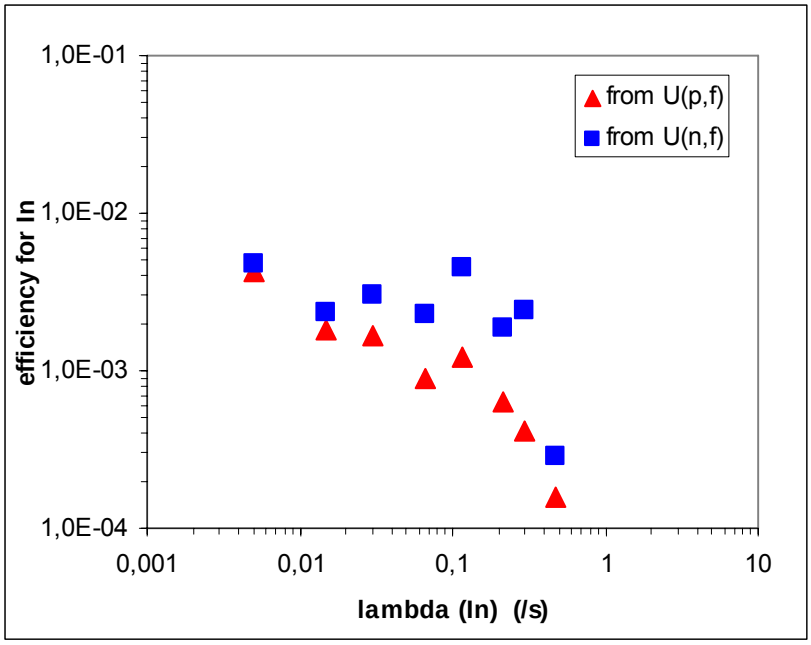

Fig. 16b: as Fig. 16a, now for indium isotopes. Note the lower scale due to lower efficiency of ionisation.

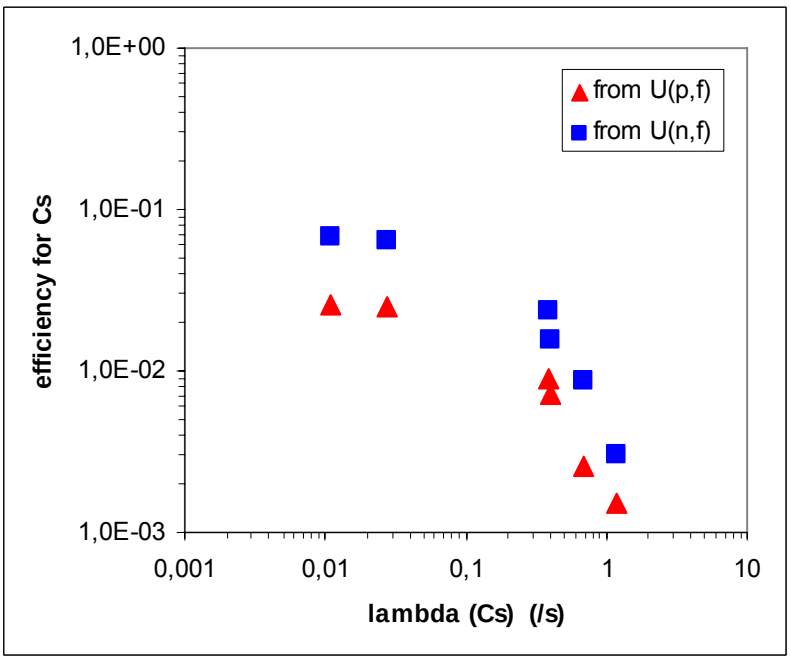

Fig. 16c: as Fig. 16a, now for caesium isotopes.

The decrease of efficiency with decreasing half-life is slower for Rb than for Cs and In. However, the yields measured for the last isotope of Rb are surprisingly high. They are probably overestimated due to interference of γ-rays. Thus, it is premature to draw a definite conclusion. The overall efficiency is higher for the alkalis Rb and Cs than for indium, likely due to the less efficient ionisation, as shown by the off-line values.

Finally we mention the evolution of target performance with temperature. The Rb and Cs yields increase by about a factor of 2 when the temperature is raised from 2100°C, for which the data have been presented in Figs. 12-16, to 2300°C. In contrast, the In yields do not increase. This shows that they have been saturated at lower temperature. Under these conditions, the diffusion-effusion efficiency is 1 by definition and the measured overall efficiency is the ionisation efficiency. The overall efficiency for In estimated from the saturation values is somewhat less than 1% and indeed is in excellent agreement with the 1-3% off-line values. The release rate of indium from the UC target has reached its maximum already below 2200°C. This conclusion does not apply to alkalis for which the highest yields are obtained at the highest temperature.

IV.2 Comparison of HDR and LDP of different densities

2a Yields and release times

Series of experiments have been performed to measure the yield and release properties of Rb and Cs neutron-rich isotopes from targets of very different densities at temperatures in the range 2000 – 2300°C. The target-ion source unit was the one shown in Fig. 2. Two kinds of target materials, both uranium carbides, have been tested: a high-density rod (HDR) (ρ = 11.2 g/cm^3, ρx = 8.2 gcm^{-2}, grain size about 200 μm*)* and a low-density powder (LDP) (ρ = 1.5 gcm^{-3}, ρx = 1.9 g/cm^2, grain size about 20 - 30 μm). Both kinds of uranium carbide target materials have been prepared at the IRIS facility from components (graphite powder and uranium dioxide) not especially manufactured as target materials for being used at an ISOL installation. It was the reason why uranium carbides were normalized for a long time at the heating test bench to outgas the unwanted impurities that reduce the ionisation efficiency. A long-lasting out-gassing procedure at high temperature might have led the grain size of the target material to grow.

A comparison of release curves, from HDR and LDP targets, for ^{139}Cs ($T_{1/2}$ = 9.27 min) is shown in Fig. 17. The counts are a good picture of the variation of the ion current of Cs after the proton beam has been switched off, when corrected by the attenuation due to the decay of the selected nucleus. The formula for the fit function is given in [22]. Both release curves are roughly exponential. However, they can be better decomposed as a sum of a fast (τ_f) and a slow (τ_s) component of about one and twenty-five minutes defined with typical errors up to 50% and 30%, respectively. The best fits are obtained for (HDR; 40 s, 1570 s) and (LDP; 80 s, 1500 s), which means that there is no definite difference in the release properties. A release curve of rubidium shows the same features (HDR; 70 s, 1680 s). It has not been measured for LDP. The presence of two components with such time constants cannot be explained by the standard diffusion formula where the curve should be a sum of terms with a well-defined relationship (the time constant associated with the kth-term varies as 1/ k^2). This issue obviously needs dedicated investigation for a hopefully better understanding.

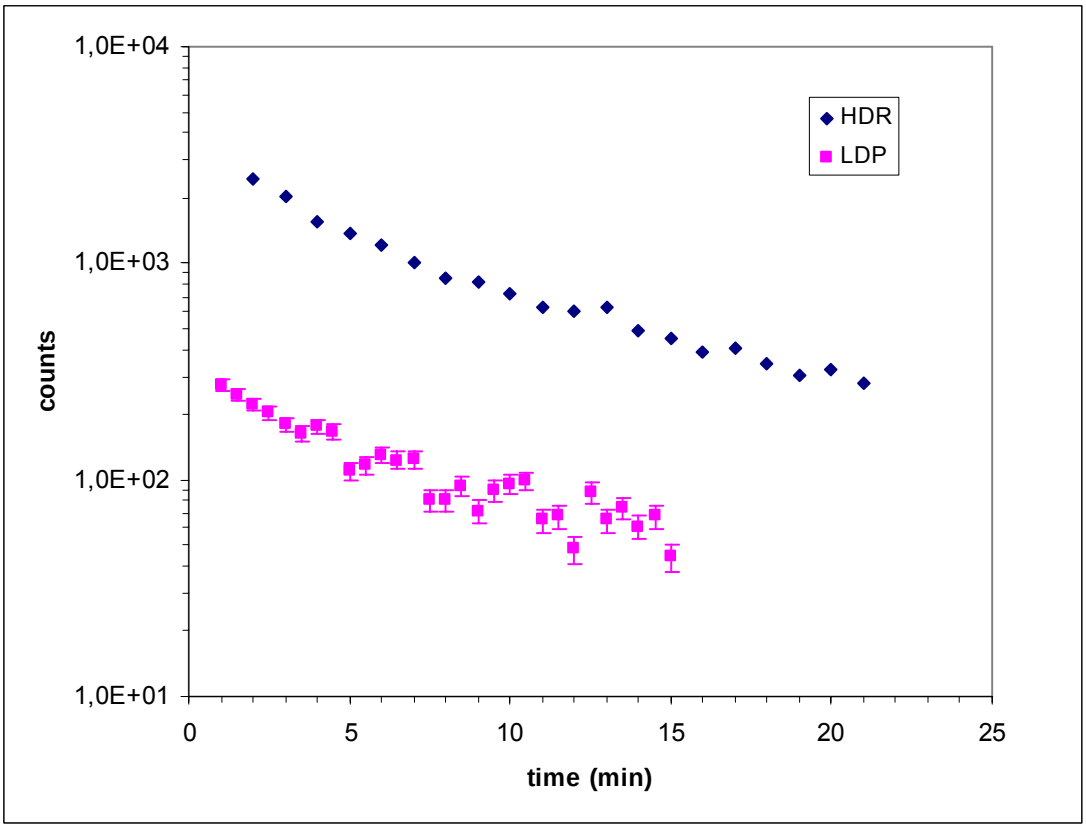

Fig. 17: Release curves of caesium measured using ^{139}Cs ($T_{½}$ = 9.27 m), for the high-density rod (HDR) at 2050(40)^{o}C and the low-density powder (LDP) at 2070(100)^{o}C.

An explanation for the shape of these release curves may invoke the decay in the target of the nuclei ^{89}Kr and ^{139}Xe with half-lives of 3.2 min and 41 s, respectively, causing a delayed production of Rb and Cs. Yields and delay times for the elements Kr and Xe have not been measured for our targets. Therefore, we investigated the influence of mother decay in the target using the link between release time and release efficiency. Two extreme cases have been considered;

a) The release times of Kr and Xe atoms are very short with respect to the radioactive half-lives of the parent isotopes ^{89}Kr and ^{139}Xe. There is little time for decays in the target. The extra contribution of the production of the parents to the yields is neglected.

b) The release times of Kr and Xe are very long. Most of the ^{89}Kr and ^{139}Xe parents decay in the target. Their production contributes considerably to the measured yields. This effect is especially important near stability, as is shown by the cross-sections, table 1, based on Ref. [14].

Table 1: Krypton, rubidium, xenon and caesium independent (in fission) production cross-sections (in mb) in fission of ^{238}U induced by 1 GeV protons [14]. Actual cross-sections for the parent nuclei must still be increased from the contribution of their own precursors, which due to their shorter half-lives, are even more likely to decay in the target. These extra contributions are negligible for the listed Xe isotopes but they amount to 30% of σ(^{89}Kr). However, they decrease rapidly with A and can be neglected against statistical errors for the isotopes heavier than ^{92}Kr.

Mass number	**89**	**90**	**91**	**92**	**93**	**94**	**95**
σ_{Kr}	6.03	5.14	3.26	1.74	0.66	0.23	0.07
σ_{Rb}	9.2	8.2	7.4	6.12	4.6	2.4	1.17
Mass number	**139**	**140**	**141**	**142**	**143**	**144**	**145**
σ_{Xe}	3.15	2.11	0.77	0.32	0.06	$0.01^{(a)}$	$0.001^{(a)}$
σ_{Cs}	3.55	3.34	3.4	2.05	1.04	0.4	0.12

According to table 1 the contribution of parents is negligible for very neutron-rich and short-lived isotopes while for those close to stability it can be more than 50% of the observed yield. In reality this contribution should be lower in the particular case of alkalis because the parent elements are noble gases. Diffusion and effusion times of noble gases are much shorter than the radioactive half-lives of those long-lived nuclei. The PARRNe-Orsay group published release times for Kr and Xe at 2080°C of 11 s and 21s [23], respectively, which imply that most of the parents close to stability are decaying after having left the target.

Fig. 18 shows the normalized yields (1 g/cm^2 of uranium, 0.1 μA proton current) of Rb and Cs neutron-rich isotopes extracted from the HDR and LDP targets at 2000°C. The highest values (triangles, exp.) are the experimental ones. They are proportional to the independent cross-section σ(Z, A) of the nucleus of interest plus an unknown fraction of the cumulative σ(Z-1, A) for the parent. The lower values (circles, cor.) are calculated by removing a fraction corresponding to the maximum possible contribution of the parent decay in the target. Note that in the section devoted to the method, we have presented an approach allowing a more realistic estimate of this fraction, which shall be applied in the analysis of forthcoming experiments.

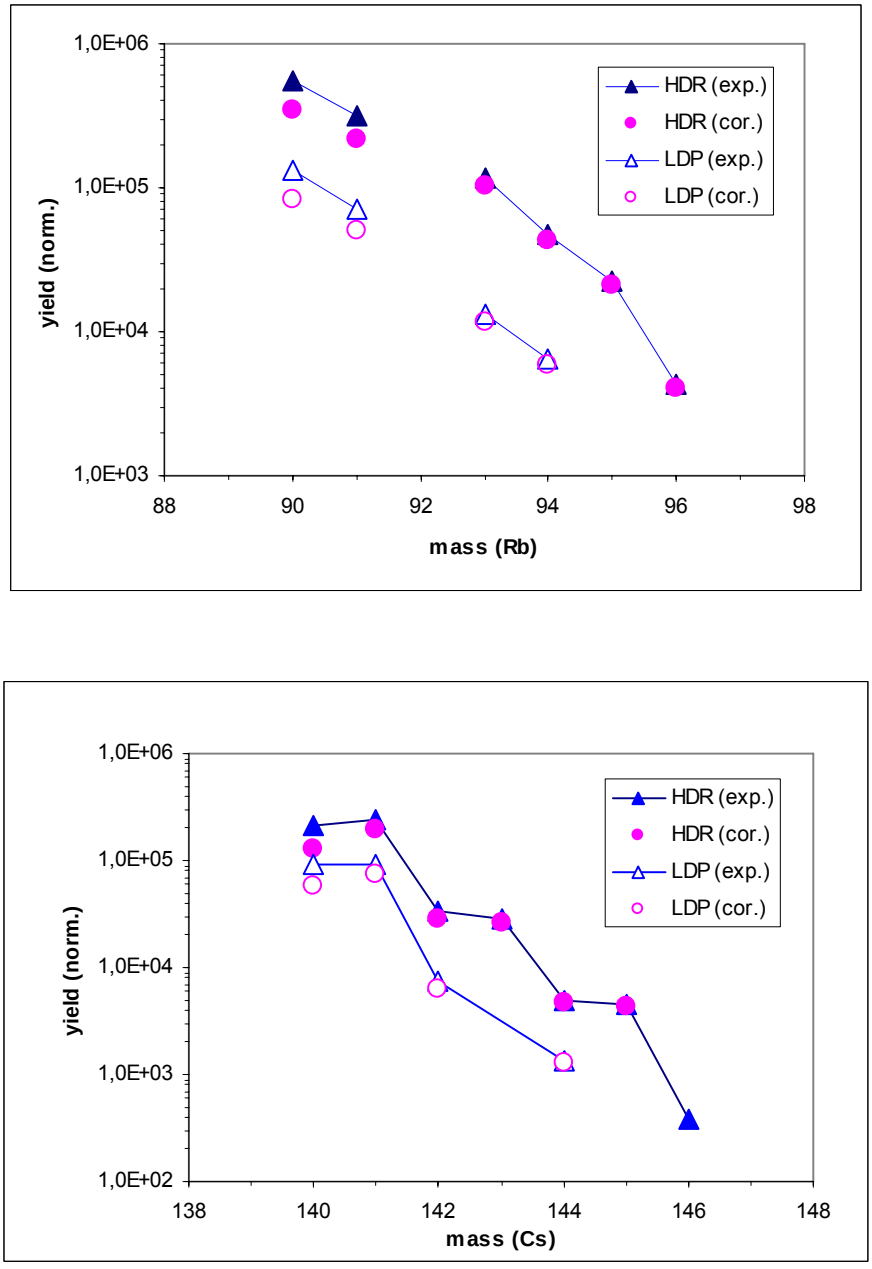

Fig. 18: Normalized yields for HDR (rod) and LDP (powder) targets at 2000°C. Subtraction of the contribution of decay in the target lowers the observed yields (triangles) to the calculated values (circles). An effect is visible only for long-lived isotopes close to stability which are near the top of cross-sections versus A. The points merge within their error bars at ^{93}Rb and ^{143}Cs and beyond.

The normalized yields at a temperature of 2000°C from the LDP target are 5-6 times lower than those from the HDR target. This fact can be explained by a high rate of out-gassing of impurities (Na, K) from the LDP target material during the first day of the on-line experiment. The working temperature, when the target is exposed at the beam, is usually higher than the temperature of the target normalized at the test bench. A high current density of ions of elements with low ionisation potentials decreases considerably the ionisation efficiency of species even with the lowest ionisation potentials such as Rb and Cs. The fact that the release curves of HDR and LDP are similar in spite of different efficiencies indeed indicates that the origin of the loss of yield is due to a change in ionisation efficiency. This effect has been confirmed in the following on-line target tests and in off-line ionisation efficiency measurements.

It is possible to match experimental and calculated yields considering efficiency factors. Ionisation efficiency is a scaling factor common to an isotopic series whereas release efficiency is a factor variable with the half-life of the isotope of interest. Figure 19 compares Rb and Cs isotope yields for the HDR and LDP targets at a temperature of 2160°C. The calculated values are based on the experimental cross-sections of Ref. [14] without considering contributions of parents. They also need to insert ionisation efficiencies, which have been found to be ε_i = 16% (Rb) and ε_i = 25% (Cs) to reach the proper scaling. These values turn out to be realistic. The experimental values are the observed ones corrected for decay losses by diffusion according to the efficiency formula for spherical grains shown in Ref. [15]. The best fit values of the parameter $T_{1/2}(\text{diff}) = \ln 2/ \mu_0$ are

for HDR (Rb: 200(60) s; Cs: 90(45) s, with $\chi^2 = 1.5$) and
for LDP (Rb: 180(50) s, Cs: 110(30) s , with $\chi^2 = 2.0$).

No appreciable differences could be observed when adding the maximum contribution of the decay of the mother nuclei to the calculated values. Therefore we cannot conclude whether the observation of two components in the release curves of ^{139}Cs originates from decay in the target of ^{139}Xe or not.

We should acknowledge that the diffusion function for spherical grains is an infinite series of terms recursively defined by the parameter μ_0 and is thus different from the empirical one with two free exponential components used to reproduce the release curve Fig. 17. The proper treatment in such a case was unknown to us at the time this work was published [22]. We have mentioned that a factor of 0.44 of T_R can be used to approximate the standard diffusion formula [15] by an exponential. After correcting downwards the above listed diffusion times to mock a pure exponential release function, they come quite close to the shortest components extracted from the release curves.

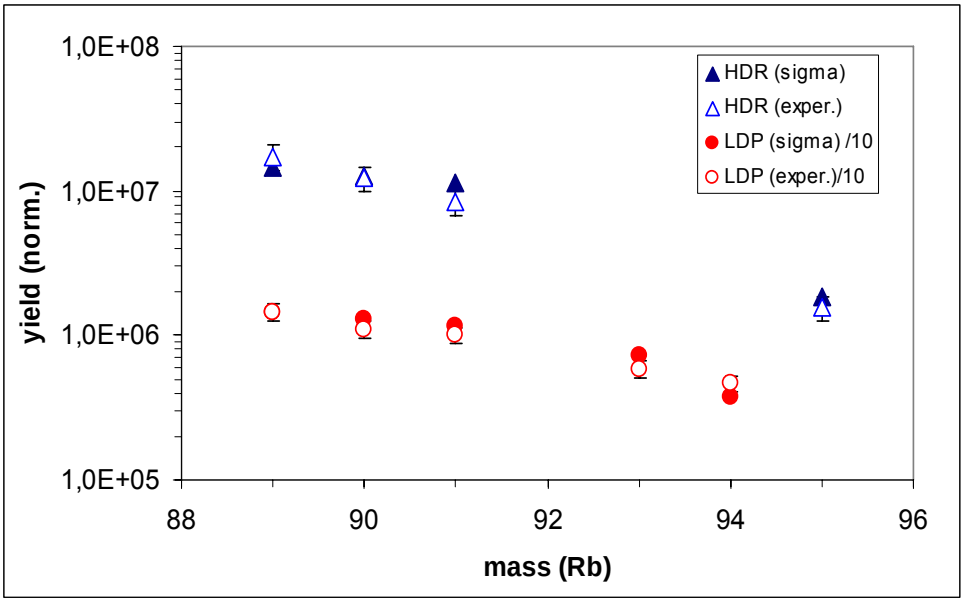

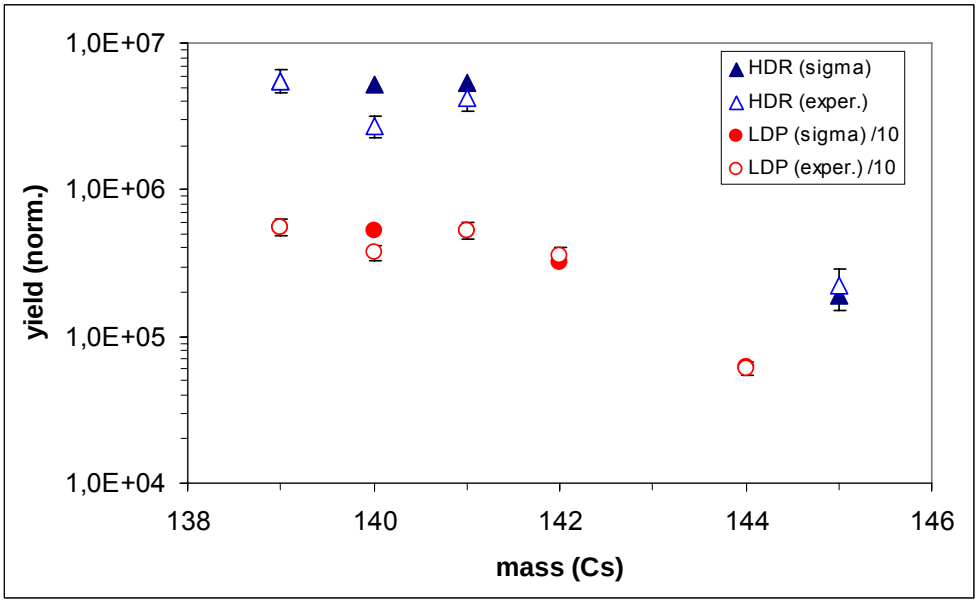

Fig. 19: Matching calculated (full symbols) and experimental yields (open symbols) using a correction for diffusion efficiency with parameters shown in the text. Data are recorded at 2160^{o}C. Yields for LDP have been divided by 10 for better visibility.

2b Enhancement of yields of n-rich isotopes

Here we present two different ways of enhancement of yields of the most neutron-rich isotopes.

a) The result of raising temperature of the HDR target is shown in Fig. 20. Higher temperature increases the Arrhenius diffusion coefficient D, increases the associated diffusion parameter μ_0 as being proportional to D, and, finally increases the diffusion efficiency according to the value of the ratio μ_0/λ (ε_D goes to 1 for very large μ_0/λ). Yields of short-lived isotopes should then increase more than those of long-lived isotopes. As expected, the yield ^{94}Rb ($T_{1/2}$ = 2.7 s) increases faster than the yield of the longer-lived ($T_{1/2}$ = 15.2 m) ^{89}Rb. In contrast, enhancement of the yield increase of ^{145}Cs ($T_{1/2}$ = 0.6 s) relative to ^{139}Cs ($T_{1/2}$ = 9.3 m) is less clear. It is obviously an interesting issue to clarify, as it could reveal differences in diffusion parameters of these elements.

.

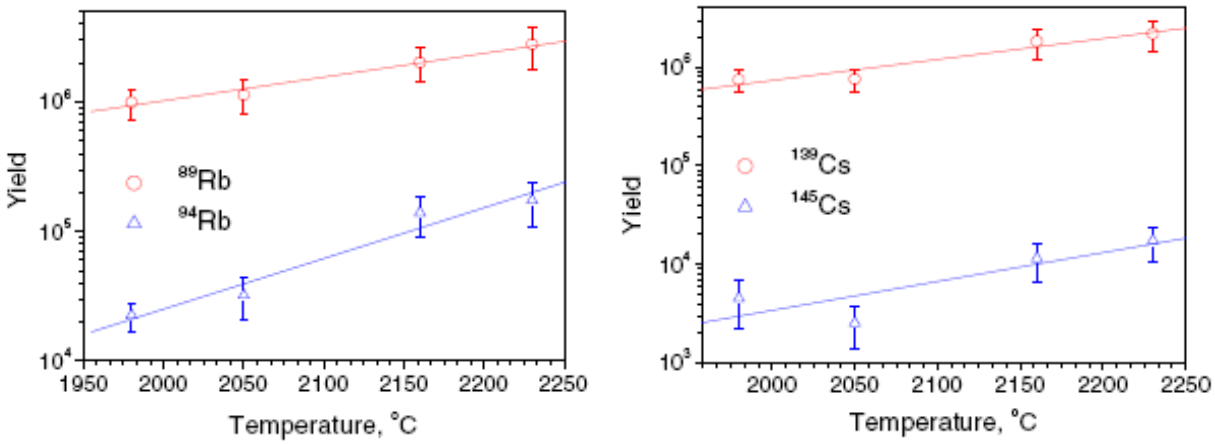

Fig. 20: Enhancement of the normalized yields with higher temperature for two isotope pairs; a long-lived one (red, upper curve) and a very short-lived (blue, lower curve) one, respectively. These yields have been measured with the HDR target. The lines are fits only to indicate the trend.

b) There is a larger chance for fission induced by secondary particles in a heavy target. These particles are mostly neutrons produced via (p,xn) spallation or accompanying fission. The cross-section for 1 GeV protons in uranium is about 30 barns [24]. The probability for a reaction per projectile is the product n.σ of the number of nuclei per surface unit (n) times the cross-section (σ). For a typical 10 g/cm^2 target, there is a chance of 0.75 to create a secondary neutron per incident proton. The n-induced fission cross-section is of about 1 barn like for p-induced fission. This adds extra cross-section σ(Z, A) with a distribution somewhat shifted towards the most n-rich isotopes. However, note that the shift is possibly less dramatic than displayed on Fig. 15 because these neutrons must be more energetic than those emitted by the Ta converter at 90 degrees.

While the primary reaction rate increases linearly with target thickness, the secondary reaction rate increases with the square of thickness. We therefore expect to see an enhancement of neutron-rich

isotopes with target thickness as long as the presumably longer release times do not increase prohibitively the decay losses. This expectation is indeed fulfilled, as it is shown in Fig. 21 that displays the ratio of yields from HDR and LDP targets y(HDR)/y(LDP) versus the atomic number of isotopes. These ratios have been scaled to be 1 for long-lived isotopes for convenience, since the overall yield for LDP was low due to insufficient out-gassing before the measurement, as it was mentioned previously. There is a clear indication of a larger enhancement of the yields of Rb isotopes far away from stability with the high density target. For Cs isotopes the effect could vanish in the limits of experimental errors but seems to be real anyway.

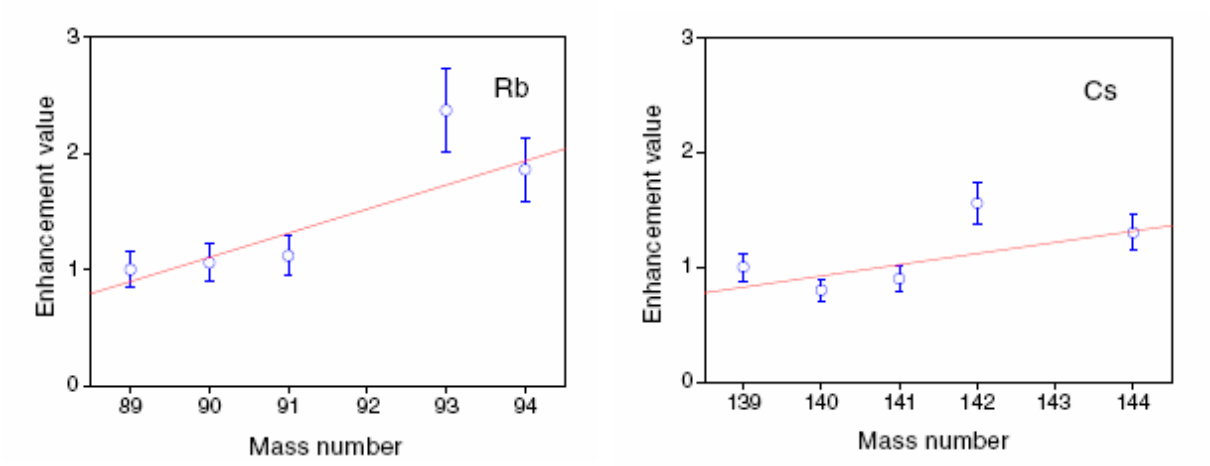

Fig. 21: Enhancement of the normalised yields of very neutron-rich Rb and Cs isotopes with target thickness is evidenced by plotting the ratio y(HDR, 8.2 g/cm^2)/y(LDP, 1.9 g/cm^2) versus isotope mass. This is ascribed to the increased rate of secondary reactions induced by neutrons that favour the more n-rich isotopes. Yield ratios are scaled to 1 for ^{89}Rb and ^{139}Cs for mere convenience of representation.

IV.3 Long-lasting uranium carbide target

3a Description and long-term stability

The new generation ISOL facilities demand targets containing a large amount of ^{238}U (up to some kilograms) to produce neutron-rich ion beams of about three order of magnitude more intense than the ones available nowadays. A serious problem arises with the replacement of the highly activated target assembly after its possible breakdown. Therefore, the new target units must be able to work for several months without failures while retaining their performance. It becomes important to know whether targets shall be able to keep their working characteristics (yields and release efficiency for produced species) during a long period of standing at high temperature.

The Long-Lasting-Target (LLT*)* unit constructively is similar to the one represented in Fig. 3, but differs from those used in our previous experiments by the increased wall thickness of target container (from 0.25 mm to now 0.50 mm). Previous experiments showed that the main reason why the uranium carbide targets break is the carbonization of the tungsten container due to the high heating temperature. In that process the resistance of the hot parts of the target container increases, thus leading to fast

destruction of the latter. The modified target construction ensures that the two cylindrical containers, respectively made of tungsten and graphite, are not in contact. Chemical reactions at high temperature are therefore avoided. The target material consists of a HDR (density 11.2 gcm^{-3} , thickness 9.2 gcm^{-2} and 200 μ grain size) like the one used for the tests described in the previous section**.**

One of the main parameters to be controlled during the experiment is the target resistance. Stable and reliable working conditions are indicated by the absence of a change of its resistance due to the heating at high temperatures (small changes of some percent are acceptable). Fig. 22 shows the target resistance measured during the off-line heating period. The resistance increase during the 2400 hours total time of heating at 2030°C (stabilized within +/-30°C) did not exceed 2%, thus suggesting that under these conditions the target could operate without any damage even for much longer time.

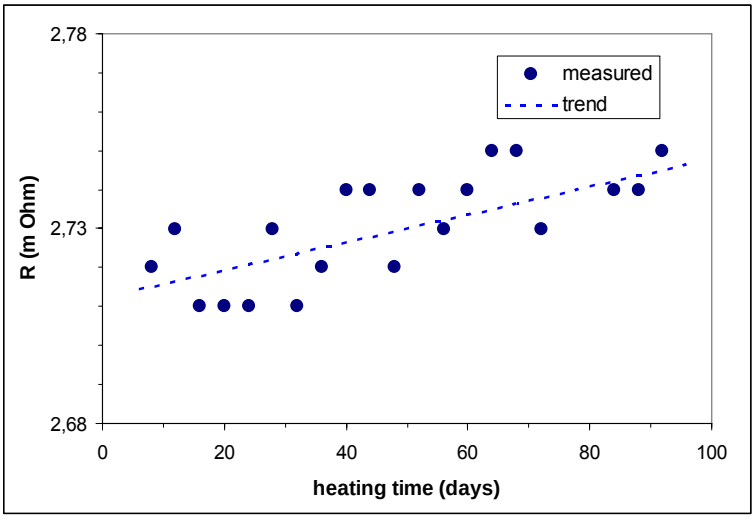

Fig. 22: Variation of target resistance during the long-term off-line heating test.

3b Yields and release times before and after long-term heating

Two series of on-line measurements separated by an interval of 3 months, during which the target has been continuously heated off-line at 2030°C, were performed. Yields of neutron-rich isotopes of Rb, Cs and In measured before [25] and after the heating test are reported in Fig. 23. The temperature was 2050 °C for all yield measurements. The yields, also those of short-lived isotopes, remained very stable. The heating did not introduce any significant change in the release properties of the target material. The grain size of this HDR target was 200 μ. It is still open whether this excellent result is valid also for targets with smaller grains and it calls for a comparable test to check whether small grains would not agglomerate to bigger clusters, making diffusion slower.

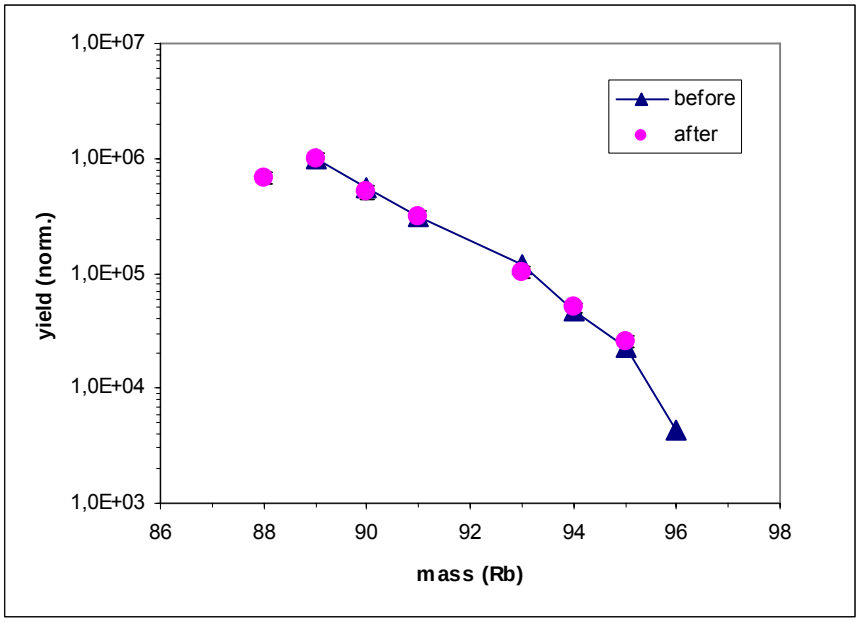

Fig. 23a: Normalized yields of rubidium isotopes measured at target temperature of 2050°C before (triangles) and after (circles) three months of continuous heating at 2030°C. The target is a HDR with 200 μ grain size. There is no significant loss of efficiency.

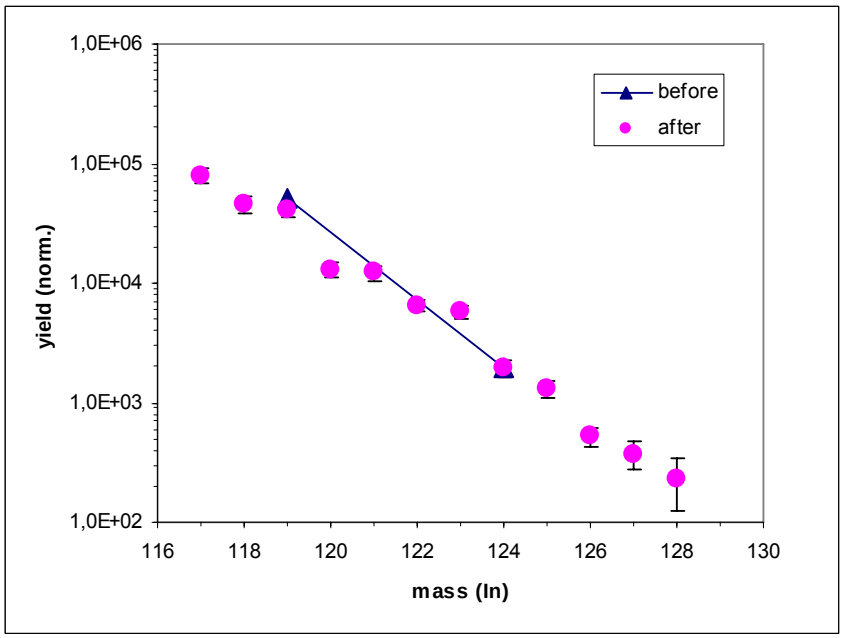

Fig. 23b: as Fig. 23a, now for indium isotopes.

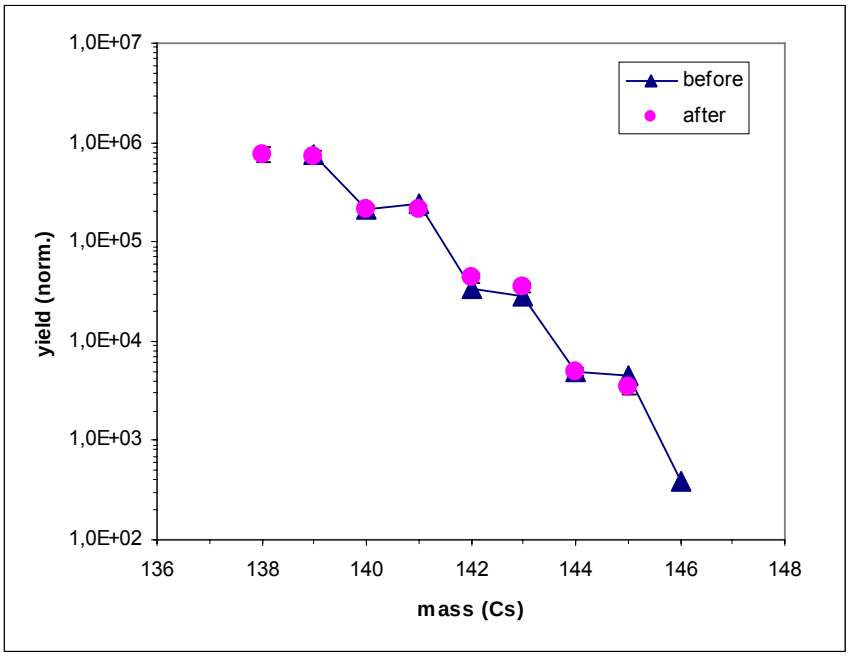

Fig. 23c: as Fig. 23a, now for caesium isotopes.

Release curves were measured for ^{139}Cs ($T_{1/2}$ = 9.27 min) at the same target temperature of 2050°C. For better comparison the curves shown in Fig. 24 have been normalised at time 0, i.e. when the proton beam is switched off. Here RT (Reference Target) refers to the measurements performed with the target at the beginning of the heating [25] and LLT refers to the measurements performed after three months of heating. In agreement with the evolution of yields shown in Fig. 23 there is hardly any difference in the release curves, except for a faint indication that the short component is stronger before the heating test. The curves, indeed, show once more a fast (τ_f) and a slow (τ_s) component, both defined with errors up to 30%, namely (RT; 40 s, 1570 s) and (LLT; 45 s, 1000 s) . The fraction of atoms (i.e. the product amplitude times τ) escaping from the target with τ_f and τ_s are 3-12% and 89-97%, respectively. Release efficiency and yield are thus mainly defined by the slow component.

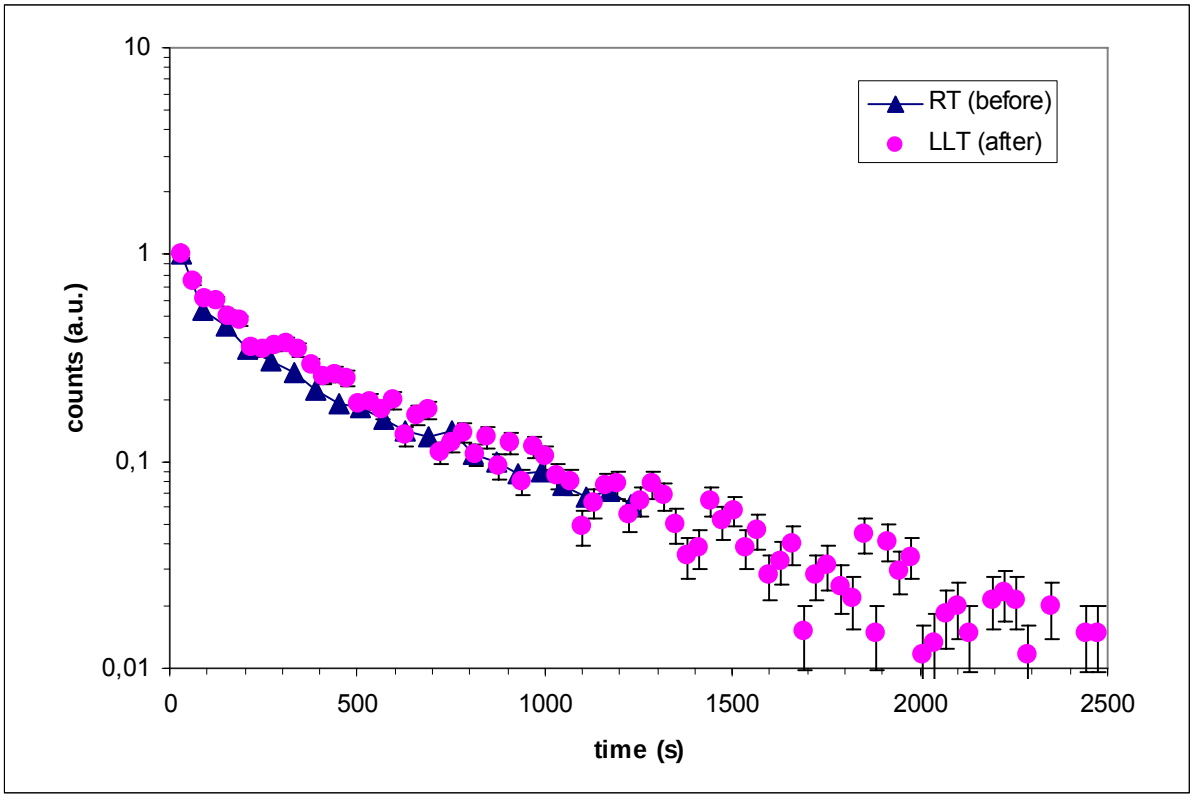

Fig. 24: Release curves for ^{139}Cs ($T_{1/2}$ = 9.27 m) before (RT) and after (LLT) three-months of continuous off-line heating of the HDR target at 2000°C. The target temperature during both measurements was 2050°C.

IV.4 Comparison of target materials using the Ionizing Target

Before extending the R&D program on uranium-carbide targets to a geometry suitable for applications at SPIRAL-II and SPES that allows to house a considerable amount of fissile material (of the order of a few kg) it was decided to evaluate future experiments with respect to a standard target geometry, called ionizing target [26]. This target was to be used to test and compare different kinds of uranium carbides. Ionisation (surface ionisation) takes place inside the container, as shown in Fig. 25. Note that, unlike in Figs. 2 and 3, the proton beam does not enter axially but is perpendicular to the container axis. As its cross-section is comparable with the diameter of the target, the usable thickness is now less than in the former geometry. Since surface ionisation is quite selective for alkalis, only Rb and Cs isotopes have been measured. There is hardly any interference of ions of other elements with higher ionisation potentials.

.

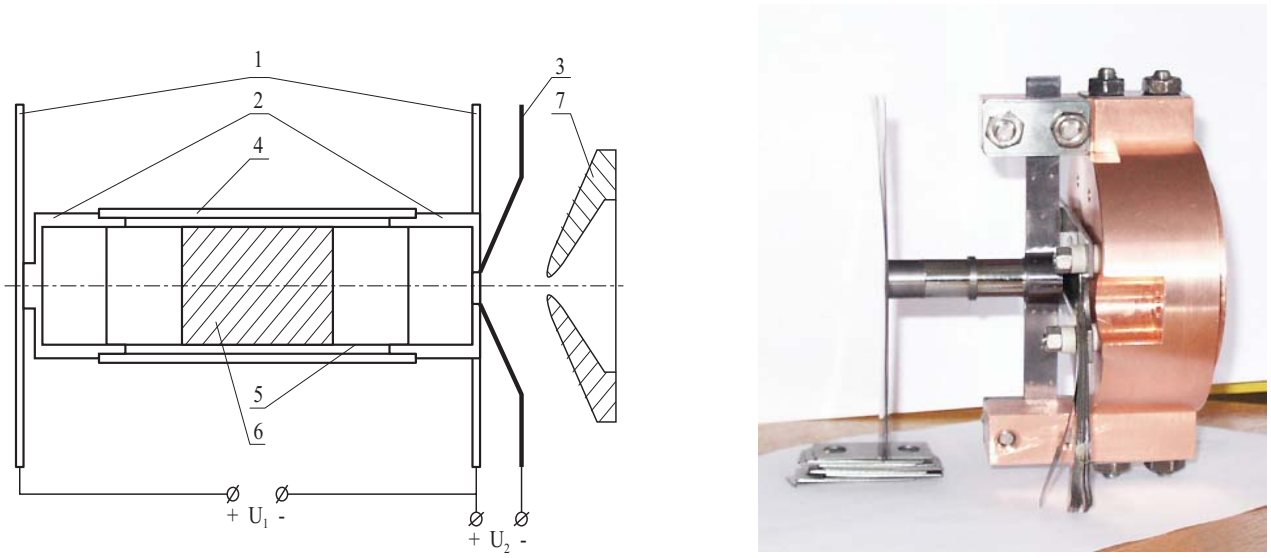

Fig. 25: Schematic drawing (left-hand side) and a picture (right-hand-side) of the reference target assembly. 1) heating conductors, 2) tantalum plugs, 3) electrode, 4) tungsten container, 5) graphite container, 6) uranium-carbide target, 7) extraction electrode. The proton beam now enters at right angle to the target cylinder axis.

The three kinds of uranium carbide material shown in Fig. 4 were tested, in the same experimental conditions. The main parameters of the tested target material are again listed below.

High Density Rod (HDR): uranium density = 11.2 g/cm^3, thickness = 6.7 g/cm^2, length = 6 mm, diameter = 11.35 mm, weight = 6.8 g, grain size = 200 μm.

Low Density Target (LDT): uranium density = *2*.32 g/cm^3, thickness = 2.8 g/cm^2, length = 12 mm, diameter = 11 mm, weight = 2.65 g, 8 pellets each of (1.2-1.6) mm thickness, grain size = 25-35 μm.

High Density Pellets (HDP): uranium density = 12.0 g/cm^3, thickness = 6.3 g/cm^2, length = 5.25 mm, diameter = 11.2 mm, weight = 6.2 g, 3 pellets each of (1.6-1.9) mm thickness, grain size = 20 μm.

The HDR material is the one used for investigating the effect of target thickness and long-term stability previously presented in this report.

The LDT material is similar to the one used at CERN-ISOLDE and at PARRNe at IPN-Orsay. For our tests it has been prepared at Gatchina by the Orsay and Gatchina groups according to the same procedure as used at ISOLDE and PARRNe. For this reason, it is especially instructive to compare our results with those reported by the ISOLDE group, because both use the same beam (1 GeV protons). A comparison with a run at PARRNe will also be shown. The pellets are shown in Fig. 26.

Our HDR and LD targets were operated in the temperatures range of 1900 – 2250°C.

The HDP target material was delivered in 2006. We present the promising results of the first tests.

Fig. 26: Low Density Target (pellets) fabricated with the technology and materials employed at PARRNe at IPN-Orsay.

We present yields versus mass number and release efficiencies as function of the isotope lifetime. The procedure to derive experimental release efficiencies has been kept simple by using the experimental cross-sections [14] instead of effective cross-sections including decay in the target. Yet, it was shown in the previous section that this contribution is not dramatically changing the effective yields for alkalis. We neither have considered the contribution of secondary neutrons. The evolutions with A of the isotope productions through fission by protons and secondary neutrons are probably not dramatically different. However, production of the most neutron-rich isotopes should be enhanced, making the efficiency to appear to be higher for short-lived isotopes. Therefore, actual release times could be longer than the currently extracted ones, especially for the thickest targets.

The conventional formulae for diffusion from spherical grains and effusion [15] involve a parameter, μ_0 for diffusion or ν for effusion. We note that considering that both processes are contributing to the delayed release requires fits with both parameters μ_0 and ν. Since they are strongly correlated, the result is quite undetermined. We have therefore only examined the limits with a sole process contributing. Even so, the conclusions are not definite. The inserts of the figures show χ^2 versus T_R for the two assumptions. The minimum value is used to show the quality of the fit, i.e. to infer which process is the most probable, while χ^2 increase and curvature are used to evaluate the errors on T_R. Let us remind that for diffusion half of the ions if they are stable have left the target at 0.44 T_R ($T_R = \ln 2/ \mu_0$), while this factor is 1 for effusion given by a single exponential ($T_R = \ln 2/ \nu$). This explains why fitted T_R (D) values are larger than those for effusion. Diffusion is more 'friendly' than effusion owing to the sum of k-terms with components in T_R/k^2. It was therefore our worry when building a target of 91 g/cm^2 that the larger dimension would make effusion prohibitively too slow. So far we know from tests carried out in the second half of 2006, this did not happen.

4a High-density rod

The normalized yields (to 1 g/cm^2 uranium and 0.1 μA beam) of Rb and Cs isotopes from the HDR target are displayed in Fig. 27. They increase by about a factor of 2 when the temperature is raised from 1900°C to 2100°C. We note that a similar increase has been observed for a powder made by smashing

a piece of this HDR material, however, when raising the temperature from 2100°C to 2300°C.

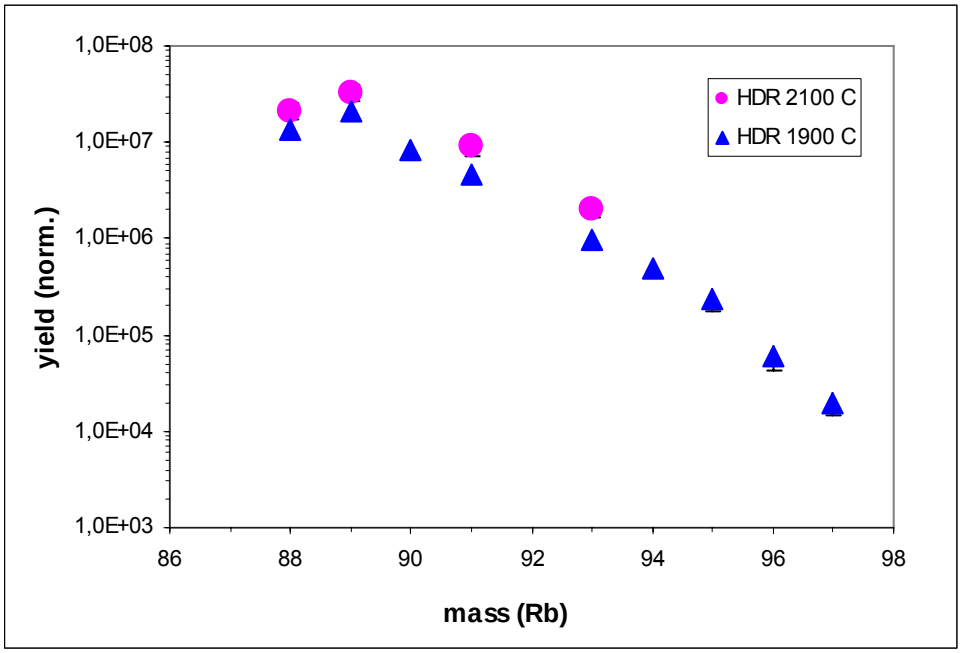

Fig. 27a: Normalized yields of Rb isotopes released from the HDR Ionizing-target. Yields for ^{92}Rb have not been measured because of the wrong branchings of γ-rays listed in the literature, later corrected by our measurement [17]. There is no sign yet of extra enhancement with temperature for the shortest-lived ^{93}Rb ($T_{1/2}$ = 5.8 s) measured, but the expected global increase is clearly seen.

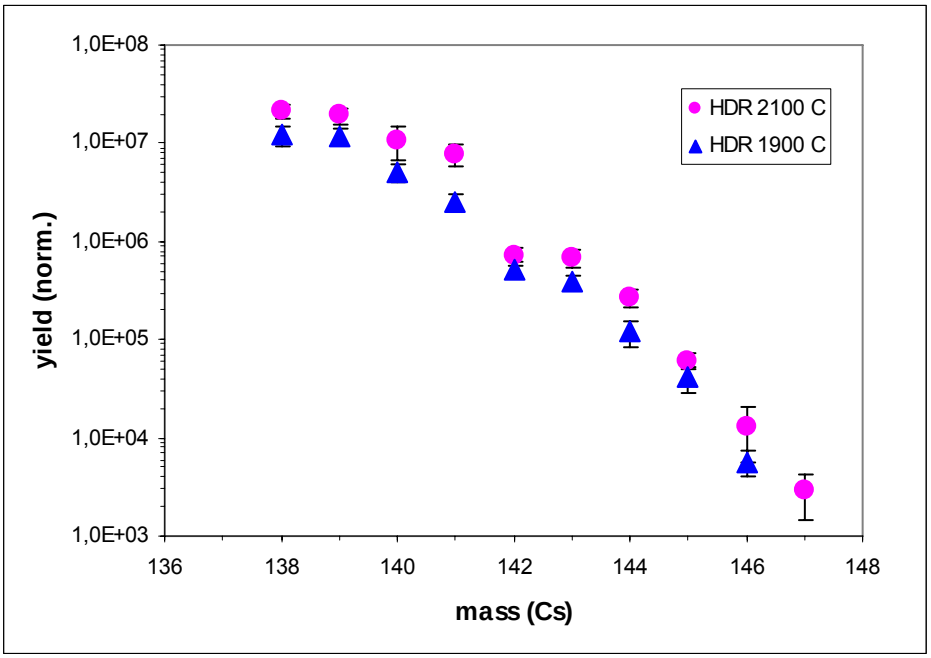

Fig. 27b: Normalized yields of Cs isotopes released from the HDR Ionizing-target. The most neutron-rich isotopes have been measured by β-counting, which is possibly the reason why the odd-even staggering observed in older pictures is absent.

The release efficiencies are shown in Fig. 28. The fits are made with two parameters: a) a free scale parameter ε(Z) representing the efficiency for stable isotopes (the release efficiency is then 1 by definition if $\lambda = 0$) and b) the parameter characteristic for the process ($\ln 2/\mu_0$ or $\ln 2/v$). For easier comparison all experimental and fitted values are divided by ε(Z) before being plotted. As can be seen from the fitted curves and from the variation of χ^2 versus release parameter (in the inserts) the quality of the fits is very similar for pure diffusion or pure effusion. This situation should last as long as we are not able to measure the very short-lived isotopes on the far right of the pictures (see Fig. 8). At the time this report is being completed the progress in the analysis of β-spectra have allowed to extend the yield measurements farther away from stability. The new yields indeed are already included in Fig. 27, but not in the release efficiency plots, Fig. 28. The presently available data give a hint that release tends to become faster with increasing temperature, in agreement with the expectations and the observed enhancement of yields of the shortest-lived isotopes discussed previously, see Fig. 20. The effect is visible in the Cs plots that span the widest temperature range (1900- 2250^{o}C).

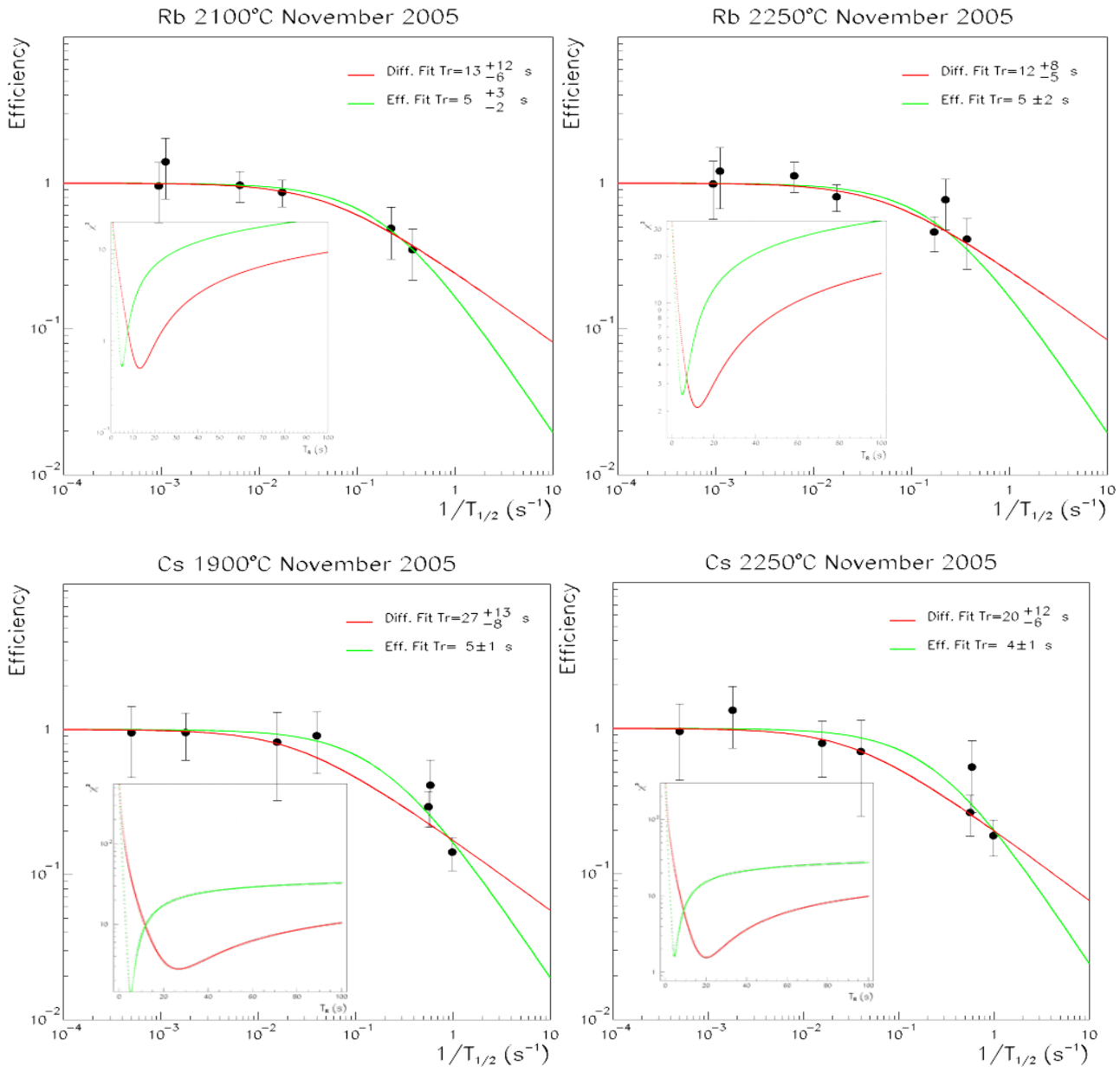

Fig. 28: Release efficiencies of rubidium and caesium for the HDR-IT. Diffusion (red) and effusion (green) mechanisms are considered separately. The quality of fits does not favour one or the other process as responsible for the delay.

4b Low-density PARRNe-like target

For comparison of high and low-density targets, measurements have been carried out with the same target geometry, under the same experimental conditions, using the LDT material. A rather small increase of yields with the temperature is observed, see Fig. 29. Especially the yields of Rb isotopes depend little on temperature, at least above 1900°C, meaning the efficiency is near to its maximum.

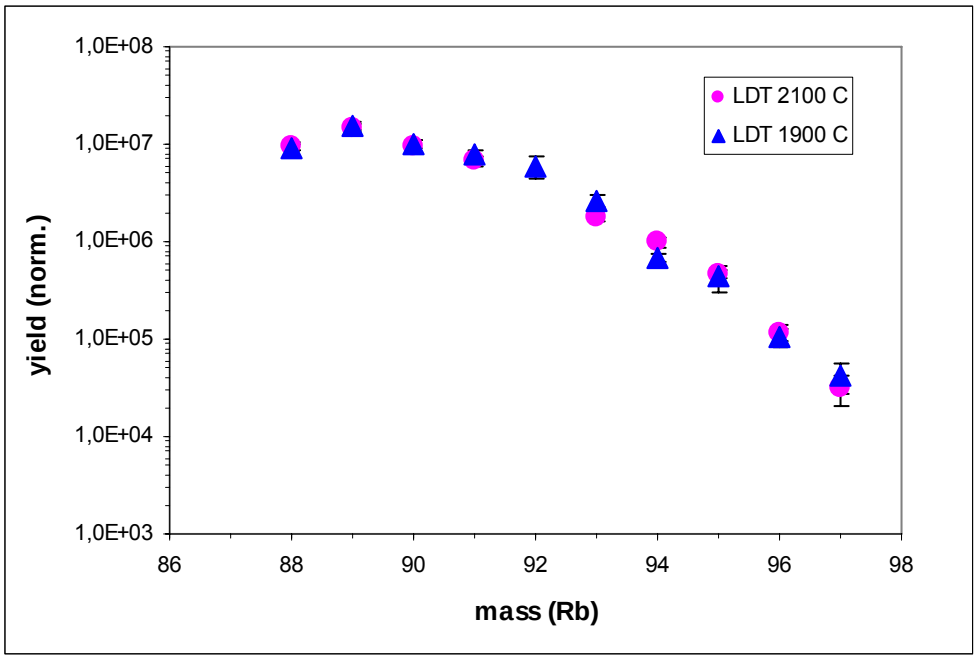

Fig. 29a: Normalized yields of Rb isotopes released from the LDT (PARRNe-like) Ionizing target. In contrast to the HDR target (Fig. 27), raising the temperature of LDT did not further improve the yields.

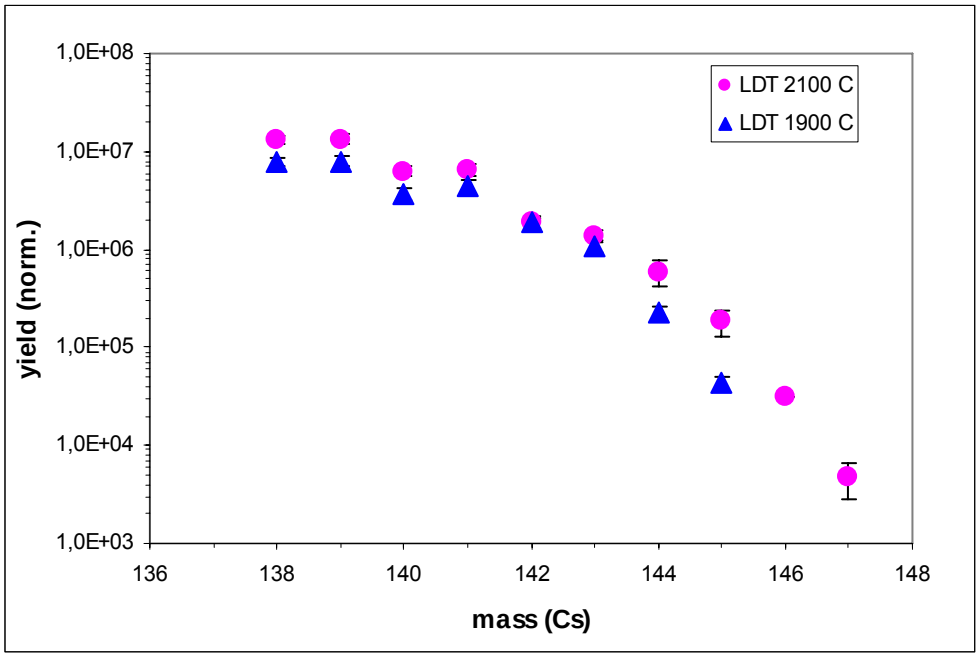

Fig. 29b: Normalized yields of Cs isotopes released from the LDT (PARRNe-like) Ionizing target. The global effect of temperature is here stronger than for rubidium and some enhancement of the shortest-lived isotopes is visible.

The release efficiency is represented in Fig. 30. The extracted release times of LDT are clearly shorter than those obtained for the HDR target. In addition, their dependence on the target temperature is weak, if any. This is consistent with the fact that the yields of the shortest-lived isotopes do not increase significantly more than those of the long-lived ones with temperature (indeed there is hardly any effect for Rb but some for Cs anyway). We conclude that the LDT target works near its best performance under the present test conditions.

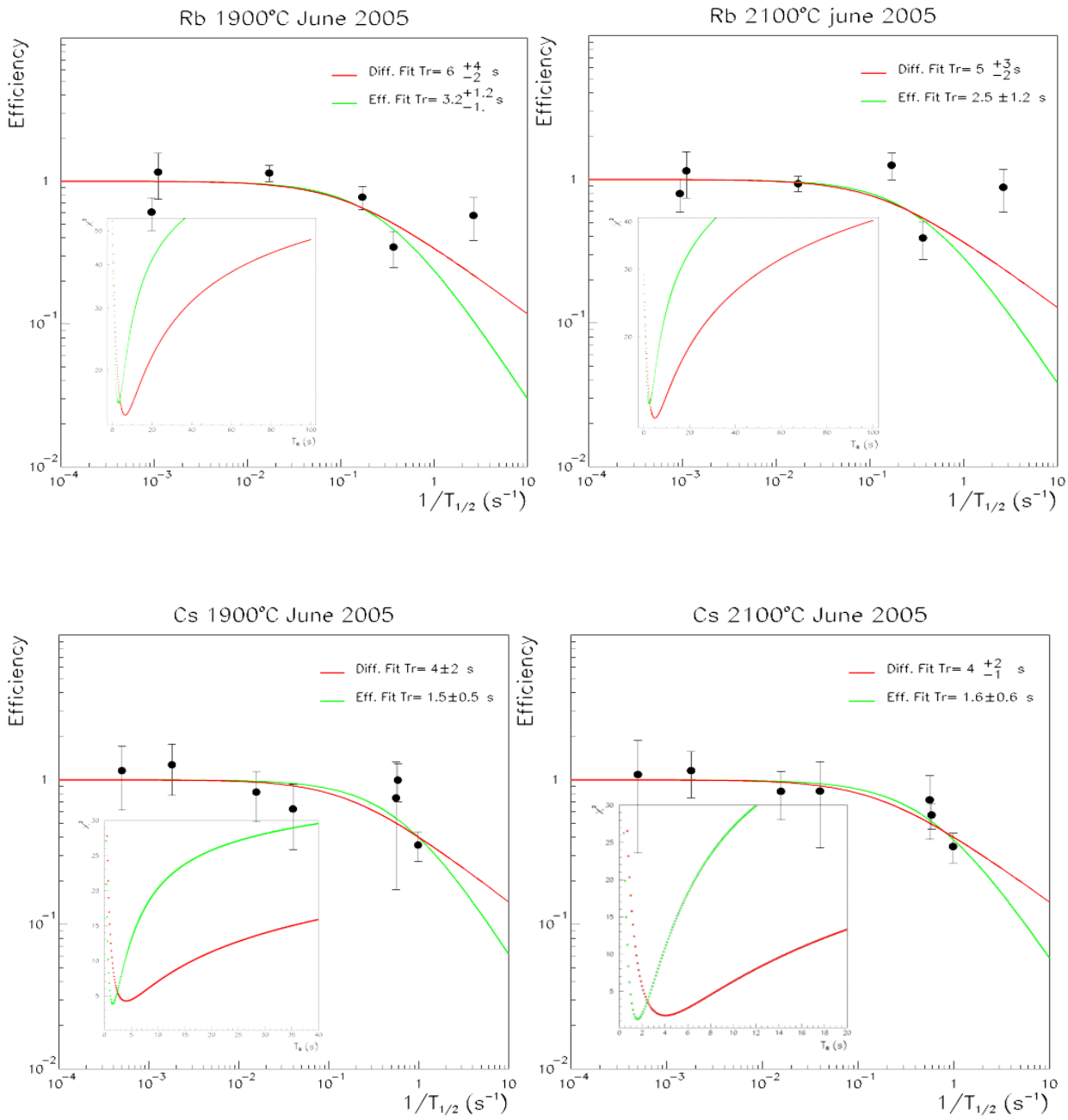

Fig. 30: Release efficiencies of rubidium and caesium for the LDT (PARNNe-like)-IT. Diffusion (red) and effusion (green) mechanisms are considered separately. As for HDR, the quality of fits does not favour one or the other process, but the characteristic times are shorter.

4c Comparison HDR/LDT

The absolute yields of Rb and Cs isotopes with the HDR and low density PARRNe-IRIS (LDT) targets can be compared (however, still for the same current of 0.1 μA) by rescaling the normalized yields, shown in Figs. 27 and 29, according to the actual target thickness. Owing to its higher density the HDR target (6.7 g/cm^2) is 2.4 times thicker than the LDT (2.8 g/cm^2). For long-lived nuclei there is an improvement of efficiency, or in other words, yields scale up faster than target thickness. We take examples measured at target temperature of 2100°C. The (HDR/LDT) yield ratios are 5.3(10) for ^{88}Rb ($T_{1/2}$ = 17.7 m) and 3.4(7) for ^{139}Cs ($T_{1/2}$ = 33.4 m). The origin of this overproduction is to be searched in fission induced by secondary neutrons. However, for the short-lived isotopes the excess is smaller, indicating a loss of efficiency of the HDR target due to slower release of the nucleus of interest. We have ratios of 3.6(8) for ^{93}Rb ($T_{1/2}$ = 5.8 s) and 1.1 for ^{144}Cs ($T_{1/2}$ = 1.0 s). Fig. 31 displays these ratios for Cs isotopes. We therefore see a clear and regular evolution of the relative efficiency with half-life, which would make HDR less competitive for the very exotic nuclei, but owing to its mass the HDR target still has the highest absolute yields for all the measured isotopes with half-lives longer than one second.

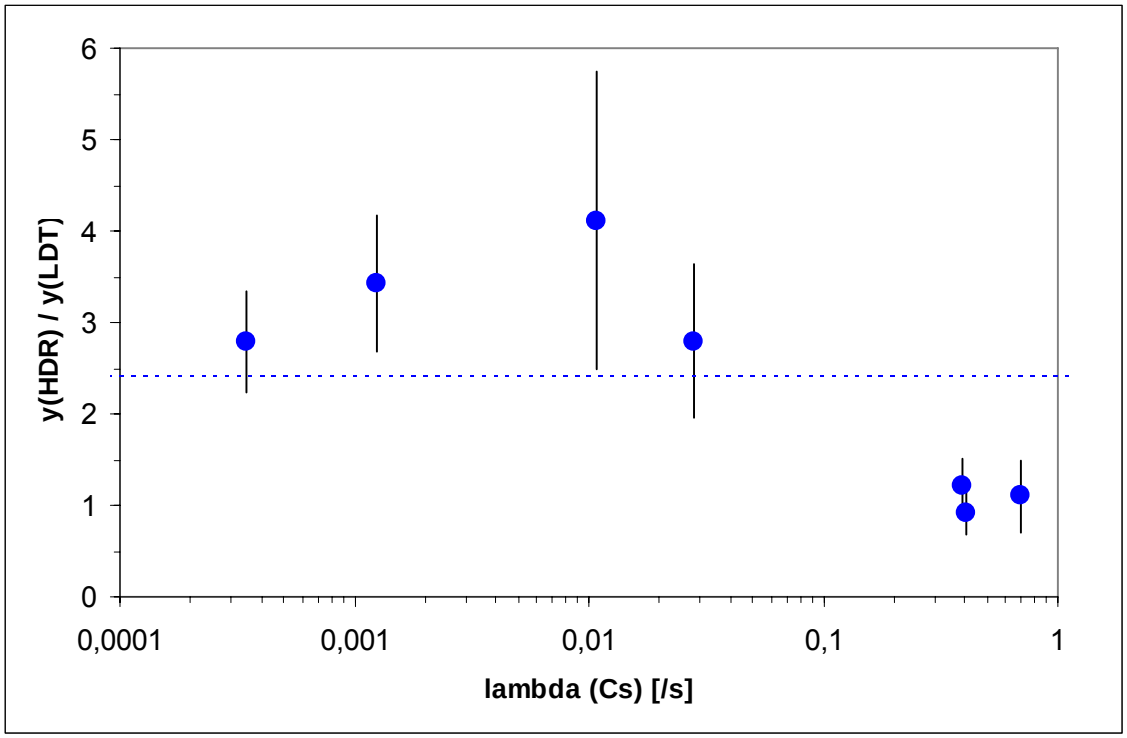

Fig. 31: Ratios of absolute yields of HDR and LDT for Cs isotopes, but scaled for the same proton current, both measured at 2100^{O}C. The yield ratio is higher than the thickness ratio of 2.4 (dash line) for half-lives longer than 100 seconds, but drops for half-lives shorter than 10 s. Yet, the HDR provides the highest yields for all shown isotopes.

Table 2 gives an overview of the release times extracted from the analysis of the efficiency curves for the LDT and HDR targets, shown in Figs. 28 and 30.

.

Table 2: Summary of releases times derived from efficiency curves versus half-life for the LDT (PARRNe-like prepared at Gatchina) and HDR targets.

Rb	Orsay Target (LDT)		Gatchina Target (HDR)	
	Tr Diffusion (s)	Tr Effusion (s)	Tr Diffusion (s)	Tr Effusion (s)
1900°C	6 (+4,-2)	3.2 (+1.2, -1.)	13 (+12, -6)	5 (+3,-2)
2000°C	-	-	-	-
2100°C	5 (+3,-2)	2.5 (±1.2)	-	-
2250°C	-	-	12 (+8,-5)	5 (± 2)

Cs	Orsay Target (LDT)		Gatchina Target (HDR)	
	Tr Diffusion (s)	Tr Effusion (s)	Tr Diffusion (s)	Tr Effusion (s)
1900°C	4 (±2)	1.5 (± 0.5)	27 (+13, -8)	5 (± 1)
2000°C	2 (±1)	1.2 (+0.1, -0.7)	-	-
2100°C	4 (+2,-1)	1.6 (±0.6)	28 (+15, -9)	5 (+2,-1)
2250°C	-	-	20 (+12, -6)	4 (± 1)

The obvious reason for the slower release time of HDR is its larger grain size of 200 microns, which is 10 times more than the 20 microns of the PARRNe-like low density pill UC_x grains. This parameter surely plays a part in the actual release time. However, if standard diffusion would apply, and effusion could be neglected, the release times in LDT would have been 100 times faster according to the R^2 (R being the grain radius) proportionality of μ_0. This factor is rather about 5 than 100. It shows that it is an oversimplification to assume standard diffusion theory for our targets. We also have to remember that the efficiency has been calculated with the cross-sections from Ref. [14], without corrections for decay in the target and contribution of fission induced by secondary neutrons. The latter probably favours production of the shortest-lived nuclei and thus makes the deduced release times, especially in HDR, to look shorter than they actually are.

The LDT target was prepared at Gatchina from the material used at IPN-Orsay at the PARRNe facility and with the same procedure originally developed at CERN-ISOLDE. Therefore, yields reported by ISOLDE are a reference for the performance of our LDT. Normalized yields of our LDT and those measured by the ISOLDE group are comparable. It confirms that in the process of the preparation of

ISOLDE type UC_x target at IRIS no noticeable changes to the target material properties were introduced and the conditions of the target maintenance at IRIS were similar to those at ISOLDE. Normalized yields of HDR, LDT and ISOLDE targets [28] are shown in Fig. 32. It is to be noted that an even better efficiency for very neutron-rich isotopes of Cs and Rb has been obtained at CERN-ISOLDE with a "cloth" uranium-carbide target. That target was used in experiments at the 600 MeV Synchrocyclotron but no longer in the experiments at the 1 GeV PS-Booster. Nowadays ISOLDE uses a "standard" 50 g/cm^2 UCx target prepared in the form of pellets from a powder with grains of 20 μ.

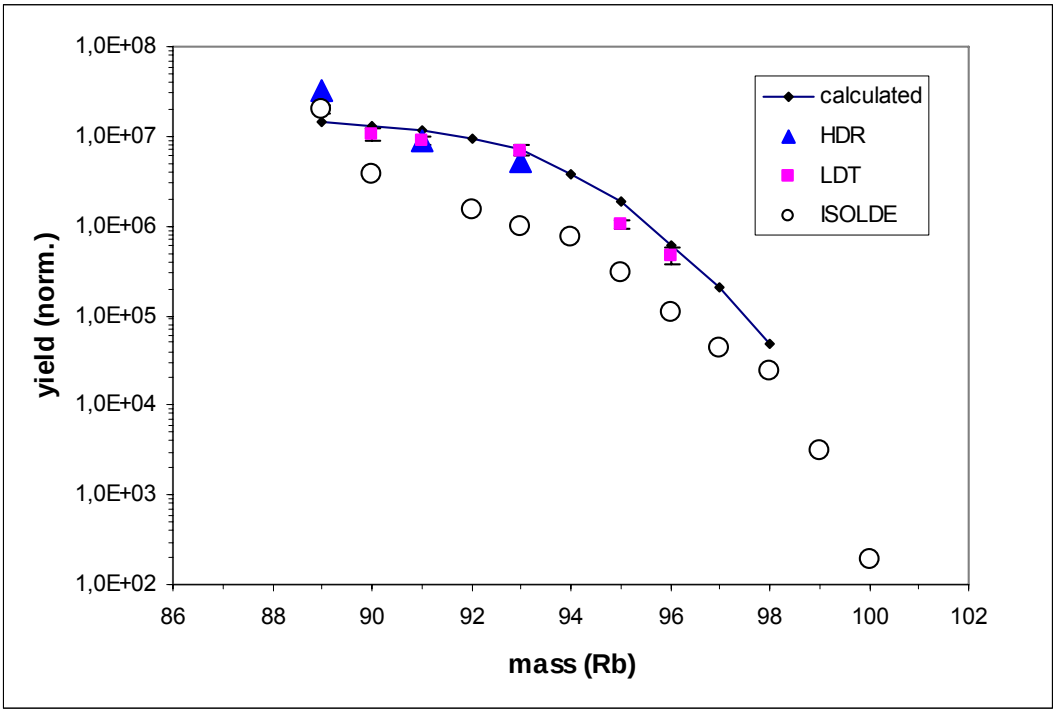

Fig. 32: Normalized production yields of rubidium isotopes from the HDR (December 2004, triangles), the PARRNe-like at IRIS LDT (June 2005, squares) both at 2100°C and the reference CERN-ISOLDE data [28] taken at about T = 2000°C (circles). The line with diamonds shows the calculated in-target production rates based only on cross-sections for p-induced fission [14], without considering fission by secondary neutrons nor decay of the parents in the target.

A puzzling result is the high yield for ^{89}Rb (both for the HDR and ISOLDE) which turns out to be higher than the calculated production rate in the target. Several effects can be invoked. Firstly, in a typical 10 g/cm^2 thick target the neutron multiplication factor is 0.75 as we mentioned previously. In other words, the effective cross-section, i.e. the sum of σ(p,f) and σ(n,f), is estimated to be 1.75 times σ(p,f). Secondly, part of the cumulated cross-section for the parent ^{89}Kr (8.1 mb) ought to be added due to decay in the target to σ(^{89}Rb) = 9.2 mb [14], but this contribution should be weak because the Kr half-life of 3.2 m is long against the presumed release times of noble gases. Yet, it still looks that the experimental points remain high.

A comparison of HDR and LDT yields with the original PARRNe data measured at Orsay is shown in Fig. 33 for the isotopes of Cs. As an exception to the rule, the yields are now presented in ions per second. The scaling of HDR and LDT yields is to a typical beam current of 50 nA and the values reflect the actual target thickness. PARRNe values are the ones in the experimental conditions [29]. They correspond to the irradiation of natural carbon with a 1 μA current of 26 MeV deuterons to generate neutrons which subsequently induce fissions in a LDT with 50 g/cm^2 of uranium. It is a comparison of fission induced by 1 GeV protons with fission induced by neutrons of 10 MeV average energy. It is therefore quite surprising that the curves are so closely parallel. Tentatively, in the slower HDR target the larger loss of short-lived isotopes could be compensated by the more flat in-target production**.** After taking into account the neutron conversion factor, that is estimated to be about n/p = 10^{-3} from early works conducted by IPN-Orsay and GANIL [30], the PARRNe yields seem to be anyway a bit low. It is worth noting that the main objective of that Cs-PARRNe experiment was a release-time measurement and the determination of the relative evolution of neutron-rich Cs isotopic chain. The Cs yields were not measured using the usual dedicated set-up. It resulted in improper beam guiding and focusing at the collection point. Thus the yields reported here can be much underestimated with respect to the best ones and the comparison with the IRIS values is only indicative.

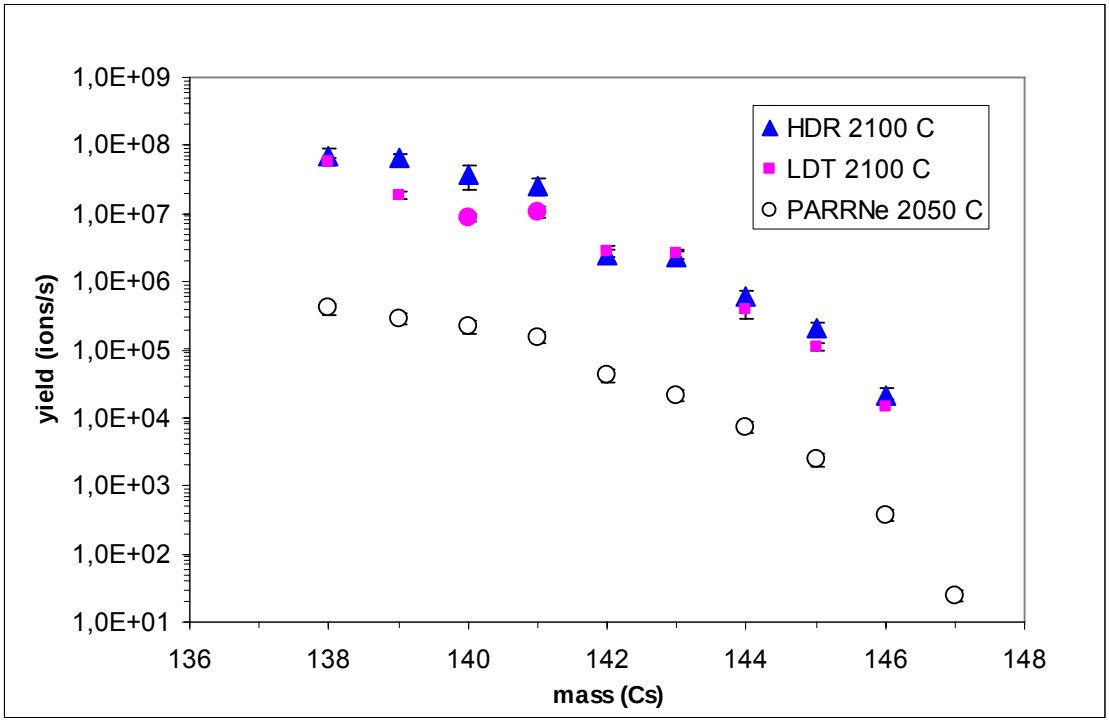

Fig. 33: Yields in ions/s produced by the ionizing target with HDR (6.7 g/cm^2), LDT (PARRNE-like) at IRIS (2.8 g/cm^2) both with 1 GeV protons of 50 nA and those reported at PARRNE-Orsay [29] in an experiment using intermediate-energy neutron-induced fission.

4d High-density pellets (HDP) of small grain size

A clear conclusion of the HDR/LDT comparison is that it is essential to use a high-density material with grain size smaller than the 200 μ of the original HDR target. A new kind of uranium carbide has therefore been tested recently with the same target geometry and under the same experimental conditions. It is the High Density Pellets (HDP) target (grain size 20 μ, density 12 g/cm^3 and pellet thickness about 2 mm) shown in Fig. 4. The effective thickness is 6.3 g/cm^2 shared on 3 pellets. The normalised yields of Cs isotopes are shown in Fig. 34. They are about 10 times lower than the best results obtained with the HDR reference target. The working temperature of the HDP ionizing target was much lower (1700°C) than the operating temperature of the HDR (2100°C). The reason was the use of a tantalum cavity as inner container for the target material housing instead of the graphite used during previous tests. The danger to melt the inner tantalum container, which was in contact with the very chemically aggressive target material led us to keep the target temperature in the interval (1500-1700) °C. The overall increase of yield from 1500°C to 1700°C was close to an order of magnitude. We therefore hope for better and competitive performance at higher temperature.

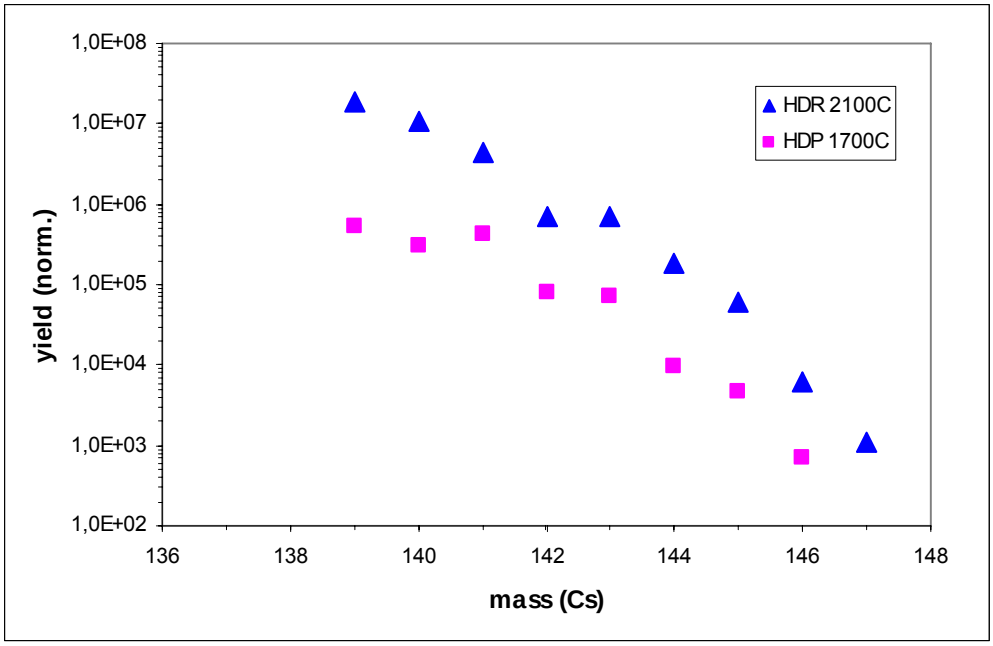

Fig. 34: Normalized yields of Cs isotopes with the new HDP target (squares) compared with best HDR performance (triangles). Note the lower operating temperature of HDP which naturally accounts for the lower yield values.

The very encouraging result was the short release times in spite of the low working temperature. For both Rb and Cs, even at the low temperature of 1700°C, the response of the target is comparable with the one of the LDT (PARRNe-IRIS) low density pill target at its normal temperature of 2100°C. In parallel with the increase of yield when raising T from 1500 to 1700°C, we definitely see a reduction of the release times that is about a factor of 5. The experiment with this target construction should be repeated at higher temperature to definitely confirm that the fast release parameters are reproducible. The ionisation efficiency will be increased by the use of a separate ionizer. The release efficiency of the HDP target in function of the isotope lifetime, for two different target temperatures is presented in Fig. 35. As before for both HDR and LDT, it is not possible to find out which process is responsible for the delay.

Nevertheless, the fast release properties were convenient to demonstrate the effect of in-target decay on experimental release curves by a comparison of the curves for $^{130}Cs^{m}$ and ^{139}Cs [17]. It might be worth to note that the unperturbed release curve for $^{130}Cs^{m}$ was fitted with a convolution of exponentials with T_R = 5.4 s (representing diffusion or effusion) and about 3 s (representing the other process). The flattening of the curve near the origin indeed implies a negative sign for the latter, which is the characteristic result of convoluting the processes. The values of the time constants are somewhat lower than those extracted from the release efficiency in Fig. 35 for the processes taken separately, which is logical. It may be tentatively stated that in the analysis of the release curve, effusion becomes visible as its time constant is now comparable with the diffusion time. It was obviously not so with the slower HDR target with 200 μ grains, having its shortest component of about 1 minute. We finally note that the diffusion process does not involve two exponentials, unlike the data shown for HDR. It is interesting to investigate if this is related to the absence of the inner graphite container.

Finally, the low temperature during this test offered the opportunity to be very selective for ionizing Rb without contamination of Sr. The γ-ray branchings in ^{92}Rb [12] were in fact measured during the first run with this target. We refer to a later section for details.

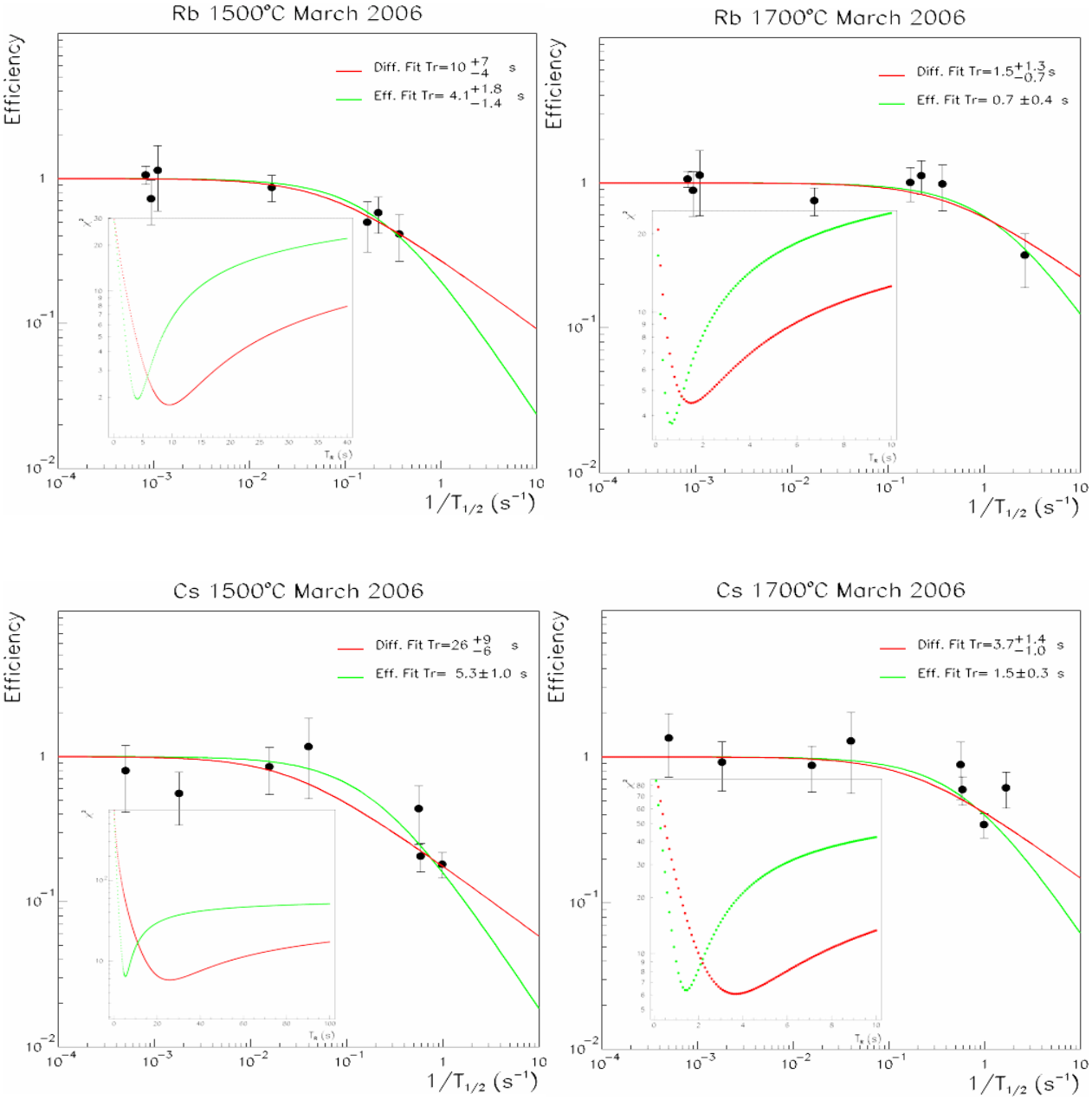

Fig. 35: Release efficiencies for rubidium and caesium from the new, small grain size, HDP target at temperatures of 1500 and 1700°C. Diffusion (red) and effusion (green) mechanisms are considered separately, but none is favoured by the fits.

Finally, we show a comparison of the evolution of yield ratios HDR/LDT, as Fig. 31, and HDR/HDP. Despite the HDP is operated at lower temperature of 1700°C instead of the aimed 2100°C the similar drop of the ratios confirms that its release of Cs is fast and compares well with the release from LDT.

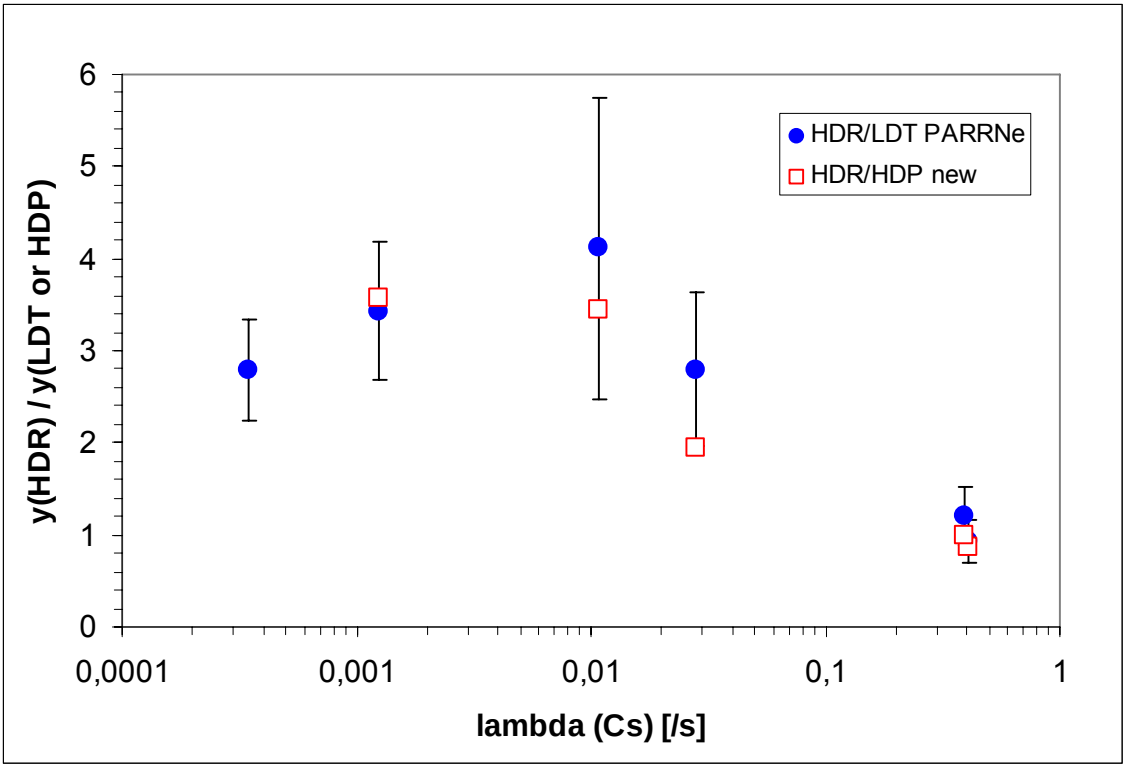

Fig. 36: Yield ratios show that the new HDP target material has as fast, and perhaps faster, release as the LDT PARRNe-like material. Note that the scale for HDR/HDP is arbitrary since the overall yield at low temperature was lower and has been scaled for better comparison. Error bars on HDR/HDP ratios are not shown for clarity, but are similar to those shown for HDR/LDT ratios.

IV.5 Francium yields

In Fig. 37 the yields of Fr isotopes from the HDR and HDP targets are presented. They have not been measured for the LDT (PARRNE-IRIS) target. The yields of very short-lived ^{214}Fr ($T_{1/2}$ = 5 ms), ^{218}Fr ($T_{1/2}$ = 1 ms) and ^{219}Fr ($T_{1/2}$ = 21 ms) were determined by measuring their characteristic α-lines with the alpha detector placed directly at the beam position. The yields of isotopes with longer half-lives were determined using both α-particles and γ-rays. As there was only one measurement (by summer 2006) of the Fr yields from the newly developed HDP target, we give here the obtained yield values from that target as being preliminary.

The Fr isotope yields obtained at ISOLDE from UC_x graphite-cloth target are also shown. The normalized yields of long-lived Fr isotopes with HDR and LDP are lower than those at ISOLDE but, at the same time, the yields of the very short-lived $^{214, 218, 219}$Fr are equal or even higher than those at ISOLDE. Low HDR and HDP target efficiency for long-lived nuclei may be explained by the low value of the ionisation efficiency of the ionizing targets used for our experiments, where ionisation takes place on the strongly carbonized inner surface of the target container. On the other hand, the high yield ratios of very short-lived Fr isotopes can only be explained if the HDR and HDP targets have the shortest release times.

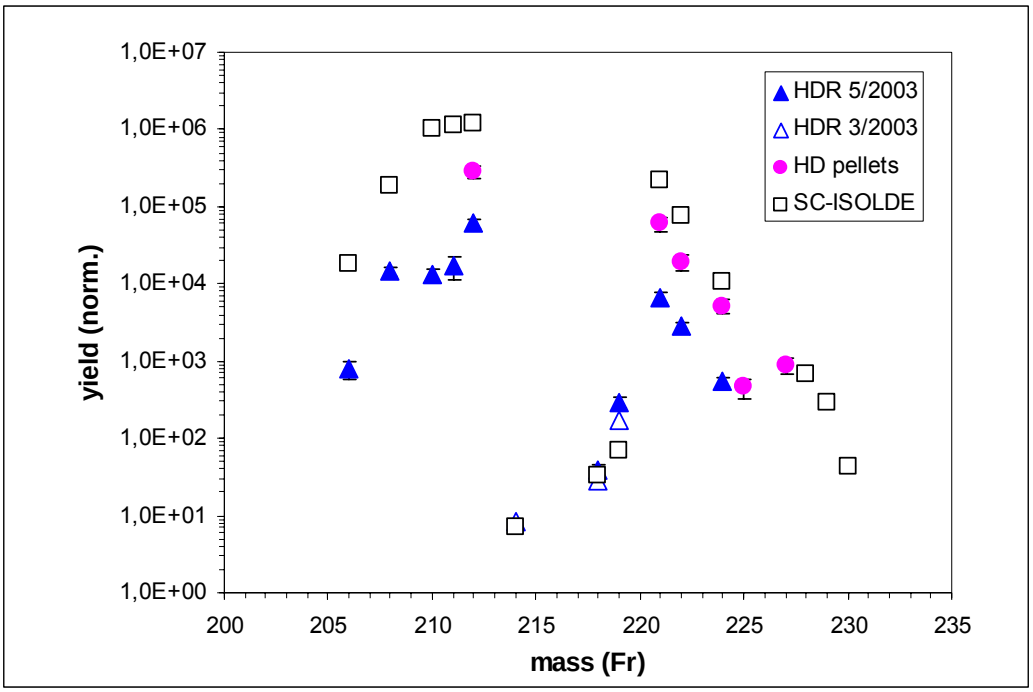

Fig. 37 Yields of francium isotopes for two experiments with the HDR (triangles), the recently developed HDP of small grain size (circles) and, for comparison, the ISOLDE graphite-cloth targets used at the former 600 MeV CERN synchrocyclotron (squares)**.**

For comparison of the Fr release efficiencies of our targets and the ISOLDE target one should first compare isotopes with same half-lives. The measured yields from ISOLDE were thus divided by our HDR and HDP yields and these ratios were subsequently normalized to unity at the long-lived (20 min) ^{212}Fr for which release times should not cause an attenuation. The obtained ratios as function of the half-lives are shown in Fig. 38. Ratios less than 0.4 clearly display the higher release efficiency of the HDR and HDP targets for short lived-isotopes ^{214}Fr (5 ms), ^{218}Fr (1 ms) and ^{219}Fr (21 ms). The performance of the new HDP target with 20 µ grains is remarkable with the corresponding ratios being less than 0.06. The fact that release efficiency for milliseconds activities is still sizeable can be explained by invoking the small volume of our high-density targets and the consequently reduced effusion times. The sticking and flight time of species produced in the IRIS tested target prototypes is about six times less than in the ISOLDE target due to the ratio of the volumes of the target containers. To confirm or reject this assumption, additional on-line tests on the short-lived Fr isotope production from the HDP target will be carried out.

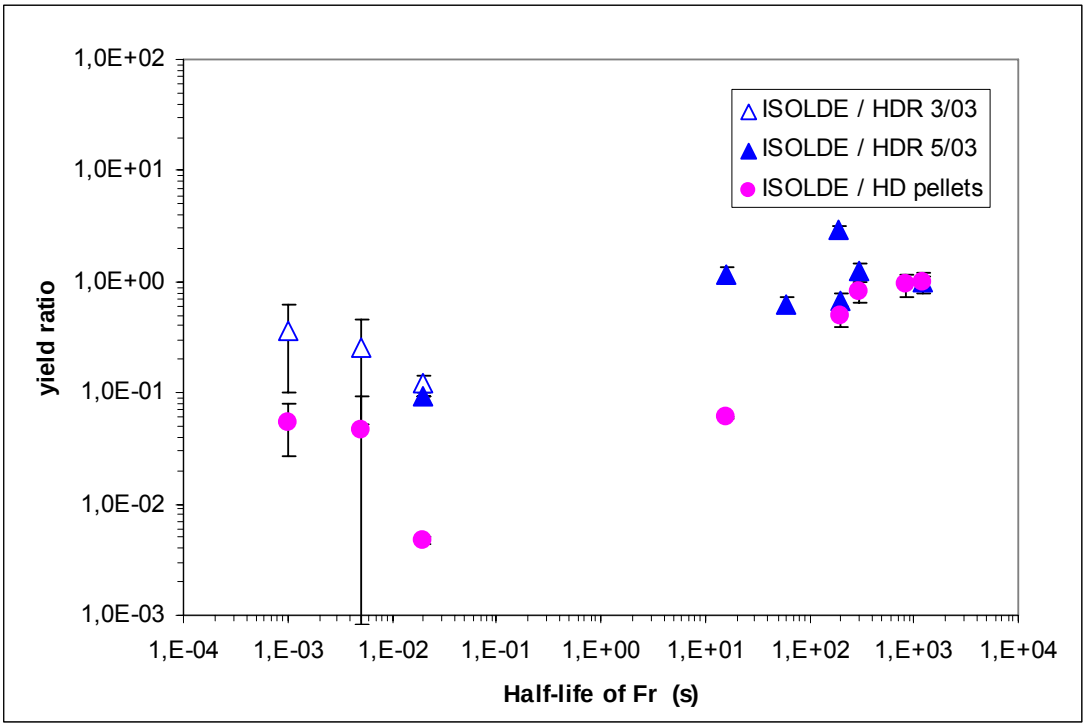

Fig. 38: Comparison of francium release efficiency of our HDR and HDP targets with the ISOLDE target. The relative efficiencies (normalized to 1 for ^{212}Fr with $T_{1/2}$ = 20 min) are plotted versus the half-life of the isotopes. Note that a low ratio means a high efficiency of the IRIS target.

IV.6 Production of other neutron-rich isotopes

In these experiments the target / ion-source construction departs from the previously used ones by the addition of an axially directed electron beam to favor ionisation of elements with higher potentials than those of alkalis and indium**.** We have selected silver and tin isotopes and a few isotopes of other elements known to be difficult cases for isotopic separation.

6a Elements with high ionisation potentials

For on-line production of Ag and Sn neutron-rich isotopes which belong to elements having high ionisation potentials ($V_i \geq 6eV$) the combined target/ ion-source (ionizing target) with electron beam ionisation inside the target container has been used [26, 27]. The construction of the target with electron-beam ionisation is shown in Fig. 39.

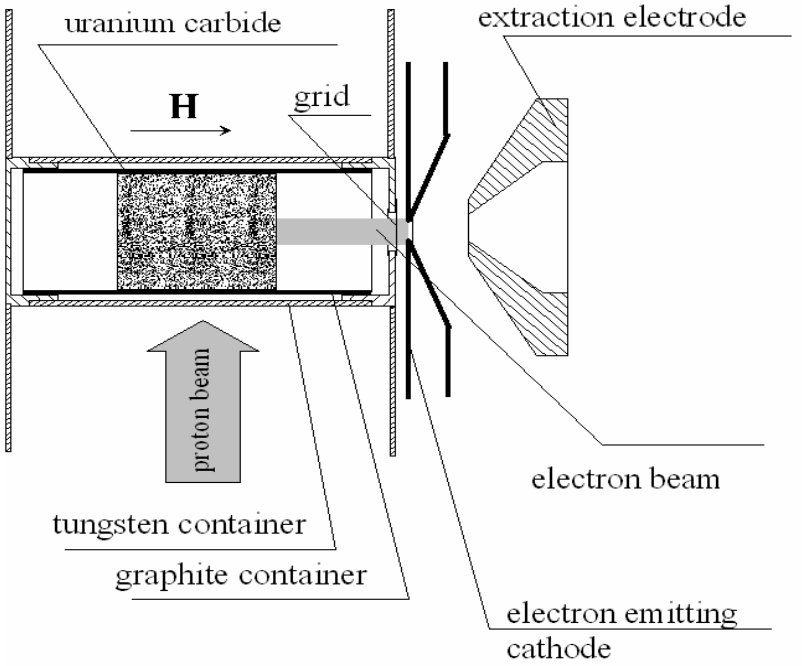

Fig. 39: Scheme of the electron beam ionizing UC target for production of neutron-rich isotopes.

The neutron-rich isotopes of Ag and Sn have been produced with ionisation efficiencies of 4% and 2%, respectively. The ionisation efficiency was calculated as the ratio of the measured isotope yields for long-lived isotopes (for which release efficiency is close to 1 by definition) and in-target productions calculated using the experimentally known cross-sections [14]. It must be mentioned that several

isotopes of Ag and Sn have 1 or even 2 isomers and that the analysis of decay data is consequently very complex. The results shown are rather preliminary. Nevertheless, the yields are believed to be correct within factors of 2- 3, which gives an indication about which efficiency and yields have been achieved so far. We note that a detailed analysis of yields of isomers and ground states is a very interesting issue since one would learn about the physics of population versus spin. Our knowledge is presently very partial and based on statistical models.

The normalization point for silver was the nucleus ^{112}Ag ($T_{1/2}$ = 3.13 h) for which a 4% overall (and also ionisation) efficiency was obtained. The normalized yields of neutron-rich isotopes of Ag obtained with a HDR target at a temperature of 2000°C are presented in Fig. 40. They do not include the yields of isomers, although it can be that part of their decays via isomeric transitions has been counted in the calculated population of the ground states. The yield drop, more than 20 times, from ^{117}Ag (73 s) to ^{121}Ag (0.8 s) suggests a large loss of release efficiency, since the cumulated cross-section for Ag [14] only drops by a factor of 3.

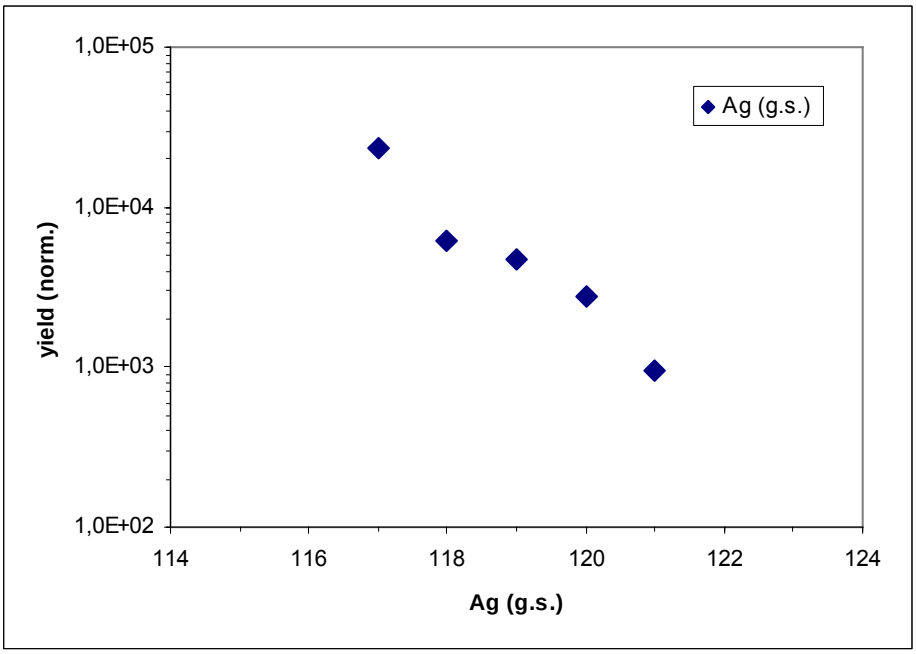

Fig. 40: Normalized Ag-isotope yields obtained with a HDR target at 2000°C. The Ionisation Target used in the comparison tests was equipped with an electron beam (Fig. 39).

The yields for Sn isotopes are shown in Fig. 41. It has been attempted to decompose the feedings of ground state and isomer(s) and their sum is also displayed. The reference for tin efficiency was the nucleus ^{128}Sn ($T_{1/2}$ = 59 m), yielding an ionisation efficiency of 2%.

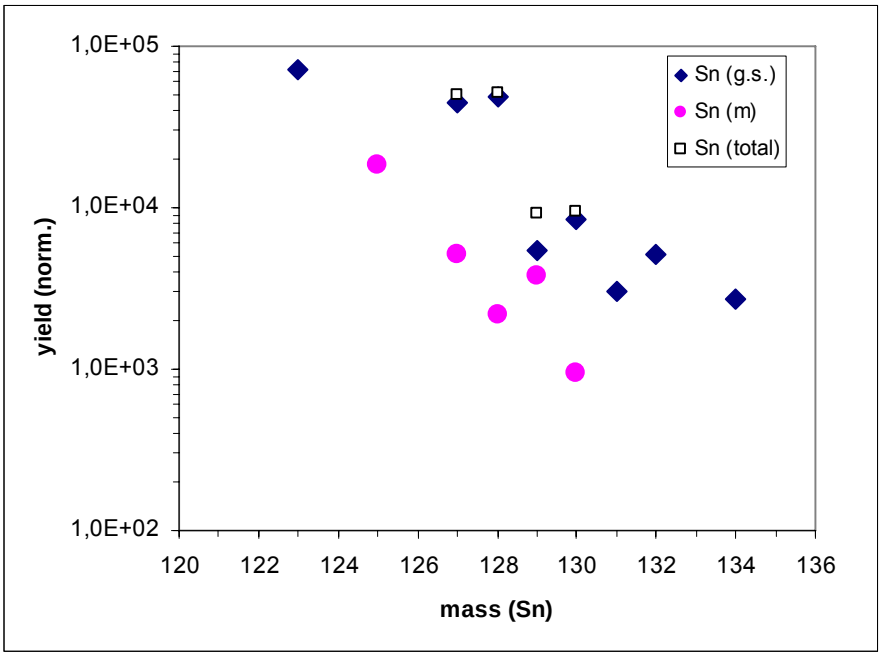

Fig. 41: Normalized yields for neutron-rich Sn isotopes in the same e-beam source and target conditions as resulting in Fig. 40 for silver. Diamonds are for ground states, circles for isomer(s) and when possible the sum (open squares) is shown.

In spite of the approximate procedure followed for the analysis, the data can be well grouped on two lines, one for the ground state with population strongly favored, and the other for the isomer. This is understood by the high spin of the isomer and low spin of the ground state. For instance, in the even-even ^{128}Sn and ^{130}Sn the isomer ($I^{\pi} = 7^{-}$) has a much higher spin than the ground state ($I^{\pi} = 0^{+}$). An exception is ^{129}Sn where both populations come closer, a fact to connect with the spins 3/2 and 11/2. This remark once more stresses the interest of accurate measurements of populations with a potential application in nuclear spectroscopy.

Despite the scattering of the data one can guess that the drop of total cross-section from (extrapolated) ^{126}Sn to ^{132}Sn is about a factor of 20 that happens to match the ratio of cumulative cross-sections [14]. Thus, there seems to be no large decay losses even for ^{132}Sn ($T_{1/2} = 40$ s).

6b Isotopes of refractory elements

For production of neutron-rich isotopes of refractory elements and of the elements with high boiling points the construction of the HDR target, but coupled with a high-temperature electron beam ion source [7], has been used (see Fig. 3). The ion-source temperature could be varied in the interval of 2100-2500°C. Absence of insulators avoids cold spots in the ion source cavity that is a very important condition for extraction of ions of refractory elements from the ion-source volume. In table 3 the on-line target-ion source efficiency is presented for some nuclides with high boiling points. The target and ion-source temperatures were respectively 2250°C and 2400°C. The quoted target-ion source efficiency is the product of the release and the ion-source ionisation efficiency. It should be pointed out that radioactive isotopes of such hard volatile elements as Co, Rh and Pd have been obtained for the first time from a 'thick' uranium-carbide target.

Table 3: Target-ion source unit efficiency (εt_{-is}) for some hard-to-be-extracted nuclides obtained with the HDR construction and material used for the early tests, supplemented with electron beam and operated at very high temperature. The value for ^{115}Pd is an upper limit because the γ-peak at 749 keV used for the measurement is contaminated by a line in ^{115}Ag decay.

Nuclide	$T_{1/2}$ (min)	$\varepsilon_{t\text{-}is}$ (%)	Boiling point (°C)
^{61}Fe	5.98	≤0.2	2861
^{62}Co	13.90	≤0.2	2927
^{68}Cu	3.75	0.4	2562
^{69}Cu	2.85	0.2	2562
^{109}Rh	1.33	5×10^{-2}	3695
^{109}Pd	4.70	0.1	2963
^{115}Pd	0.83	0.25	2963

.

IV.7 Branchings of gamma-rays

7a Procedure

Branching of a γ-ray is the probability of this γ-ray to be emitted per decay. The number of decays is obtained either by comparison with a γ–ray of known branching in the same decay chain or with the number of β-particles emitted by the nucleus of interest. To be reliable the decomposition of decay curves requires either very high statistics or that the lifetimes of the nucleus of interest and of its daughters are sufficiently different. The alternative is to use a selective ion source to avoid production of ions of daughters and apply conservation of the total number of nuclei. For ionisation of ^{92}Rb and ^{144}Cs, which are alkalis, we used surface ionisation. Under normal working conditions around 2000^{0}C there is a small chance to ionize also the earth-alkali elements Sr (^{92}Sr is the β-decay daughter of ^{92}Rb) and Ba (Cs daughter). The conditions for suppression of Sr and Ba beams are met by decreasing the surface temperature. As shown in Fig. 42, the intensity ratio of γ-lines emitted in ^{94}Sr (1428 keV) and ^{94}Rb (837 keV) decays decreases, witnessing the decrease of the ^{94}Sr ion current. When a plateau is reached, one concludes that all the lines originate from mass separated ^{94}Rb only.

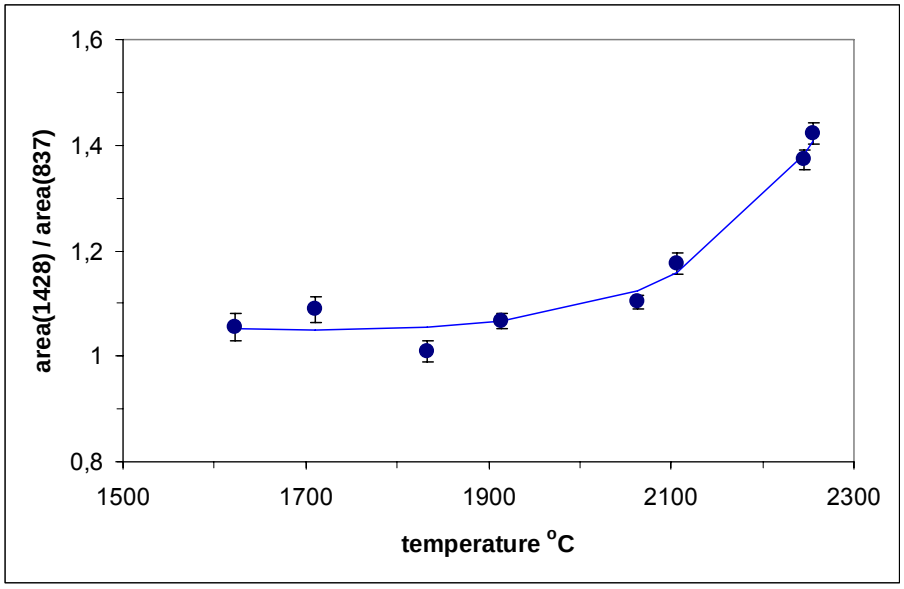

Fig. 42: The temperature dependence of the intensity ratio of lines in ^{94}Sr and ^{94}Rb decay measured with the new high-density pellets target. The ion source is selective for rubidium below 1800^{o}C. The measurement is performed at 1700^{o}C.

7b The ^{92}Rb case

We obtained for the 2^+ to 0^+ ground-state transition in ^{92}Sr a feeding $b_\gamma(815) = 0.032(4)$ per decay of ^{92}Rb. This value is 10 times lower than is quoted in literature. The yield now increases by a factor of 10 and removes a discontinuity in yield measurements of rubidium isotopes [12], see Fig. 43.

The revised value implies either or both of the following alternatives;

a) without changing the decay scheme, a large increase of the ground-state β-branching is needed, making this transition one of the fastest first-forbidden transitions known, together with the one in ^{142}Ba, discussed below,

b) without changing the ground-state β-branching one must have failed to observe a large amount of γ-strength composed of very high-energy transitions directly populating the ground state of ^{92}Sr while by-passing the 815 keV transition. This alternative could be checked with modern highly efficient Ge-arrays such as EXOGAM installed at an isotope separator, e.g. PARRNe.

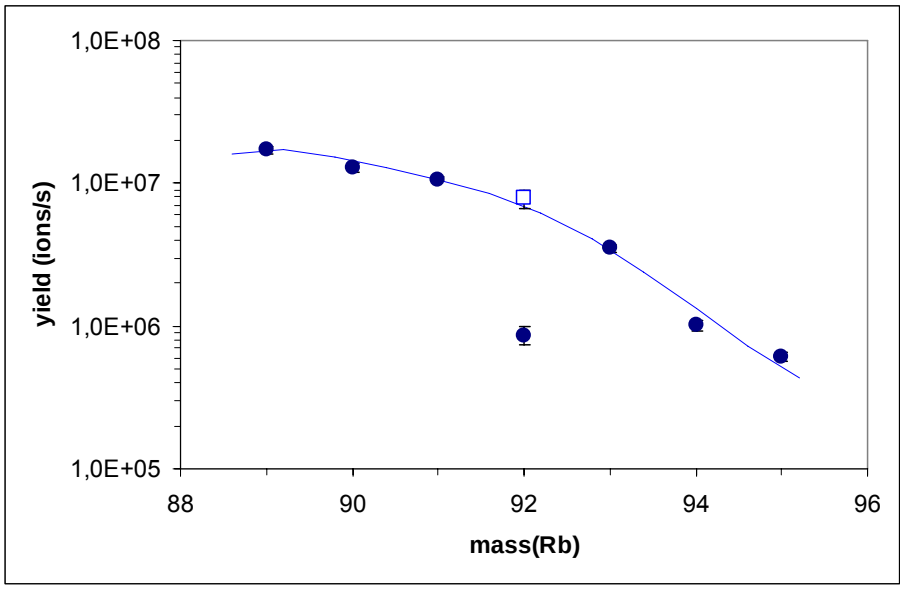

Fig. 43: When using the revised branchings the yield deduced for ^{92}Rb is inside a smooth trend versus mass number (square), while it was an order of magnitude too low if calculated with the branching value adopted by the Nuclear Data Group (circle).

7c Cs isotopes and future measurements

We also obtained preliminary results for some Cs isotopes by the γ method. A small staggering of yields is seen in the region of A = 141 to 143. There is a discontinuity visible in all yields plots for Cs, the yield calculated for ^{142}Cs being lower than for its odd-A neighbours. The case of ^{142}Cs deserves special interest since it defines the lowest logft limit for well-established first-forbidden (ff) β-transitions. The ff-transition to the ^{142}Ba ground state (logft = 5.6) is twice faster than the lower limit (logft = 5.9) recommended as guideline by the Nuclear Data group. The ENDSF quoted value was confirmed within our still large error. We obtained $b_\gamma(360) = 0.25(5)$ per decay of Cs (compare with 0.27(3) in ENDSF). The alternative would be that the yields for the odd-A neighbours are overestimated. This issue should be investigated by comparison of γ and β rates for the whole Cs chain.

The branching of the 2^+ to g.s. transition in ^{144}Ba (199 keV) is deduced to be 0.55(6) per decay of ^{144}Cs. It was so far unknown and allows us to extend our yield systematic by the γ method to a short-lived isotope of Cs ($T_{1/2}$ = 1 s). The deduced logft value for the (probably 1^- Cs) to 0^+ first-forbidden transition of 6.0 is near the lower limit for such transitions and therefore within the expected range.

As final remark, there is a need for more reliable decay branchings of γ-transitions. They are needed for yield measurements, and especially for release efficiency which is very sensitive to small changes of the yields. In order to estimate the errors one should compare the results of the γ-method with those of the β-γ comparison method. The former implies that one can trust the reported γ-ray branchings in the daughter decay to obtain a normalisation. The latter is free of such assumptions but is sensitive to ratios of detector efficiencies and to the decomposition of the β-spectrum into its components, which also limit the accuracy. The perfect agreement we obtained for ^{92}Rb confirms that the spectroscopic input data for ^{92}Sr decay are correct, but our most recent measurements do not show agreement for $^{142, 144}$Cs decays. Future investigations of the Cs isotopic chain with β-γ and γ measurements are thus needed to derive the correct γ-ray branchings for these decays.

V. SUMMARY AND OUTLOOK

The first part of the R&D program on uranium-carbide targets, carried out in the framework of the SPES, SPIRAL-2 and EURISOL projects, has been completed. Series of off-line and on-line experiments have been performed to investigate high-density uranium carbide targets and compare their characteristics with low-density UC_x targets. For that purpose several units of different construction, containing different structure and density target materials have been employed. In particular, the technology of high-density uranium carbides has been developed and the performances of High Density Rod (HDR) and High Density Pellets (HDP) targets have been investigated in detail.

We have identified problems in the analysis of the data, possibly leading to erroneous yield values (e.g. in case of isomers or incorrect spectroscopic data) and developed more elaborate methods for their evaluation. We have revisited the formalism and extended it to take β-decay in the target into account as well in calculation of the effective cross-section needed for calculating the efficiency as for the calculation of perturbation of experimental release curves. We thus have developed suitable tools to evaluate and compare the performances of various targets. However, while the calculation of experimental yields is a purely mathematical problem and is under control, the understanding of the release data is still a remote goal. It implies testing various assumptions which unfortunately do not produce very different observables. Therefore, considerable effort is still needed before we will be able to predict the properties of more massive targets. In any case, it is necessary to use a unified formalism to treat yield and release instead of the independent empirical approaches often used in our older publications. It is in addition worth to note that yield measurements are very sensitive to details of the decay schemes. This offers tools to determine decay branchings of γ-transitions and relative feedings of ground states and isomers in fission, both of interest to nuclear physicists.

Comparison tests of 1 GeV proton-induced fission and neutron-induced fission, where the neutrons are generated by the protons impinging on a massive tantalum converter, were carried out with a high-density powder of large grain size (200 μ) coupled with a W-surface-ionizing source. Neutron-induced fission enhances the yields of very neutron-rich isotopes when normalized to those of isotopes close to the stability.

The performance of a high-density rod target (HDR) has been compared with the one of a low-density powder target of same grain size. The HDR target enhances the production yields for short-lived nuclei far from beta-stability. This is attributed to fissions induced by secondary particles, mostly neutrons, in agreement with the enhancement observed in the experiments with Ta-converter. The number of secondary neutrons produced by 1 GeV protons in a 10 g/cm^2 uranium target is not negligible. It indeed doubles the production rates. An extra enhancement with temperature is also observed for the most n-rich isotopes. It means that the characteristic release times are not negligible with respect to the nuclear half-lives although they do not yet deplete the yields of the very short-lived nuclei too dramatically. The release curves for rubidium and cesium have been recorded. They can be separated into 2 components, a short one of about 0.5 – 1 min, and another of about 25 min. We do not understand the origin of these components. It is a bit confusing and contradictory with this observation that release efficiencies can be quite well reproduced with standard diffusion theory with the μ_0 parameter associated with times $\ln 2/\mu_0$ of 100-200 seconds. All in all, there was no striking difference in release properties of the rod and powder.

Another direction of our efforts was the building and test of a new target unit able to work effectively for some months without failures, the Long-Lasting Target (LLT). The target was a modified HDR. The new feature is a stronger W second target container with 0.5 mm thickness (formerly 0.25 mm) physically separated from the inner graphite container to prevent its carbonization. This target-ion source unit was tested on-line before and after three-month heating at 2000°C at the test bench. The efficiency and release properties were essentially unchanged.

The performances of the HDR and of a very recently developed high-density pellet target (HDP) with smaller grain size have been compared with those of the low-density targets in use at PARRNe-Orsay and ISOLDE. For this purpose, a low-density UC_x powder material (of grain size 20-30 μ) has been prepared at IRIS (the so-called LDT) using the procedures developed at ISOLDE and adopted at PARRNe. The same target construction (ionizing target) has been used for all tests. The evolution of yields versus half-lives demonstrated that the release process of Rb and Cs is fastest for the LDT, resulting in higher normalized yields (per g of uranium and for a reference beam current) of short-lived neutron-rich isotopes. However, as the uranium thickness is 2.4 higher in HDR for targets having same volume, the absolute yields of the measured short-lived isotopes with $T_{1/2}$ as short as 200 ms are still the highest for the HDR target. The uranium carbide HDR target material, which was for the first time used at IRIS was not initially produced for that purpose. The obvious next step of development was thus to manufacture a material with high density of 11-12 g/cm^3, but with a grain size comparable with the one of the ISOLDE target material. We received this material at the end of 2005 as high-density pills (12 g/cm^3) of the geometry similar to ISOLDE pills and having a grain size ≤ 20 microns. The first results for this target, the high-density pellet target (HDP), in early 2006 readily demonstrated that its release properties are considerably better than those of the HDR material and very close to those of LDT, in spite of its operation at low temperature caused by a technical problem. The release times of HDR, LDT and new HDP were estimated from the efficiencies using the same method for all of them. The time constants for Rb and Cs drop from about 25 s for the HDR with 200 μ grains to typically 5 s for the LDT and HDP with 20 μ grains. Yet, the lower ionisation efficiency of the HDP target, due to the low operation temperature, should be increased making use of a separate ionizer before the yields can compare with the best ones provided by the HDR target.

Although somewhat outside the scope of PLOG, the performance of the high-density rod and new pellets for Fr isotopes has been tested and is reported here. We obtained a quite unexpected but very encouraging result: the normalized yields of extremely short-lived Fr isotopes (a few ms) are equal or even higher than those from the graphite-cloth ISOLDE target that were the best ever reported. We attribute this to the smaller size of our target, made possible by its high density, and the resulting smaller effusion time. Francium isotopes offer a very interesting testing ground for release properties of alkalis owing to the very short lifetimes of the isotopes and the fact that they are produced by spallation instead of fission, which makes an estimate of cross-sections easier.

Production of elements with high ionisation potentials or hardly volatile was studied with the HDR target material. The ionizing target employed for comparisons of HDR, LDT and HDP was used with an electron beam. For the separation of refractory elements the temperature could reach as high as 2500^{o}C. Ionisation efficiencies or 2% for Sn and 4% for Ag have been obtained while, for the first time to our knowledge, isotopes of refractory elements such as Co, Rh and Pd have been produced on-line from a uranium-carbide thick target.

To summarize, the high-density targets did not show any dramatic loss of efficiency with respect to

thinner targets. This was an issue that was under debate before our investigations. The firstly used high-density rod HDR UC (11g/cm^3 with 200 μ grain size), owing to the larger mass fitting in the same volume and despite higher decay losses, provides higher yields in ions/s than the 2.3 g/cm^3 UC_x Orsay-ISOLDE pills (LDT), even for Rb and Cs isotopes of half-life shorter than one second. The release times of the newly manufactured HD target pellets (HDP) with 20 μ grains are comparable with those of the LDT. Yields could not be measured under the best temperature conditions, but from the above said we expect them to become even better than those of the HDR, the most substantial improvements being awaited for the most short-lived nuclei. The study of the HDP clearly is a priority for the coming investigations.

The shortening of release times when the grains become smaller indicates that diffusion is the main cause for the delay time. The Fr results showed that the compact construction is the key to ensure fast effusion, allowing observation of millisecond activities with unprecedented efficiency. We therefore conclude that UC high-density targets offer the best perspectives for delivering high-intensity neutron-rich beams and their development must be continued.

As mentioned, we do not have enough insight in the mechanism of release, which so far one can judge seems to be dominated by diffusion for UC targets of typically 10 g. It is thus necessary to continue these studies. We are not able to predict the properties of a massive target (about 1 kg) from our present results. Loss of release efficiency by longer effusion path and increase of the number of secondary fissions work in opposite ways. Measurements with heavier targets should be a step forward. Thus, in June 2006 the first on-line experiment on the study of the heavy target with the thickness of uranium of 91 g/cm^2 was carried out. This target used the new HD pill target material and was constructed by adding another container placed symmetrically of the usual one with respect to the extracted ion beam axis. The first tests showed that there is little loss of efficiency, i.e. of normalized yield, even for activities as short as a few seconds. Therefore, small grain size is definitely a key parameter. Accordingly, target material with even smaller grains (1 and 5 μ) shall be delivered soon by the Lutch Scientific Industrial Association, a joint venture of PNPI with local industry. We shall also carry out the tests of long-lasting targets with these new materials.

Finally, there is a problem with the absolute yields obtained in the experiments at IRIS. It seems that the overall efficiency of the system can vary almost a factor of 10 between different runs. As long as our investigations rely on relative yields (release efficiency) or even are independent of the yield scale (release curves) this is not an issue. However, for actual RIB experiments it is fundamental to keep a reproducible performance. We should therefore investigate this carefully.

On the basis of the present experience, the second part of the R&D program, to be developed in the framework of the ISTC project #2965, foresees the development of massive target units (up to 1 kg of high-density uranium carbide) and the investigation of their performances.

Acknowledgements

We acknowledge the financial support of the European Community under the FP6 "Research Infrastructure Action - Structuring the European Research Area" EURISOL DS Project Contract no. 515768 RID IDS referring to LNL, GANIL and Orsay and financial support of ISTC in the frames of ISTC Project No. 2965 referring to PNPI. The EC is not liable for any use that can be made on the information contained herein.

References

[1] the SPES project; A. Bracco and A. Pisent; LNL-INFN (Rep) 181/02 (2002).

[2] M.G. Saint-Laurent et al.; SPIRAL phase II European RTD report, GANIL R 01-03-2001.

[3] V.A. Nazarevicz and R.F. Casten; Nucl. Phys. A **682** (2001) 295-309.

[4] M. Portillo et al..; Nucl. Instrum. and Meth. in Phys. Res. B **194** (2002) 193.

[5] V.A. Bolshakov et al.; Nucl. Instrum. and Meth., in Phys. Res. B **70** (1992) 69-74.

[6] G.D. Alton at al.; Nucl. Instrum. and Meth. in Phys. Res. B **66** (1992) 492.

[7] V.N. Panteleev et al.; Rev. Sci. Instrum. **73** (2002) 738, and Rev. Sci. Instrum. **75** (2004) 1634.

[8] A. Andrighetto et al.; Nucl. Instrum. and Meth. in Phys. Res. B **204** (2003) 267.

[9] C. M. Baglin; Nuclear Data Sheets **91** (2000) 423.

[10] G. Lhersonneau et al.; Eur. Phys. J.A **9** (2000) 385.

[11] L. Stroe et al.; Eur. Phys. J. A **17** (2003) 57.

[12] G. Lhersonneau et al.; Phys. Rev. C **74** (2006) 017308.

[13] V. Rizzi et al.; proc. RNB7, Cortina, Italy, July 2006, to be published in Eur. Phys. J. A.

[14] M. Bernas et al.; Nucl. Phys. A**725** (2003) 213.

[15] R. Kirchner; Nucl. Instrum. Meth. in Phys. Res. B**70** (1992) 186.

[16] B. Roussière et al. ; Nucl. Instrum. Meth. in Phys. Res. B**194** (2002) 151.

[17] G. Lhersonneau et al. ; Nucl. Instrum, Meth. in Phys. Res. A**566** (2006) 465.

[18] D.G. Madland and T.R. England ; Nucl. Sci. Eng. **64** (1977) 859.

[19] A.E. Barzakh et al; Eur. Phys. J. A**19** (2004) 341-345.

[20] L.S. Waters, Editor; MCNPx User Manual, Version 2.1.5, TPO-EG83-G-UG-X-00001, (1999).

[21] N. Lecesne et al.; Nucl. Instrum. and Meth. in Phys. Res. **B**126 (1997) 141.

[22] V.N. Panteleev et al.; Nucl. Phys. A**701** (2002) 470.

[23] B. Roussière et al.; Nucl. Instrum. Meth. in Phys. Res. B**246** (2006) 288

[24] A. Herrera-Martinez; EURISOL project, multi –MW target design study, CERN thesis 2005-033.

[25] A. Andrighetto et al.; Eur. Phys. J. A**23** (2005) 257-264.

[26] V.N. Panteleev et al.; Nucl. Instrum. Meth. in Phys. Res. B**240** (2005) 888.

[27] V.N. Panteleev et al.; Rev. Sci. Instrum. **77** (2006) 03A705.

[28] ISOLDE user's guide, http://isolde.web.cern.ch/ISOLDE/.

[29] C. Lau et al.; Nucl. Instrum. Meth. In Phys. Res. B**204** (2003) 257.

[30 N. Pauwels et al.; http://www.nea.fr/html/science/satif/satifs_pauwels.pdf.

List of reviewed publications published by the PLOG collaboration

1. V.N. Panteleev et al.; Rev. Sci. Instrum. **73** (2002) 738.

2. V.N. Panteleev et al.; Nucl. Phys. A **701** (2002) 470.

3. A. Andrighetto et al.; Nucl. Instrum. and Meth. in Phys. Res. B **204** (2003) 267.

4. V.N. Panteleev et al.; Nucl. Instrum. and Meth. in Phys. Res. B **204** (2003) 382.

5. V.N. Panteleev et al.; Rev. Sci. Instrum. **75** (2004) 1634.

6. A.E. Barzakh et al.; Eur. Phys. J. A **19** (2004) 341.

7. V.N. Panteleev et al.; Nucl. Instrum. Meth. in Phys. Res. B **240** (2005) 888.

8. A. Andrighetto et al.; Eur. Phys. J. A **23** (2005) 257.

9. G. Lhersonneau et al.; Phys. Rev. C **74** (2006) 017308.

10. V.N. Panteleev et al.; Rev. Sci. Instrum. **77** (2006) 03A705.

11. V. Rizzi et al.; Proc.RNB7, Cortina, Italy, 2006, to be published in Eur. Phys.J. A.

12. G. Lhersonneau et al.; Nucl. Instrum, Meth. in Phys. Res. A **566** (2006) 465.

13. V.N. Panteleev et al.; ibid. 11

APPENDIX 1

Yield formulae for up to 2 isomers and ground state

Introduction

We explicit the calculation of yields in case the nucleus has one or two isomers. In that case, transitions used for analysis can be fed in several decay modes and with different probabilities. This formalism has been applied to the analysis of data obtained at IRIS, Gatchina, since 2004 by V. Rizzi for isotopes of Rb and Cs with occasionally one isomer. The situation is sketched in Fig. 1.

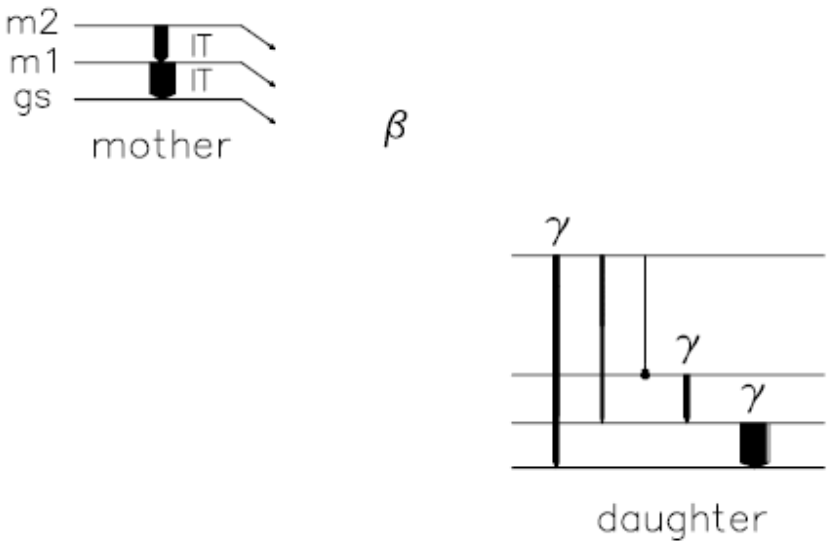

Figure 1: Schematic decay scheme of a nucleus with 2 isomers. Isomers and the ground state are populated in fission as well as possibly in β decay of a still more exotic nucleus. The yield is the number of nuclei (for each of these states) that are delivered by the mass separator per time unit. This number reflects fission cross-sections and isobaric decays of precursors. Isomers and ground state are linked by isomeric transitions (IT) and can also undergo β decay. Each one of the γ rays marked in the daughter nucleus can be populated in each decay mode of the parent. It is therefore needed to analyse at least 3 γ rays from different levels (a necessary condition to ensure different population probabilities) to disentangle the primary productions.

This presents a complete description of the solving method for yields (ion currents in continuous irradiation) determined by γ spectroscopy. A linear 3 x 3 system of equations is associated with decays from ground state and up to 2 isomers.
An ion current collected on the movable tape is denoted by p assumed to be constant during a cycle, while
n is a number of nuclei currently either collected or in front of the detector.
Both p and n are vectors up to (3). For the whole system indices are (i= 1; the highest isomer, i= 2; the lowest isomer and i= 3; g the ground state). If there is only one isomer the indices are (i= 1; the isomer and i= 2; g). If there is only a ground state obviously i= 1, and the system collapses to the well known formulae used by excel fans and in our older papers.
The variable $b(i, j)$ is the branching from level i to level j via the isomeric transition (IT).

step1. Number of decays during measurement

The starting point is writing the equations that describe the beam on part of the cycle

$$\begin{aligned} dn(1)/dt &= p(1) - \lambda(1)\, n(1) \\ dn(2)/dt &= p(2) + b(1,2)\, \lambda(1)\, n(1) - \lambda(2)\, n(2) \\ dn(3)/dt &= p(3) + b(2,3)\, \lambda(2)\, n(2) - \lambda(3)\, n(3) \end{aligned}$$

Initial conditions are no nuclei at starting time $n(i) = 0$. The solution is conveniently put as a matrix equation

$$n(t) \;=\; M_{irr}(t)\;\; p$$

where the matrix is triangular. The number of nuclei collected at the end of collection is thus $n(t_c)$, with t_c the collection time.

In order to remain compact we set some definitions with the convention that the decay is $i \rightarrow j \rightarrow k$

$$\begin{aligned}
f_{irr}(i) &= \frac{1 - e^{-\lambda(i)t}}{\lambda(i)} \\
f_{dec}(i,j) &= \frac{e^{-\lambda(i)t} - e^{-\lambda(j)t}}{\lambda(j) - \lambda(i)} \\
f_{ddd}(i,j,k) &= \lambda(j) \frac{f_{dec}(i,k) - f_{dec}(j,k)}{\lambda(j) - \lambda(i)} \\
f_{idc}(i,j) &= f_{irr}(j) - f_{dec}(i,j) \\
f_{grd}(i,j,k) &= f_{idc}(j,k) - f_{ddd}(i,j,k)
\end{aligned}$$

The elements of M_{irr} as shown below are evaluated at $t = t_c$ to give the number of nuclei on the tape when the transport starts.

$$\begin{vmatrix}
f_{irr}(1) & 0 & 0 \\
f_{idc}(2,1)\, b(1,2) & f_{irr}(2) & 0 \\
f_{grd}(3,2,1)\, b(1,2)\, b(2,3) & f_{idc}(3,2)\, b(2,3) & f_{irr}(3)
\end{vmatrix}$$

The next step is to get the activity during measurement. It starts with the number of nuclei. The equations are

$$\begin{aligned}
dn(1)/dt &= -\lambda(1)\, n(1) \\
dn(2)/dt &= b(1,2)\, \lambda(1)\, n(1) - \lambda(2)\, n(2) \\
dn(3)/dt &= b(2,3)\, \lambda(2)\, n(2) - \lambda(3)\, n(3)
\end{aligned}$$

with the initial conditions $n_0 = n(i, t = 0) = n_c(i)$, the number of nuclei collected at $t = t_c$, calculated from above. Note that the time is reset at end of collection for convenience. The beam is switched off at $t = 0$ and decay begins.

Counting shall start after the transport is completed at a time t_t and shall last for a time t_c. The number of nuclei collected at time t during decay is given by another matrix equation.

$$n(t) = M_{dec}(t)\ n_0$$

where the elements of M_{dec} are

$$\begin{vmatrix}
e^{-\lambda(1)t)} & 0 & 0 \\
\lambda(1)\, f_{dec}(1,2)\, b(1,2) & e^{-\lambda(2)t} & 0 \\
\lambda(1)\, f_{ddd}(1,2,3)\, b(1,2)\, b(2,3) & \lambda(2)\, f_{dec}(2,3)\, b(1,2) & e^{-\lambda(3)t}
\end{vmatrix}$$

The number of decays of each mode i observed after transport during measurement is the integral of the activity

$$N_{dec} \;=\; \int_{t_1}^{t_2} \lambda\, n(t)\, dt$$

with $t_1 = t_t$ and $t_2 = t_1 + t_c$.
Multiplication introduces a new matrix M_λ with elements $\lambda(i)$ on its diagonal.
The result of integration is to substitute the former diagonal elements of $M_{dec}(t)$ with

$$u(i) \;=\; \frac{e^{-\lambda(i)t_1} - e^{-\lambda(i)t_2}}{\lambda(i)}$$

while for off-diagonal elements it is sufficient to redefine

$$f_{dec}(i,j) \;=\; \frac{u(i) - u(j)}{\lambda(j) - \lambda(i)}$$

The number of decays $N_{dec}(i)$ is expressed by a matrix product. The new matrix M is a 3 x 3 matrix totally calculable from nuclear lifetimes and cycle times. The elements can be considered to have no errors.

$$\begin{aligned} N_{dec}(t_c, t_t, \lambda' s) \;&=\; M_\lambda(\lambda' s)\;\; M_{dec}(t_c, t_t, \lambda' s)\;\; p \\ &=\; M\;\; p \end{aligned}$$

step.2 Gamma peak area

The observed peak area A of the γ ray is a superposition of contributions from all the decay modes, each with it own probability $b(i)$ to emit the transition.Thus, with ε the efficiency to detect the γ-ray in a peak, the area is

$$A \;=\; \varepsilon \sum_i b(i)\, N_{dec}(i)$$

We introduce a matrix M_ε with equal elements ε on the diagonal and a covariant vector for the decay branchings B of the transition.

$$\begin{aligned} M_\varepsilon(i,j) \;&=\; \varepsilon\;\; \delta(i,j) \\ B(j) \;&=\; (\, b(1)\, b(2)\, b(3)\,) \\ A \;&=\; (M_\varepsilon\, B)\;\; (\, M\, p) \end{aligned}$$

The factorisation has the advantage to separate the sources of coefficients (literature nuclear data, detector, measurement times and lifetimes) in a way transparent enough to easily implement changes if needed. It also shows that A retains a linear form in p.

$$A \;=\; \sum_i c(i)\, p(i)$$

How to get p from A is only mathematics.

step.3 Solving area(p)

In order to solve the system for each $p(i)$ it is thus needed to have at least as many lines as there are decay modes. If more γ peaks, with experimental area A_k and error δ_k) are available, this problem can be treated by the χ^2 method. The expression to be minimized versus the components of the vector p has the form

$$\chi^2(p) \;=\; \sum_k \left(\frac{A_k(experimental) - A_k(p)}{\delta_k}\right)^2$$

Searching the minimum of $\chi^2(p)$ by setting the derivatives

$$\frac{d\chi^2}{dp(i)} \;=\; 0$$

gives another linear system with M_{norm} the normal matrix formed of half of the second derivatives of $\chi^2(p)$and D the vector of half of first derivatives, that has to be solved for p.

$$M_{norm}\, p \;=\; D$$

with elements

$$\begin{aligned} M_{norm}(i,j) &= \sum_k w(k)\, c(i,k)\, c(j,k) \\ D(i) &= \sum_k w(k)\, c(i,k)\, A(k) \end{aligned}$$

where the weights are $w(k) = (1/\delta_k)^2$ if one considers only statistical errors due to counting.

The matrix to solve the system is the so-called covariance matrix

$$M_{cov} \;=\; M_{norm}^{-1}$$

Following standard procedures standard deviations on $p(i)$ are $\sigma(i) = \sqrt{M_{cov}}$. If the ratio χ^2/nf, (nf being the number of degrees of freedom) is larger than 1, σ's shall be scaled up by $\sqrt{\chi^2/nf}$. For the total yield

$$p = \sum_i p(i)$$

the error is

$$\begin{aligned} \delta p &= \sqrt{\sum_{i,j} (\frac{dp}{dp(i)})(\frac{dp}{dp(j)})\, M_{cov}(i,j)} \\ &= \sqrt{\sum_{i,j} M_{cov(i,j)}} \end{aligned}$$

Branchings of γ lines are not free of errors. The analytical calculation of how these errors propagate on the final result is less simple. It is easier to repeat the calculation with modified branchings ($b(i) \rightarrow b(i) + \delta b(i)$) for each decay mode one by one and compute the resulting increments of each $p(i)$. Finally, these increments are added quadratically to the fit errors.
The error on detector efficiency ε can be split into a scale error and a relative (energy dependent) error. The former has to be added at the very end, together with other scale uncertainties such as those on beam current, transmission, etc. The latter is the error on the variation of the ratio of efficiencies for different γ-ray energies. It is at most of a few percents and can be neglected in practice.

Erratum:

In the matrix M_{irr} the order of the indices for λ's in functions f_{idc} and f_{grd} must be reversed, i.e. they must read: (1,2), (2,3) and (1,2,3). Another, and more compact, expression of M_{irr} (3,3) is $f_{irr}(3) - (\lambda_2 f_{dec}(3,1) - \lambda_1 f_{dec}(3,2)) / (\lambda_2 - \lambda_1)$.

APPENDIX 2

Tables of experimental yields

Yields are shown as 'absolute ', i.e. expressed in ions/second (left-hand side) and as 'normalized', i.e. scaled for a target mass of 1 g/cm^2 of uranium and a proton beam current of 0.1 μA (right-hand side). The usual measurement method is γ-spectroscopy, but β-counting has been used occasionally.

A2.1
June 2002 (HDR powder; 19.8 g/cm^2; surface ionisation source; direct and with Ta converter)

This is the first used high-density UCx with grains of about 200 microns.

Cesium at T=2100°C-direct			HDR Powder		
A	**T1/2 [s]**	**Yield [1/s]**	**Err Yield [1/s]**	**Norm.Yield [1/s]**	**Err. Norm. [1/s]**
140	63,7	4,73E+06	9,46E+05	1,59E+06	3,18E+05
141	24,94	3,89E+06	7,78E+05	1,31E+06	2,62E+05
142	1,7	9,68E+05	1,94E+05	3,26E+05	6,52E+04
143	1,78	8,49E+05	1,70E+05	2,86E+05	5,72E+04
144	1,01	2,11E+05	4,23E+04	7,11E+04	1,42E+04
145	0,6	1,04E+05	2,08E+04	3,50E+04	7,00E+03

Cesium at T=2100°C-converter			HDR Powder		
A	**T1/2 [s]**	**Yield [1/s]**	**Err Yield [1/s]**	**Norm.Yield [1/s]**	**Err. Norm. [1/s]**
140	63,7	2,82E+07	5,64E+06	9,50E+06	1,90E+06
141	24,94	2,55E+07	5,09E+06	8,57E+06	1,71E+06
142	1,7	6,88E+06	1,38E+06	2,32E+06	4,63E+05
143	1,78	5,76E+06	1,15E+06	1,94E+06	3,88E+05
144	1,01	1,83E+06	3,66E+05	6,16E+05	1,23E+05
145	0,6	5,31E+05	1,06E+05	1,79E+05	3,58E+04

Rubidium at T=2100°C-direct			HDR Powder		
A	**T1/2 [s]**	**Yield [1/s]**	**Err Yield [1/s]**	**Norm.Yield [1/s]**	**Err. Norm. [1/s]**
90	258	1,60E+07	3,20E+06	5,39E+06	1,08E+06
91	58,4	2,91E+06	5,81E+05	9,79E+05	1,96E+05
92	4,49	1,81E+06	3,62E+05	6,09E+05	1,22E+05
93	5,84	8,06E+05	1,61E+05	2,71E+05	5,43E+04
94	2,7	5,84E+05	1,17E+05	1,97E+05	3,94E+04
95	0,38	1,60E+07	3,20E+06	5,39E+06	1,08E+06

Rubidium at T=2100°C-converter HDR Powder					
A	**T1/2 [s]**	**Yield [1/s]**	**Err Yield [1/s]**	**Norm.Yield [1/s]**	**Err. Norm. [1/s]**
90	258	4,42E+07	8,84E+06	1,49E+07	2,97E+06
91	58,4	1,23E+07	2,47E+06	4,16E+06	8,32E+05
92	4,49	1,13E+07	2,26E+06	3,80E+06	7,60E+05
93	5,84	5,11E+06	1,02E+06	1,72E+06	3,44E+05
94	2,7	3,14E+06	6,29E+05	1,06E+06	2,12E+05
95	0,38	4,42E+07	8,84E+06	1,49E+07	2,97E+06

Indium at T=2100°C-direct HDR Powder					
A	**T1/2 [s]**	**Yield [1/s]**	**Err Yield [1/s]**	**Norm.Yield [1/s]**	**Err. Norm. [1/s]**
119	138	1,89E+06	3,79E+05	6,38E+05	1,28E+05
120	46,2	7,82E+05	1,56E+05	2,63E+05	5,27E+04
121	23	6,96E+05	1,39E+05	2,35E+05	4,69E+04
122	10,5	3,57E+05	7,14E+04	1,20E+05	2,41E+04
123	6	4,55E+05	9,09E+04	1,53E+05	3,06E+04
124	3,2	1,84E+05	3,67E+04	6,18E+04	1,24E+04
125	2,3	1,13E+05	2,25E+04	3,79E+04	7,59E+03
126	1,45	3,79E+04	7,57E+03	1,27E+04	2,55E+03
127	3,7	3,33E+03	6,67E+02	1,12E+03	2,24E+02

Indium at T=2100°C-converter HDR Powder					
A	**T1/2 [s]**	**Yield [1/s]**	**Err Yield [1/s]**	**Norm.Yield [1/s]**	**Err. Norm. [1/s]**
119	138	1,56E+06	3,12E+05	5,25E+05	1,05E+05
120	46,2	8,06E+05	1,61E+05	2,71E+05	5,43E+04
121	23	1,29E+06	2,57E+05	4,33E+05	8,67E+04
122	10,5	8,04E+05	1,61E+05	2,71E+05	5,42E+04
123	6	1,51E+06	3,02E+05	5,08E+05	1,02E+05
124	3,2	7,41E+05	1,48E+05	2,49E+05	4,99E+04
125	2,3	5,23E+05	1,05E+05	1,76E+05	3,52E+04
126	1,45	1,45E+05	2,90E+04	4,89E+04	9,77E+03
127	3,7	1,10E+04	2,21E+03	3,71E+03	7,43E+02

A2.2
May 2003 (HDR; 8.2 g/cm^2; surface ionisation source)
In form of a rod.

Cesium at T=1980°C			HDR		
A	**T1/2 [s]**	**Yield [1/s]**	**Err Yield [1/s]**	**Norm.Yield [1/s]**	**Err. Norm. [1/s]**
139	556,2	4,30E+06	5,47E+05	7,49E+05	9,53E+04
140	63,7	1,23E+06	1,47E+05	2,14E+05	2,56E+04
141	24,94	1,40E+06	1,74E+05	2,44E+05	3,03E+04
142	1,7	1,90E+05	2,15E+04	3,31E+04	3,75E+03
143	1,78	1,60E+05	1,73E+04	2,79E+04	3,01E+03
144	1,01	2,80E+04	3,07E+03	4,88E+03	5,35E+02
145	0,6	2,59E+04	6,51E+03	4,51E+03	1,13E+03
146	0,34	2,20E+03	9,87E+02	3,83E+02	1,72E+02

Cesium at T=2050°C			HDR		
A	**T1/2 [s]**	**Yield [1/s]**	**Err Yield [1/s]**	**Norm.Yield [1/s]**	**Err. Norm. [1/s]**
139	556,2	4,38E+06	5,59E+05	7,63E+05	9,74E+04
140	63,7	1,19E+06	1,42E+05	2,07E+05	2,47E+04
141	24,94	1,25E+06	1,59E+05	2,18E+05	2,77E+04
142	1,7	2,90E+05	3,25E+04	5,05E+04	5,66E+03
143	1,78	2,30E+05	2,61E+04	4,01E+04	4,55E+03
144	1,01	2,35E+04	2,87E+03	4,09E+03	5,00E+02
145	0,6	1,45E+04	3,28E+03	2,53E+03	5,71E+02

Cesium at T=2160°C			HDR		
A	**T1/2 [s]**	**Yield [1/s]**	**Err Yield [1/s]**	**Norm.Yield [1/s]**	**Err. Norm. [1/s]**
139	556,2	1,05E+07	1,84E+06	1,83E+06	3,21E+05
140	63,7	3,21E+06	5,34E+05	5,59E+05	9,30E+04
141	24,94	3,55E+06	6,50E+05	6,18E+05	1,13E+05
145	0,6	6,60E+04	1,42E+04	1,15E+04	2,47E+03

Cesium at T=2230°C			HDR		
A	**T1/2 [s]**	**Yield [1/s]**	**Err Yield [1/s]**	**Norm.Yield [1/s]**	**Err. Norm. [1/s]**
139	556,2	1,27E+07	2,19E+06	2,21E+06	3,82E+05
140	63,7	4,17E+06	7,16E+05	7,26E+05	1,25E+05
141	24,94	4,57E+06	8,37E+05	7,96E+05	1,46E+05
145	0,6	1,00E+05	1,92E+04	1,74E+04	3,34E+03

Rubidium at T=1980°C			HDR		
A	**T1/2 [s]**	**Yield [1/s]**	**Err Yield [1/s]**	**Norm.Yield [1/s]**	**Err. Norm. [1/s]**
89	909	5,70E+06	7,50E+05	9,93E+05	1,31E+05
90	258	3,20E+06	4,10E+05	5,57E+05	7,14E+04
91	58,4	1,80E+06	2,13E+05	3,14E+05	3,71E+04
92	4,49	1,48E+05	2,00E+04	2,58E+04	3,48E+03
93	5,84	6,80E+05	8,42E+04	1,18E+05	1,47E+04
94	2,7	2,75E+05	3,20E+04	4,79E+04	5,57E+03
95	0,38	1,30E+05	1,60E+04	2,26E+04	2,79E+03

Rubidium at T=2050°C			HDR		
A	**T1/2 [s]**	**Yield [1/s]**	**Err Yield [1/s]**	**Norm.Yield [1/s]**	**Err. Norm. [1/s]**
89	909	6,50E+06	9,68E+05	1,13E+06	1,69E+05
91	258	1,60E+06	2,43E+05	2,79E+05	4,23E+04
95	0,38	1,85E+05	3,27E+04	3,22E+04	5,70E+03

Rubidium at T=2160°C			HDR		
A	**T1/2 [s]**	**Yield [1/s]**	**Err Yield [1/s]**	**Norm.Yield [1/s]**	**Err. Norm. [1/s]**
89	909	1,16E+07	1,67E+06	2,02E+06	2,91E+05
90	258	7,64E+06	1,09E+06	1,33E+06	1,90E+05
91	58,4	3,77E+06	4,86E+05	6,57E+05	8,47E+04
95	0,38	8,06E+05	1,38E+05	1,40E+05	2,41E+04

Rubidium at T=2230°C			HDR		
A	**T1/2 [s]**	**Yield [1/s]**	**Err Yield [1/s]**	**Norm.Yield [1/s]**	**Err. Norm. [1/s]**
89	909	1,60E+07	2,96E+06	2,79E+06	5,16E+05
90	258	8,17E+06	1,46E+06	1,42E+06	2,54E+05
91	58,4	4,40E+06	7,69E+05	7,67E+05	1,34E+05
95	0,38	1,00E+06	1,89E+05	1,74E+05	3,29E+04

Francium at T=1980°C			HDR		
A	**T1/2 [s]**	**Yield [1/s]**	**Err Yield [1/s]**	**Norm.Yield [1/s]**	**Err. Norm. [1/s]**
206	15,9	4,51E+03	6,53E+02	1,10E+03	1,59E+02
208	59,1	8,47E+04	4,69E+03	2,07E+04	1,14E+03
210	190,8	7,59E+04	5,20E+02	1,85E+04	1,27E+02
211	186	9,71E+04	2,58E+03	2,37E+04	6,30E+02
212	1200	3,43E+05	3,94E+03	8,38E+04	9,61E+02
221	294	3,81E+04	1,77E+03	9,29E+03	4,31E+02
222	852	1,61E+04	9,39E+02	3,92E+03	2,29E+02
224	199,8	3,07E+03	1,55E+02	7,50E+02	3,79E+01

A2.3
June 2003 (LDP; 1.86 g/cm^2; surface ionisation source)
Still made of UCx with large grains.

Rubidium at T=1990°C			LDP		
A	**T1/2 [s]**	**Yield [1/s]**	**Err Yield [1/s]**	**Norm.Yield [1/s]**	**Err. Norm. [1/s]**
89	909	3,25E+05	6,04E+04	2,53E+05	4,71E+04
90	258	1,75E+05	2,82E+04	1,36E+05	2,19E+04
91	58,4	9,34E+04	2,19E+04	7,28E+04	1,71E+04
93	5,84	1,74E+04	2,53E+03	1,36E+04	1,97E+03
94	2,702	8,33E+03	3,83E+02	6,49E+03	2,98E+02

Rubidium at T=2160°C			LDP		
A	**T1/2 [s]**	**Yield [1/s]**	**Err Yield [1/s]**	**Norm.Yield [1/s]**	**Err. Norm. [1/s]**
89	909	3,30E+06	5,69E+05	2,58E+06	4,43E+05
90	258	1,94E+06	2,68E+05	1,51E+06	2,09E+05
91	58,4	1,13E+06	1,70E+05	8,80E+05	1,32E+05
93	5,84	2,26E+05	2,65E+04	1,76E+05	2,07E+04
94	2,702	1,27E+05	2,58E+03	9,90E+04	2,01E+03

Rubidium at T=2240°C			LDP		
A	**T1/2 [s]**	**Yield [1/s]**	**Err Yield [1/s]**	**Norm.Yield [1/s]**	**Err. Norm. [1/s]**
89	909	3,98E+06	6,82E+05	3,10E+06	5,32E+05
90	258	1,84E+06	2,58E+05	1,43E+06	2,01E+05
91	58,4	9,72E+05	1,47E+05	7,57E+05	1,15E+05
93	5,84	1,62E+05	1,93E+04	1,26E+05	1,51E+04
94	2,702	8,40E+04	1,91E+03	6,55E+04	1,49E+03

Cesium at T=1990°C			LDP		
A	**T1/2 [s]**	**Yield [1/s]**	**Err Yield [1/s]**	**Norm.Yield [1/s]**	**Err. Norm. [1/s]**
139	556,2	3,43E+05	1,63E+05	2,68E+05	1,27E+05
140	63,7	8,77E+04	7,74E+03	6,84E+04	6,03E+03
141	24,94	1,20E+05	2,36E+04	9,33E+04	1,84E+04
142	1,7	9,67E+03	2,38E+03	7,53E+03	1,86E+03
144	1,01	1,73E+03	3,10E+02	1,35E+03	2,42E+02

Cesium at T=2160°C			LDP		
A	**T1/2 [s]**	**Yield [1/s]**	**Err Yield [1/s]**	**Norm.Yield [1/s]**	**Err. Norm. [1/s]**
139	556,2	1,64E+06	7,42E+05	1,28E+06	5,78E+05
140	63,7	5,18E+05	4,09E+04	4,04E+05	3,19E+04
141	24,94	6,92E+05	1,15E+05	5,40E+05	8,97E+04
142	1,7	1,45E+05	2,55E+04	1,13E+05	1,99E+04
144	1,01	1,85E+04	9,65E+02	1,44E+04	7,52E+02

Cesium at T=2240°C			LDP		
A	**T1/2 [s]**	**Yield [1/s]**	**Err Yield [1/s]**	**Norm.Yield [1/s]**	**Err. Norm. [1/s]**
139	556,2	1,82E+06	8,32E+05	1,42E+06	6,48E+05
140	63,7	4,55E+05	3,61E+04	3,55E+05	2,82E+04
141	24,94	4,70E+05	8,07E+04	3,66E+05	6,29E+04
142	1,7	1,06E+05	1,90E+04	8,26E+04	1,48E+04
144	1,01	1,28E+04	7,63E+02	9,96E+03	5,95E+02

Francium at T=2250°C			LDP		
A	**T1/2 [s]**	**Yield [1/s]**	**Err Yield [1/s]**	**Norm.Yield [1/s]**	**Err. Norm. [1/s]**
206	15,9	5,90E+03	6,84E+02	4,60E+03	5,34E+02
208	59,1	1,06E+05	5,15E+03	8,25E+04	4,01E+03
210	190,8	1,18E+05	7,81E+02	9,21E+04	6,09E+02
212	1200	4,07E+05	4,91E+03	3,17E+05	3,83E+03
221	294	5,72E+04	2,57E+03	4,46E+04	2,00E+03
224	199,8	5,77E+03	2,23E+02	4,50E+03	1,73E+02
225	240	1,41E+03	1,92E+02	1,10E+03	1,50E+02
227	148,2	1,37E+03	7,30E+01	1,07E+03	5,69E+01
228	38	1,57E+03	6,17E+02	1,23E+03	4,81E+02
219	0,02	5,25E+01		4,09E+01	

A2.4

December 2003 (HDR; 9.8 g/cm^2; e-beam ion source)

Electron beam allows observation of Ag and Sn, not detailed here**.**

Indium at T=1900°C(1)			HDR		
A	**T1/2 [s]**	**Yield [1/s]**	**Err Yield [1/s]**	**Norm.Yield [1/s]**	**Err. Norm. [1/s]**
119	144	4,79E+04	8,78E+03	7,44E+03	1,36E+03
120	47,3	1,33E+04	2,33E+03	2,06E+03	3,62E+02
121	23,1	1,16E+04	2,29E+03	1,80E+03	3,56E+02
122	10,8	6,58E+03	1,13E+03	1,02E+03	1,76E+02
123	5,98	4,77E+03	1,12E+03	7,40E+02	1,74E+02
124	3,7	2,73E+03	6,49E+02	4,23E+02	1,01E+02

Indium at T=2000°C(1)			HDR		
A	**T1/2 [s]**	**Yield [1/s]**	**Err Yield [1/s]**	**Norm.Yield [1/s]**	**Err. Norm. [1/s]**
119	144	3,10E+04	5,72E+03	4,81E+03	8,88E+02
120	47,3	1,18E+04	2,40E+03	1,38E+03	3,21E+02
121	23,1	1,06E+04	2,15E+03	1,64E+03	3,33E+02
122	10,8	4,33E+03	8,60E+02	6,72E+02	1,34E+02
123	5,98	5,61E+03	1,25E+03	8,71E+02	1,93E+02
124	3,7	1,18E+03	3,99E+02	1,84E+02	6,20E+01
125	2,36	1,50E+03	4,07E+02	2,33E+02	6,33E+01

Indium at T=2100°C(1)			HDR		
A	**T1/2 [s]**	**Yield [1/s]**	**Err Yield [1/s]**	**Norm.Yield [1/s]**	**Err. Norm. [1/s]**
119	144	1,35E+05	2,46E+04	2,10E+04	3,81E+03
120	47,3	5,08E+04	7,74E+03	7,89E+03	1,20E+03
121	23,1	5,29E+04	1,02E+04	8,22E+03	1,58E+03
122	10,8	2,19E+04	3,63E+03	3,40E+03	5,64E+02
123	5,98	2,02E+04	3,80E+03	3,14E+03	5,91E+02
124	3,7	8,57E+03	1,75E+03	1,33E+03	2,72E+02
125	2,36	5,58E+03	1,09E+03	8,67E+02	1,69E+02

Indium at T=1900°C(2)			HDR		
A	**T1/2 [s]**	**Yield [1/s]**	**Err Yield [1/s]**	**Norm.Yield [1/s]**	**Err. Norm. [1/s]**
119	144	5,21E+04	9,53E+03	8,09E+03	1,48E+03
120	47,3	2,73E+04	4,70E+03	4,24E+03	7,30E+02
121	23,1	2,24E+04	4,35E+03	3,47E+03	6,75E+02
122	10,8	1,29E+04	2,03E+03	2,00E+03	3,15E+02
123	5,98	9,00E+03	1,76E+03	1,40E+03	2,73E+02
124	3,7	3,51E+03	8,45E+02	5,45E+02	1,31E+02
125	2,36	2,44E+03	5,54E+02	3,79E+02	8,61E+01

Indium at T=2000°C(2)			HDR		
A	**T1/2 [s]**	**Yield [1/s]**	**Err Yield [1/s]**	**Norm.Yield [1/s]**	**Err. Norm. [1/s]**
119	144	7,00E+04	1,28E+04	1,09E+04	1,99E+03
123	5,98	1,07E+04	2,08E+03	1,66E+03	3,23E+02
124	3,7	4,82E+03	1,07E+03	7,48E+02	1,66E+02
125	2,36	3,32E+03	6,92E+02	5,16E+02	1,07E+02

Indium at T=2100°C(2)			HDR		
A	**T1/2 [s]**	**Yield [1/s]**	**Err Yield [1/s]**	**Norm.Yield [1/s]**	**Err. Norm. [1/s]**
119	144	8,74E+04	1,59E+04	1,36E+04	2,47E+03
120	47,3	3,46E+04	5,46E+03	5,37E+03	8,48E+02
121	23,1	3,36E+04	6,49E+03	5,22E+03	1,01E+03
122	10,8	1,54E+04	2,70E+03	2,39E+03	4,19E+02
123	5,98	1,33E+04	2,55E+03	2,07E+03	3,96E+02
124	3,7	4,72E+03	1,02E+03	7,33E+02	1,58E+02
125	2,36	3,60E+03	7,40E+02	5,59E+02	1,15E+02

Indium at T=2000°C(3)			HDR		
A	**T1/2 [s]**	**Yield [1/s]**	**Err Yield [1/s]**	**Norm.Yield [1/s]**	**Err. Norm. [1/s]**
119	144	4,46E+04	8,15E+03	6,92E+03	1,27E+03
120	47,3	2,43E+04	3,87E+03	3,77E+03	6,01E+02
121	23,1	2,57E+04	5,01E+03	3,99E+03	7,78E+02
122	10,8	1,05E+04	1,94E+03	1,63E+03	3,01E+02
123	5,98	9,26E+03	1,82E+03	1,44E+03	2,82E+02
124	3,7	3,41E+03	8,40E+02	5,30E+02	1,30E+02
125	2,36	2,25E+03	5,27E+02	3,49E+02	8,18E+01

Indium at T=2100°C(3)			HDR		
A	**T1/2 [s]**	**Yield [1/s]**	**Err Yield [1/s]**	**Norm.Yield [1/s]**	**Err. Norm. [1/s]**
119	144	5,41E+04	9,90E+03	8,41E+03	1,54E+03
120	47,3	1,81E+04	2,95E+03	2,81E+03	4,58E+02
121	23,1	1,44E+04	2,85E+03	2,24E+03	4,42E+02
122	10,8	6,88E+03	1,30E+03	1,07E+03	2,02E+02
123	5,98	5,23E+03	1,13E+03	8,11E+02	1,76E+02
124	3,7	2,43E+03	8,20E+02	3,77E+02	1,27E+02
125	2,36	1,70E+03	4,10E+02	2,64E+02	6,36E+01

Indium at T=2200°C(3)			HDR		
A	**T1/2 [s]**	**Yield [1/s]**	**Err Yield [1/s]**	**Norm.Yield [1/s]**	**Err. Norm. [1/s]**
119	144	3,60E+04	6,63E+03	5,58E+03	1,03E+03
120	47,3	1,44E+04	2,50E+03	2,24E+03	3,88E+02
121	23,1	1,28E+04	2,56E+03	1,99E+03	3,97E+02
122	10,8	6,47E+03	1,24E+03	1,00E+03	1,93E+02
123	5,98	5,20E+03	1,13E+03	8,07E+02	1,75E+02
124	3,7	2,40E+03	8,80E+02	3,73E+02	1,37E+02
125	2,36	1,29E+03	3,54E+02	2,00E+02	5,50E+01

A2.5

June 2004 Run 1 (HDR; 9.2 g/cm^2; surface ionisation source; 3 months target)

Yields after 3 months of heating.

Rubidium at T=1900°C			HDR		
A	**T1/2 [s]**	**Yield [1/s]**	**Err Yield [1/s]**	**Norm.Yield [1/s]**	**Err. Norm. [1/s]**
88	1067	4,34E+06	4,77E+05	6,74E+05	7,41E+04
89	909	6,36E+06	7,00E+05	9,88E+05	1,09E+05
90	258	3,28E+06	5,00E+05	5,09E+05	7,76E+04
91	58,4	2,00E+06	2,70E+05	3,11E+05	4,19E+04
92	4,49	1,39E+06	1,79E+05	2,16E+05	2,78E+04
93	5,84	6,59E+05	7,65E+05	1,02E+05	1,19E+05
94	2,702	3,24E+05	3,71E+05	5,03E+04	5,76E+04
95	0,377	1,63E+05	1,79E+05	2,53E+04	2,78E+04

Cesium at T=1900°C			HDR		
A	**T1/2 [s]**	**Yield [1/s]**	**Err Yield [1/s]**	**Norm.Yield [1/s]**	**Err. Norm. [1/s]**
138	2004,60	4,93E+06	9,37E+05	7,66E+05	1,45E+05
139	556,20	4,74E+06	6,37E+05	7,36E+05	9,89E+04
140	63,70	1,35E+06	1,52E+05	2,10E+05	2,36E+04
141	24,94	1,35E+06	1,68E+05	2,10E+05	2,61E+04
142	1,70	2,79E+05	3,00E+04	4,33E+04	4,66E+03
143	1,78	2,24E+05	2,80E+04	3,48E+04	4,35E+03
144	1,01	3,19E+04	3,39E+03	4,95E+03	5,26E+02
145	0,59	2,22E+04	3,62E+03	3,45E+03	5,62E+02

Cesium at T=2050°C			HDR		
A	**T1/2 [s]**	**Yield [1/s]**	**Err Yield [1/s]**	**Norm.Yield [1/s]**	**Err. Norm. [1/s]**
139	556,20	4,59E+06	6,19E+05	7,13E+05	9,61E+04
141	24,94	1,34E+06	1,80E+05	2,08E+05	2,80E+04
143	1,78	2,45E+05	2,84E+04	3,80E+04	4,41E+03
145	0,59	2,23E+04	3,84E+03	3,46E+03	5,96E+02

Cesium at T=2150°C			HDR		
A	**T1/2 [s]**	**Yield [1/s]**	**Err Yield [1/s]**	**Norm.Yield [1/s]**	**Err. Norm. [1/s]**
139	556,20	4,58E+06	6,16E+05	7,11E+05	9,57E+04
141	24,94	1,41E+06	1,88E+05	2,19E+05	2,92E+04
143	1,78	2,79E+05	3,23E+04	4,33E+04	5,02E+03
145	0,59	2,38E+04	6,59E+03	3,70E+03	1,02E+03

Indium at T=1900°C(1)			HDR		
A	**T1/2 [s]**	**Yield [1/s]**	**Err Yield [1/s]**	**Norm.Yield [1/s]**	**Err. Norm. [1/s]**
117	2592	5,17E+05	7,56E+04	8,03E+04	1,17E+04
118	8.50-267	2,93E+05	4,30E+04	4,55E+04	6,68E+03
119	144	2,61E+05	3,19E+04	4,05E+04	4,95E+03
120	47,3	8,36E+04	1,27E+04	1,30E+04	1,97E+03
121	23,1	7,93E+04	1,16E+04	1,23E+04	1,80E+03
122	10,3	4,21E+04	4,70E+03	6,54E+03	7,30E+02
123	5,98	3,69E+04	5,00E+03	5,73E+03	7,76E+02
124	3,11	1,25E+04	2,12E+03	1,94E+03	3,29E+02
125	2,36	8,44E+03	1,51E+03	1,31E+03	2,34E+02
126	1,6	3,36E+03	6,20E+02	5,22E+02	9,63E+01
127	3,67	2,39E+03	6,20E+02	3,71E+02	9,63E+01
128	0,72	1,51E+03	6,93E+02	2,34E+02	1,08E+02

Indium at T=2050°C(1)			HDR		
A	**T1/2 [s]**	**Yield [1/s]**	**Err Yield [1/s]**	**Norm.Yield [1/s]**	**Err. Norm. [1/s]**
119	144	1,47E+05	1,74E+03	2,28E+04	2,70E+02
121	23,1	6,28E+04	8,64E+03	9,75E+03	1,34E+03
123	5,98	2,48E+04	3,59E+03	3,85E+03	5,57E+02
125	2,36	7,32E+03	1,10E+03	1,14E+03	1,71E+02
127	3,67	2,56E+03	5,70E+02	3,98E+02	8,85E+01

A2.6
June 2004 Run 2 (HDR; 11.2 g/cm^2; new e-beam source)

Rubidium at T=1950°C			HDR		
A	**T1/2 [s]**	**Yield [1/s]**	**Err Yield [1/s]**	**Norm.Yield [1/s]**	**Err. Norm. [1/s]**
88	1067	1,55E+06	2,58E+05	2,73E+05	4,57E+04
90	258	2,76E+06	4,43E+05	4,89E+05	7,83E+04
91	58,4	1,94E+06	3,04E+05	3,43E+05	5,37E+04
93	5,84	4,64E+05	7,21E+04	8,20E+04	1,28E+04
95	0,377	6,38E+04	1,04E+04	1,13E+04	1,83E+03

Cesium at T=1950°C			HDR		
A	**T1/2 [s]**	**Yield [1/s]**	**Err Yield [1/s]**	**Norm.Yield [1/s]**	**Err. Norm. [1/s]**
138	2004,60	3,09E+06	7,97E+04	5,47E+05	1,41E+04
139	556,20	4,43E+06	3,37E+05	7,83E+05	5,96E+04
140	63,70	1,26E+06	3,64E+04	2,24E+05	6,43E+03
141	24,94	1,28E+06	1,42E+05	2,27E+05	2,51E+04
143	1,78	2,47E+05	4,37E+03	4,37E+04	7,72E+02
145	0,59	3,79E+04	8,08E+03	6,71E+03	1,43E+03

Indium at T=1950°C(1)			HDR		
A	**T1/2 [s]**	**Yield [1/s]**	**Err Yield [1/s]**	**Norm.Yield [1/s]**	**Err. Norm. [1/s]**
119	144	5,53E+04	6,60E+03	9,78E+03	1,17E+03
121	23,1	3,67E+04	4,11E+03	6,48E+03	7,26E+02
122	10,3	1,33E+04	1,62E+03	2,36E+03	2,87E+02
123	5,98	1,77E+04	1,94E+03	3,13E+03	3,43E+02
125	2,36	3,62E+03	4,12E+02	6,41E+02	7,28E+01

Indium at T=2100°C(1)			HDR		
A	**T1/2 [s]**	**Yield [1/s]**	**Err Yield [1/s]**	**Norm.Yield [1/s]**	**Err. Norm. [1/s]**
119	144	7,26E+04	8,65E+03	1,28E+04	1,53E+03
121	23,1	5,19E+04	5,79E+03	9,17E+03	1,02E+03
123	5,98	1,96E+04	2,21E+03	3,47E+03	3,90E+02
125	2,36	4,38E+03	5,16E+02	7,74E+02	9,12E+01

A2.7

December 2004 Run 1 (HDR; 4.5 g/cm^2; e-beam ion source)

Elements Ag and Sn have been seen (not detailed here).

Cesium at T=1900°C			HDR		
A	**T1/2 [s]**	**Yield [1/s]**	**Err Yield [1/s]**	**Norm.Yield [1/s]**	**Err. Norm. [1/s]**
138	0,34	4,93E+06	9,37E+05	7,66E+05	1,45E+05
139	556,2	4,74E+06	6,37E+05	7,36E+05	9,89E+04
140	63,7	1,35E+06	1,52E+05	2,10E+05	2,36E+04
141	24,94	1,35E+06	1,68E+05	2,10E+05	2,61E+04
142	1,7	2,79E+05	3,00E+04	4,33E+04	4,66E+03
143	1,78	2,24E+05	2,80E+04	3,48E+04	4,35E+03
144	1,01	3,19E+04	3,39E+03	4,95E+03	5,26E+02
145	0,6	2,22E+04	3,62E+03	3,45E+03	5,62E+02

Cesium at T=2050°C			HDR		
A	**T1/2 [s]**	**Yield [1/s]**	**Err Yield [1/s]**	**Norm.Yield [1/s]**	**Err. Norm. [1/s]**
139	556,2	4,59E+06	6,19E+05	7,13E+05	9,61E+04
141	24,94	1,34E+06	1,80E+05	2,08E+05	2,80E+04
143	1,78	2,48E+05	2,84E+04	3,85E+04	4,41E+03
145	0,6	2,23E+04	3,84E+03	3,89E+03	6,69E+02

Cesium at T=2100°C			HDR		
A	**T1/2 [s]**	**Yield [1/s]**	**Err Yield [1/s]**	**Norm.Yield [1/s]**	**Err. Norm. [1/s]**
139	556,2	4,58E+06	6,16E+05	7,11E+05	9,57E+04
141	24,94	1,41E+06	1,88E+05	2,19E+05	2,92E+04
143	1,78	2,79E+05	3,23E+04	4,33E+04	5,02E+03
145	0,6	2,38E+04	6,59E+03	4,15E+03	1,15E+03

A2.8
December 2004 Run 2 (HDR; 6.7 g/cm^2; surface ionisation source)

Some yields have been measured by β-counting and γ-spectroscopy. The discrepancies are assumed to originate from incorrect spectroscopic information, but this needs to be clarified. In such cases, the yields by β-counting are those shown in the figures.

Cesium at T=1900°C				HDR			
A	$T_{1/2}$ [s]	Yield [1/s] gamma	Err Yield [1/s]	Norm. Yield [1/s] gamma	Err. Norm. [1/s]	Norm. Yield [1/s] beta	Err. norm. [1/s]
138	2004,60	5,16E+07	1,31E+07	1,10E+07	2,79E+06		
138m	174,60	5,76E+06	1,02E+06	1,23E+06	2,18E+05		
139	556,20	5,48E+07	1,01E+07	1,17E+07	2,15E+06		
140	63,70	2,37E+07	4,83E+06	5,05E+06	1,03E+06		
141	24,94	1,17E+07	2,31E+06	2,50E+06	4,92E+05		
142	1,70	2,45E+06	4,55E+05	5,23E+05	9,71E+04		
143	1,78	1,81E+06	3,28E+05	3,86E+05	6,99E+04		
144	1,01	4,34E+05	9,01E+04	9,25E+04	1,92E+04	1,20E+05	3,42E+04
145	0,594	1,06E+05	1,98E+04	2,27E+04	4,22E+03	4,10E+04	1,20E+04
146	0,321	1,81E+04	5,69E+03	3,85E+03	1,21E+03	5,73E+03	1,65E+03
147	0,225					8,74E+02	3,78E+02
148	0,158					4,07E+01	2,20E+01

Cesium at T=2050°C				HDR			
A	$T_{1/2}$ [s]	Yield [1/s]	Err Yield [1/s]	Norm. Yield [1/s] gamma	Err. Norm. [1/s]	Norm. Yield [1/s] beta	Err. Norm. [1/s]
138	2004,60	3,34E+07	6,11E+06	7,12E+06	1,30E+06		
138m	174,60	1,41E+07	2,50E+06	3,00E+06	5,34E+05		
139	556,20	9,68E+07	2,49E+07	2,06E+07	5,31E+06		
140	63,70	3,03E+07	7,03E+06	6,47E+06	1,50E+06		
142	1,70	2,89E+06	5,40E+05	6,16E+05	1,15E+05		
143	1,78	2,34E+06	4,32E+05	5,00E+05	9,22E+04		
144	1,01	9,77E+05	2,03E+05	2,08E+05	4,33E+04		
145	0,594	2,29E+05	4,26E+04	4,88E+04	9,09E+03		
146	0,321	4,89E+04	1,29E+04	1,04E+04	2,75E+03	1,24E+04	2,42E+03
147	0,225					2,73E+03	6,44E+02

Cesium at T=2100°C			HDR				
A	T1/2 [s]	**Yield [1/s]**	**Err Yield [1/s]**	**Norm. Yield [1/s] gamma**	**Err. Norm. [1/s]**	**Norm. Yield [1/s] beta**	**Err. Norm. [1/s]**
120m	57	>5,00E+03	1,68E+03	>1,07E03	3,57E+02		
120	64	no gammas					
121m	122	3,19E+04	8,24E+03	6,81E+03	1,76E+03		
121	155	<1,2E+04		<2,6E+03			
122	21	8,73E+04	1,74E+04	1,86E+04	3,71E+03		
122m	222	<2,8E+04		<6,0E+03			
123+123m	356,4+1,64	7,55E+05	1,73E+05	1,61E+05	3,68E+04		
124	30,8	1,06E+06	2,17E+05	2,26E+05	4,64E+04		
124m	6,3	3,03E+04	6,48E+03	6,47E+03	1,38E+03		
125	2700	9,40E+06	1,89E+06	2,00E+06	4,02E+05		
126	98,4	5,94E+06	1,20E+06	1,27E+06	2,56E+05		
128	219,6	1,81E+07	3,22E+06	3,86E+06	6,87E+05		
130	1752,6	2,38E+07	7,83E+06	5,08E+06	1,67E+06		
130m	207,6	1,61E+07	2,78E+06	3,43E+06	5,93E+05		
138	2004,60	8,23E+07	1,49E+07	1,76E+07	3,19E+06		
138m	174,60	1,77E+07	3,17E+06	3,78E+06	6,76E+05		
139	556,20	9,01E+07	1,65E+07	1,92E+07	3,53E+06		
140	63,70	5,09E+07	1,91E+07	1,08E+07	4,08E+06		
141	24,94	3,60E+07	9,23E+06	7,68E+06	1,97E+06		
142	1,70	3,36E+06	6,51E+05	7,17E+05	1,39E+05		
143	1,78	3,26E+06	6,74E+05	6,96E+05	1,44E+05		
144	1,01	1,27E+06	2,66E+05	2,71E+05	5,66E+04		
145	0,60	2,88E+05	5,27E+04	6,15E+04	1,12E+04		
146	0,321	5,21E+04	1,69E+04	1,11E+04	3,61E+03	1,32E+04	7,44E+03
147	0,225					2,87E+03	1,44E+03
148	0,158					4,30E+02	2,88E+02

Rubidium at T=1900°C			HDR				
A	**$T_{1/2}$ [s]**	**Yield [1/s]**	**Err Yield [1/s]**	**Norm. Yield [1/s] gamma**	**Err. Norm. [1/s]**	**Norm. Yield [1/s] beta**	**Err. Norm. [1/s]**
88	1066,8	6,47E+07	1,13E+07	1,38E+07	2,41E+06		
89	909	9,71E+07	1,79E+07	2,07E+07	3,82E+06		
90m	258	2,99E+07	5,72E+06	6,38E+06	1,22E+06		
90	158	9,00E+06	2,00E+06	1,92E+06	4,26E+05		
91	58,4	2,19E+07	4,02E+06	4,66E+06	8,57E+05		
93	5,84	4,45E+06	8,25E+05	9,49E+05	1,76E+05		
94	2,7	2,33E+06	4,15E+05	4,96E+05	8,84E+04		
95	0,38	6,86E+05	1,20E+05	1,46E+05	2,55E+04	2,34E+05	6,19E+04
96	0,199	1,62E+05	8,88E+04	3,46E+04	1,89E+04	6,03E+04	1,66E+04
97	0,1699					2,00E+04	5,22E+03
98	0,114					2,97E+03	9,55E+02

Rubidium at T=2100°C			HDR		
A	**$T_{1/2}$ [s]**	**Yield [1/s]**	**Err Yield [1/s]**	**Norm. Yield [1/s]**	**Err. Norm. [1/s]**
79	1374	3,41E+05	7,58E+04	7,28E+04	1,62E+04
80	34	3,62E+05	8,04E+04	7,72E+04	1,71E+04
88	1066,8	1,00E+08	1,75E+07	2,14E+07	3,73E+06
89	909	1,53E+08	2,86E+07	3,27E+07	6,10E+06
91	58,4	4,22E+07	8,07E+06	9,00E+06	1,72E+06
93	5,84	9,37E+06	1,74E+06	2,00E+06	3,70E+05

Indium at T=2100°C			HDR		
A	**T1/2 [s]**	**Yield [1/s]**	**Err Yield [1/s]**	**Norm.Yield [1/s]**	**Err. Norm. [1/s]**
117	2592,00	8,45E+06	1,73E+06	1,80E+06	3,69E+05
118	267-8.50	7,50E+06	1,92E+06	1,60E+06	4,09E+05
119	144,00	7,55E+06	1,36E+06	1,61E+06	2,90E+05
120	46.20 - 47.30	2,09E+06	9,37E+05	4,45E+05	2,00E+05
121	23,1	2,12E+06	3,84E+05	4,52E+05	8,20E+04
122	10.30-10.80	8,27E+05	2,36E+05	1,76E+05	5,03E+04
123	5.98-47.80	6,44E+05	1,71E+05	1,37E+05	3,64E+04
124	3.11-3.70	1,65E+05	8,24E+04	3,52E+04	1,76E+04
125	2.36-12.20	8,71E+04	1,07E+05	1,86E+04	2,29E+04
126	1.60-1.64	3,13E+04	7,92E+03	6,67E+03	1,69E+03
127	1.09-3.67	2,53E+04	1,27E+04	5,40E+03	2,71E+03

A2.9 (a)

June 2005 Run 1 (LDT – PARRNe Target; 2.8 g/cm^2 ; surface ionisation source)

Target manufactured at Gatchina according to ISOLDE specifications.

Rubidium at T=1900°C			LDT		
A	**T1/2 [s]**	**Yield [1/s]**	**Err Yield [1/s]**	**Norm.Yield [1/s]**	**Err. Norm. [1/s]**
79	1374	2,12E+04	3,68E+03	1,08E+04	1,88E+03
80	34	9,53E+04	1,26E+04	4,86E+04	6,41E+03
88	1066,8	1,82E+07	1,54E+06	9,30E+06	7,84E+05
89	909	3,03E+07	2,76E+06	1,55E+07	1,41E+06
90m	258	1,46E+07	1,77E+06	7,46E+06	9,05E+05
90	158	4,88E+06	5,81E+05	2,49E+06	2,96E+05
91	58,4	1,53E+07	1,95E+06	7,80E+06	9,95E+05
92	4,498	1,15E+07	2,91E+06	5,89E+06	1,48E+06
93	5,84	5,20E+06	6,98E+05	2,65E+06	3,56E+05
94	2,7	1,34E+06	1,43E+05	6,81E+05	7,28E+04
95	0,38	8,48E+05	2,54E+05	4,33E+05	1,30E+05
96	0,199	2,05E+05	4,10E+04	1,05E+05	2,09E+04
97	0,1699	8,23E+04	2,88E+04	4,20E+04	1,47E+04

Rubidium at T=2000°C			LDT		
A	**T1/2 [s]**	**Yield [1/s]**	**Err Yield [1/s]**	**Norm.Yield [1/s]**	**Err. Norm. [1/s]**
88	1066,8	1,88E+07	1,61E+06	9,61E+06	8,20E+05
89	909	2,86E+07	2,61E+06	1,46E+07	1,33E+06
90m	258	1,07E+07	1,91E+06	5,44E+06	9,74E+05
90	158	8,07E+06	2,83E+06	4,12E+06	1,44E+06
91	58,4	1,32E+07	1,70E+06	6,72E+06	8,69E+05
93	5,84	3,00E+06	3,58E+05	1,82E+06	2,33E+05
94	2,7	1,95E+06	2,42E+05	9,93E+05	1,23E+05
95	0,38	9,02E+05	8,14E+04	4,60E+05	4,15E+04
96	0,199	2,30E+05	4,60E+04	1,17E+05	2,35E+04
97	0,1699	6,24E+04	2,18E+04	3,18E+04	1,11E+04

Rubidium at T=2100°C			LDT		
A	**T1/2 [s]**	**Yield [1/s]**	**Err Yield [1/s]**	**Norm.Yield [1/s]**	**Err. Norm. [1/s]**
88	1066,8	3,11E+07	2,59E+06	1,59E+07	1,32E+06
89	909	4,01E+07	3,48E+06	2,05E+07	1,77E+06
90m	258	2,04E+07	3,31E+06	1,04E+07	1,69E+06
90	158	9,22E+06	1,49E+06	4,70E+06	7,60E+05
91	58,4	2,44E+07	3,40E+06	1,25E+07	1,74E+06
93	5,84	9,32E+06	1,67E+06	4,76E+06	8,54E+05
94	2,7	2,93E+06	8,94E+05	1,50E+06	4,56E+05
95	0,38	1,96E+06	2,53E+05	9,98E+05	1,29E+05
96	0,199	4,74E+05	9,47E+04	2,42E+05	4,83E+04
97	0,1699	1,75E+05	6,12E+04	8,92E+04	3,12E+04

Cesium at T=1900°C			LDT		
A	**T1/2 [s]**	**Yield [1/s]**	**Err Yield [1/s]**	**Norm.Yield [1/s]**	**Err. Norm. [1/s]**
138	2004,60	1,23E+07	1,41E+06	6,26E+06	7,19E+05
138m	174,60	3,15E+06	3,66E+05	1,61E+06	1,87E+05
139	556,20	1,56E+07	1,77E+06	7,94E+06	9,04E+05
140	63,70	7,34E+06	9,47E+05	3,74E+06	4,83E+05
141	24,94	8,60E+06	1,45E+06	4,39E+06	7,40E+05
142	1,70	3,66E+06	4,96E+05	1,87E+06	2,53E+05
143	1,78	2,14E+06	3,08E+05	1,09E+06	1,57E+05
144	1,01	4,50E+05	7,21E+04	2,30E+05	3,68E+04
145	0,594	8,50E+04	1,55E+04	4,33E+04	7,92E+03

Cesium at T=2000°C			LDT				
A	**$T_{1/2}$ [s]**	**Yield [1/s]**	**Err Yield [1/s]**	**Norm.Yield [1/s] gamma**	**Err. Norm. [1/s]**	**Norm. Yield [1/s] beta**	**Err. Norm. [1/s]**
120m	57	>1,37E+03	2,76E+02	>7,01E+02	1,41E+02		
120	64	no					
121m	122	1,47E+04	1,98E+03	7,49E+03	1,01E+03		
121	155	<2,40E+03		<5,13E+02			
122	21	5,13E+04	4,41E+03	2,62E+04	2,25E+03		
122m	222	<1,48E+04		<3,15E+03			
123+123m	356,4+1,64	3,02E+05	5,48E+04	1,54E+05	2,80E+04		
124	30,8	8,63E+05	8,02E+04	4,40E+05	4,09E+04		
124m	6,3	1,89E+04	2,67E+03	9,65E+03	1,36E+03		
125	2700	2,82E+06	2,47E+05	1,44E+06	1,26E+05		
126	98,4	1,98E+06	1,69E+05	1,01E+06	8,61E+04		
128	219,6	4,27E+06	3,49E+05	2,18E+06	1,78E+05		
130	1752,6	3,82E+06	1,58E+06	8,15E+05	3,36E+05		
130m	207,6	4,14E+06	3,66E+05	2,11E+06	1,87E+05		
138	2004,60	1,09E+07	1,14E+06	5,58E+06	5,83E+05		
138m	174,60	4,31E+06	4,12E+05	2,20E+06	2,10E+05		
139	556,20	1,54E+07	1,48E+06	7,83E+06	7,56E+05		
140	63,70	7,40E+06	7,89E+05	3,77E+06	4,02E+05		
141	24,94	8,04E+06	1,18E+06	4,10E+06	6,05E+05		
142	1,70	2,78E+06	2,84E+05	1,42E+06	1,45E+05	1,95E+06	5,43E+05
143	1,78	1,99E+06	2,12E+05	1,01E+06	1,08E+05	1,10E+06	2,99E+05
144	1,01	5,84E+05	1,10E+05	2,98E+05	5,62E+04	3,68E+05	1,25E+05
145	0,594	1,61E+05	2,50E+04	8,23E+04	1,27E+04	1,02E+05	3,58E+04
146	0,321	1,90E+04	6,48E+03	9,71E+03	3,30E+03	2,02E+04	5,59E+03
147	0,225					2,96E+03	1,09E+03
148	0,158					2,30E+02	1,50E+02

Cesium at T=2100°C			LDT				
A	**$T_{1/2}$ [s]**	**Yield [1/s]**	**Err Yield [1/s]**	**Norm. Yield [1/s] gamma**	**Err. Norm. [1/s]**	**Norm. Yield [1/s] beta**	**Err. Norm. [1/s]**
120m	57	>1,83E+03	4,85E+02	>9,33E+02	2,47E+02		
120	64	no gammas					
121m	122	8,66E+03	3,58E+03	4,42E+03	1,83E+03		
121	155	<7,40E+03		<1,58E+03			
122	21	5,60E+04	6,84E+03	2,86E+04	3,49E+03		
122m	222	<2,75E+04		<5,87E+03			
123+123m	356,4+1,64	4,66E+05	1,11E+05	2,38E+05	5,65E+04		
124	30,8	1,12E+06	1,55E+05	5,71E+05	7,90E+04		
124m	6,3	3,07E+04	5,51E+03	1,56E+04	2,81E+03		
125	2700	2,53E+06	4,28E+05	1,29E+06	2,18E+05		
126	98,4	2,26E+06	2,71E+05	1,15E+06	1,38E+05		
128	219,6	6,06E+06	6,92E+05	3,09E+06	3,53E+05		
130	1752,6	4,56E+06	2,55E+06	9,73E+05	5,43E+05		
130m	207,6	6,26E+06	7,45E+05	3,19E+06	3,80E+05		
138	2004,60	1,87E+07	2,28E+06	9,53E+06	1,16E+06		
138m	174,60	7,55E+06	9,37E+05	3,85E+06	4,78E+05		
139	556,20	2,63E+07	3,27E+06	1,34E+07	1,67E+06		
140	63,70	1,24E+07	1,58E+06	6,31E+06	8,05E+05		
141	24,94	1,29E+07	2,02E+06	6,57E+06	1,03E+06		
142	1,70	3,64E+06	5,95E+05	1,86E+06	3,04E+05		
143	1,78	2,70E+06	4,13E+05	1,38E+06	2,11E+05		
144	1,01	7,35E+05	1,38E+05	3,75E+05	7,06E+04	5,91E+05	1,73E+05
145	0,594	1,58E+05	2,07E+04	8,06E+04	1,06E+04	1,84E+05	5,44E+04
146	0,321	3,46E+04	1,23E+04	1,77E+04	6,28E+03	3,06E+04	3,77E-02
147	0,225					4,72E+03	1,94E+03
148	0,158					2,21E+02	1,02E+02

A2.9 (b)
June 2005 Run 2 (LDT – PARRNe Target; 2.8 g/cm^2 ; surface ionisation source)

Rubidium at T=1900°C			LDT		
A	**T1/2 [s]**	**Yield [1/s]**	**Err Yield [1/s]**	**Norm.Yield [1/s]**	**Err. Norm. [1/s]**
84m	1215,600	8,42E+06	7,33E+05	4,30E+06	3,74E+05
86m	61,02	3,15E+07	2,50E+06	1,61E+07	1,27E+06
88	1066,80	4,14E+07	3,28E+06	2,11E+07	1,67E+06
89	909,00	4,28E+07	4,77E+06	2,18E+07	2,43E+06
91	58,40	1,08E+07	1,83E+06	5,49E+06	9,34E+05
93	5,84	4,07E+06	4,58E+05	2,07E+06	2,33E+05
95	0,378	2,03E+06	2,54E+05	1,04E+06	1,30E+05

Rubidium at T=2100°C			LDT		
A	**T1/2 [s]**	**Yield [1/s]**	**Err Yield [1/s]**	**Norm.Yield [1/s]**	**Err. Norm. [1/s]**
86m	61,02	4,34E+07	3,37E+06	2,21E+07	1,72E+06
89	909,00	3,18E+07	3,26E+06	1,62E+07	1,67E+06
91	58,40	2,25E+07	3,22E+06	1,15E+07	1,64E+06
93	5,84	6,00E+06	8,31E+05	3,06E+06	4,24E+05
95	0,378	3,22E+06	3,74E+05	1,64E+06	1,91E+05
96	1,070	3,90E+05	3,52E+04	1,99E+05	1,79E+04

Cesium at T=1900°C			LDT		
A	**T1/2 [s]**	**Yield [1/s]**	**Err Yield [1/s]**	**Norm.Yield [1/s]**	**Err. Norm. [1/s]**
128	219,600	2,08E+06	1,65E+05	1,06E+06	8,39E+04
130m	207,600	2,04E+06	1,72E+05	1,04E+06	8,79E+04
138m	174,60	1,91E+06	1,77E+05	9,73E+05	9,05E+04
138	2004,60	1,76E+07	1,33E+06	8,98E+06	6,81E+05
140	63,70	4,97E+06	5,56E+05	2,53E+06	2,84E+05
141	24,94	4,05E+06	5,78E+05	2,07E+06	2,95E+05
143	1,78	1,26E+06	1,19E+05	6,41E+05	6,07E+04
145	0,600	5,75E+04	9,83E+03	2,93E+04	5,01E+03

Cesium at T=2000°C			LDT		
A	**T1/2 [s]**	**Yield [1/s]**	**Err Yield [1/s]**	**Norm.Yield [1/s]**	**Err. Norm. [1/s]**
120m	57	1,37E+03	2,76E+02	7,01E+02	1,41E+02
121m	122	1,47E+04	1,98E+03	7,49E+03	1,01E+03
122	21	5,13E+04	4,41E+03	2,62E+04	2,25E+03
123	356,4	3,99E+05	7,74E+04	2,04E+05	3,95E+04
124	30,8	8,63E+05	8,02E+04	4,40E+05	4,10E+04
125	2700	2,82E+06	2,47E+05	1,44E+06	1,26E+05
126	98,4	1,98E+06	1,69E+05	1,01E+06	8,61E+04
128	219,6	4,27E+06	3,49E+05	2,18E+06	1,78E+05
130m	207,6	4,14E+06	3,66E+05	2,11E+06	1,87E+05
138	2004,6	3,96E+07	3,14E+06	2,02E+07	1,60E+06
139	556,2	1,54E+07	1,48E+06	7,83E+06	7,56E+05
140	63,7	7,40E+06	7,89E+05	3,77E+06	4,02E+05
141	24,94	8,50E+06	1,50E+06	4,34E+06	7,67E+05
142	1,7	2,98E+06	3,40E+05	1,52E+06	1,74E+05
143	1,78	2,52E+06	2,80E+05	1,29E+06	1,43E+05
144	1,01	4,50E+05	1,08E+05	2,30E+05	5,49E+04
145	0,6	1,61E+05	2,50E+04	8,23E+04	1,27E+04
146	0,321	1,08E+04	3,34E+03	5,54E+03	1,71E+03

Cesium at T=2100°C			LDT		
A	**T1/2 [s]**	**Yield [1/s]**	**Err Yield [1/s]**	**Norm.Yield [1/s]**	**Err. Norm. [1/s]**
120m	57	1,83E+03	4,85E+02	9,33E+02	2,47E+02
121m	122	8,66E+03	3,58E+03	4,42E+03	1,83E+03
122	21	5,60E+04	6,84E+03	2,86E+04	3,49E+03
123	356,4	4,66E+05	1,11E+05	2,38E+05	5,65E+04
124	30,8	1,12E+06	1,55E+05	5,71E+05	7,90E+04
125	2700	2,53E+06	4,28E+05	1,29E+06	2,18E+05
126	98,4	2,31E+06	3,25E+05	1,18E+06	1,66E+05
128	219,6	6,06E+06	6,92E+05	3,09E+06	3,53E+05
130m	207,6	6,26E+06	7,45E+05	3,19E+06	3,80E+05
138	2004,6	7,48E+07	8,35E+06	3,82E+07	4,26E+06
139	556,2	1,62E+07	2,00E+06	8,27E+06	1,02E+06
140	63,7	1,24E+07	1,58E+06	6,31E+06	8,05E+05
141	24,94	1,49E+07	2,63E+06	7,60E+06	1,34E+06
142	1,7	3,98E+06	7,00E+05	2,03E+06	3,57E+05
143	1,78	3,62E+06	5,89E+05	1,85E+06	3,00E+05
144	1,01	5,28E+05	1,22E+05	2,69E+05	6,21E+04
145	0,6	1,58E+05	2,07E+04	8,06E+04	1,06E+04
146	0,321	1,97E+04	6,41E+03	1,01E+04	3,27E+03

A2.10
November 2005 (HDR; 7 g/cm^2; surface ionisation source; rhenium ionizer)

Cesium at T=1970°C			HDR		
A	**T1/2 [s]**	**Yield [1/s]**	**Err Yield [1/s]**	**Norm.Yield [1/s]**	**Err. Norm. [1/s]**
138m	174,60	6,44E+05	1,02E+05	1,32E+05	2,09E+04
140	63,70	3,01E+06	5,37E+05	6,15E+05	1,10E+05
141	24,94	1,14E+06	2,40E+05	2,33E+05	4,90E+04
142	1,70	1,58E+05	2,27E+04	3,23E+04	4,64E+03
143	1,78	1,20E+05	1,89E+04	2,44E+04	3,86E+03
144	1,01	1,28E+04	2,21E+03	2,62E+03	4,52E+02

Cesium at T=2175°C			HDR		
A	**T1/2 [s]**	**Yield [1/s]**	**Err Yield [1/s]**	**Norm.Yield [1/s]**	**Err. Norm. [1/s]**
123	356,40	1,13E+05	2,66E+04	2,30E+04	5,43E+03
126	98,40	4,71E+05	8,28E+04	9,63E+04	1,69E+04
128	219,60	1,29E+06	2,27E+05	2,64E+05	4,64E+04
130	207,60	1,10E+06	1,95E+05	2,25E+05	3,99E+04
138m	174,60	1,70E+06	3,11E+05	3,47E+05	6,35E+04
139	556,20	7,43E+06	1,35E+06	1,52E+06	2,75E+05
140	63,70	5,42E+06	9,64E+05	1,11E+06	1,97E+05
141	24,94	4,03E+06	7,51E+05	8,24E+05	1,53E+05
142	1,70	3,47E+05	6,19E+04	7,09E+04	1,26E+04
143	1,78	2,64E+05	4,79E+04	5,39E+04	9,79E+03
144	1,01	3,25E+04	5,94E+03	6,63E+03	1,21E+03

Rubidium at T=2175°C			HDR		
A	**T1/2 [s]**	**Yield [1/s]**	**Err Yield [1/s]**	**Norm.Yield [1/s]**	**Err. Norm. [1/s]**
84m	1215,60	2,16E+06	3,65E+05	4,40E+05	7,45E+04
89	909	8,47E+06	1,71E+06	1,73E+06	3,50E+05
90m	258	4,38E+06	7,94E+05	8,95E+05	1,62E+05
91	58,4	2,63E+06	4,94E+05	5,37E+05	1,01E+05
93	5,84	5,84E+05	1,10E+05	1,19E+05	2,25E+04
94	2,702	2,77E+05	4,72E+04	5,65E+04	9,63E+03

Gallium at T=2290°C			HDR		
A	**T1/2 [s]**	**Yield [1/s]**	**Err Yield [1/s]**	**Norm.Yield [1/s]**	**Err. Norm. [1/s]**
73	17496,00	7,41E+04	1,26E+04	1,51E+04	2,57E+03
74	487,20	4,07E+04	6,91E+03	8,67E+03	1,41E+03
75	126,00	8,89E+03	1,51E+03	1,81E+03	3,09E+02
76	32,60	3,95E+03	6,90E+02	8,06E+02	1,41E+02
77	13,20	3,37E+02	7,23E+01	6,87E+01	1,47E+01
78	5,09	3,23E+02	2,22E+02	6,59E+01	4,53E+01

Indium at T=2290°C			HDR		
A	**T1/2 [s]**	**Yield [1/s]**	**Err Yield [1/s]**	**Norm.Yield [1/s]**	**Err. Norm. [1/s]**
119	144	4,62E+05	8,24E+04	9,56E+04	1,71E+04
120	46,2	1,61E+05	2,81E+04	3,34E+04	5,82E+03
121	23,1	1,85E+05	3,22E+04	3,84E+04	6,66E+03
122	10,8	3,09E+04	5,23E+03	6,40E+03	1,08E+03
123	5,98	5,27E+04	9,25E+03	1,09E+04	1,92E+03
124	3,17	2,29E+04	5,15E+03	4,75E+03	1,07E+03

A2.11

December 2005 (HDP; 4.5 g/cm^2; surface ionisation source)

High density new pellets, now with small grain size.

Rubidium at T=2080°C			HDP		
A	**T1/2 [s]**	**Yield [1/s]**	**Err Yield [1/s]**	**Norm.Yield [1/s]**	**Err. Norm. [1/s]**
88	1066,80	3,65E+06	1,27E+06	1,16E+06	4,02E+05
89	909,00	7,40E+06	1,53E+06	2,35E+06	4,86E+05
90	158,00	3,34E+06	7,62E+05	1,06E+06	2,42E+05
91	58,40	3,07E+06	6,93E+05	9,75E+05	2,20E+05
93	5,84	8,82E+05	1,93E+05	2,80E+05	6,12E+04
94	2,70	4,60E+05	1,00E+05	1,46E+05	3,19E+04
95	0,378	1,72E+05	3,78E+04	5,46E+04	1,20E+04

Rubidium at T=2190°C			HDP		
A	**T1/2 [s]**	**Yield [1/s]**	**Err Yield [1/s]**	**Norm.Yield [1/s]**	**Err. Norm. [1/s]**
88	1066,80	4,19E+06	9,14E+05	1,33E+06	2,90E+05
89	909,00	4,47E+06	9,32E+05	1,42E+06	2,96E+05
90	158,00	1,48E+06	3,87E+05	4,69E+05	1,23E+05
91	58,40	1,96E+06	4,22E+05	6,22E+05	1,34E+05
93	5,84	6,99E+05	1,49E+05	2,22E+05	4,72E+04
94	2,70	3,24E+05	7,06E+04	1,03E+05	2,24E+04
95	0,378	1,35E+05	2,93E+04	4,30E+04	9,31E+03

Cesium at T=2000°C			HDP		
A	**T1/2 [s]**	**Yield [1/s]**	**Err Yield [1/s]**	**Norm.Yield [1/s]**	**Err. Norm. [1/s]**
130m	207,600	5,51E+05	1,17E+05	1,75E+05	3,73E+04
138m	174,60	5,58E+05	1,31E+05	1,77E+05	4,15E+04
139	556,20	2,75E+06	5,86E+05	8,72E+05	1,86E+05
140	63,70	1,08E+06	2,37E+05	3,42E+05	7,53E+04
141	24,94	8,52E+05	2,10E+05	2,70E+05	6,66E+04
142	1,700	1,86E+05	3,86E+04	5,90E+04	1,23E+04
143	1,78	1,70E+05	3,52E+04	5,39E+04	1,12E+04
144	1,01	2,44E+04	5,18E+03	7,75E+03	1,64E+03
145	0,600	3,05E+04	2,60E+04	9,68E+03	8,26E+03

Cesium at T=2070°C			HDP		
A	**T1/2 [s]**	**Yield [1/s]**	**Err Yield [1/s]**	**Norm.Yield [1/s]**	**Err. Norm. [1/s]**
130m	207,600	8,03E+05	1,68E+05	2,55E+05	5,34E+04
139	556,20	4,23E+06	9,01E+05	1,34E+06	2,86E+05
141	24,94	1,35E+06	2,89E+05	4,28E+05	9,17E+04
143	1,78	2,75E+05	5,66E+04	8,72E+04	1,80E+04
144	1,01	3,88E+04	8,05E+03	1,23E+04	2,55E+03

Francium at T=2000°C			HDP		
A	**T1/2 [s]**	**Yield [1/s]**	**Err Yield [1/s]**	**Norm.Yield [1/s]**	**Err. Norm. [1/s]**
206	15,90	1,17E+04	3,02E+03	3,73E+03	9,58E+02
208	59,10	2,02E+05	4,14E+04	6,41E+04	1,32E+04
210	190,8	2,24E+05	4,57E+04	7,10E+04	1,45E+04
212	1200	6,45E+05	1,34E+05	2,05E+05	4,27E+04
221	294,0	1,05E+05	2,27E+04	3,34E+04	7,21E+03
222	852,0	4,08E+04	9,67E+03	1,30E+04	3,07E+03
224	199,8	1,31E+04	2,97E+03	4,17E+03	9,44E+02
225	240	2,29E+03	6,42E+02	7,26E+02	2,04E+02
227	148,2	2,17E+03	5,35E+02	6,89E+02	1,70E+02

A2.12
March 2006 (HDP; 6.3 g/cm^2; surface ionisation source)
Small grains.

Rubidium at T=1500°C			HDP		
A	**T1/2 [s]**	**Yield [1/s]**	**Err Yield [1/s]**	**Norm.Yield [1/s]**	**Err. Norm. [1/s]**
80	34,40	4,75E+03	7,89E+02	1,08E+03	1,79E+02
84m	1215,60	7,93E+04	9,91E+03	1,80E+04	2,25E+03
86m	61,02	2,52E+05	1,76E+04	5,71E+04	4,00E+03
88	1066,8	3,40E+05	3,51E+04	7,72E+04	7,95E+03
89	909	4,35E+05	6,46E+04	9,86E+04	1,46E+04
90	158	5,99E+05	8,59E+04	1,36E+05	1,95E+04
91	58,4	2,10E+05	2,35E+04	4,76E+04	5,32E+03
92	4,492	1,02E+05	1,01E+04	2,31E+04	2,28E+03
93	5,84	5,83E+04	1,21E+04	1,32E+04	2,73E+03
94	2,702	2,45E+04	1,83E+03	5,55E+03	4,14E+02

Rubidium at T=1700°C			HDP		
A	**T1/2 [s]**	**Yield [1/s]**	**Err Yield [1/s]**	**Norm.Yield [1/s]**	**Err. Norm. [1/s]**
79	1374,00	7,92E+03	2,20E+03	1,80E+03	4,99E+02
80	34,40	3,02E+04	4,82E+03	6,85E+03	1,09E+03
84m	1215,60	1,05E+06	7,18E+04	2,38E+05	1,63E+04
88	1066,8	2,68E+06	2,78E+05	6,08E+05	6,30E+04
89	909	2,27E+06	3,06E+05	5,16E+05	6,94E+04
90	158	3,42E+06	4,96E+05	7,75E+05	1,12E+05
91	58,4	1,17E+06	1,44E+05	2,66E+05	3,27E+04
92	4,492	1,27E+06	1,05E+05	2,87E+05	2,39E+04
93	5,84	7,55E+05	6,87E+04	1,71E+05	1,56E+04
94	2,702	3,68E+05	2,74E+04	8,34E+04	6,22E+03
95	0,3775	5,54E+04	8,81E+03	1,26E+04	2,00E+03

Cesium at T=1500°C			HDP		
A	**T1/2 [s]**	**Yield [1/s]**	**Err Yield [1/s]**	**Norm.Yield [1/s]**	**Err. Norm. [1/s]**
121	122,00	7,82E+03	1,05E+03	1,77E+03	2,38E+02
122	222,00	1,89E+04	2,80E+03	4,29E+03	6,34E+02
123	356,40	4,47E+04	8,56E+03	1,01E+04	1,94E+03
124	30,80	6,05E+04	7,18E+03	1,37E+04	1,63E+03
125	2700,00	1,80E+05	8,20E+04	4,08E+04	1,86E+04
126	98,40	1,65E+05	1,90E+04	3,73E+04	4,30E+03
127	22500,00	7,07E+05	1,12E+05	1,60E+05	2,54E+04
128	219,60	6,23E+05	7,08E+04	1,41E+05	1,61E+04
129	1,15E+05	1,73E+06	4,36E+05	3,93E+05	9,90E+04
130	207,60	2,67E+05	3,59E+04	6,05E+04	8,13E+03
138	207,60	2,35E+05	2,80E+04	5,32E+04	6,35E+03
140	63,70	2,86E+05	3,38E+04	6,48E+04	7,67E+03
141	24,94	3,17E+05	4,32E+04	7,18E+04	9,80E+03
142	1,70	2,65E+04	3,19E+03	6,01E+03	7,22E+02
143	1,78	2,89E+04	3,86E+03	6,56E+03	8,76E+02
144	1,01	4,52E+03	6,32E+02	1,02E+03	1,43E+02
145	0,59	1,14E+04	2,62E+03	2,58E+03	5,93E+02

Cesium at T=1700°C			HDP		
A	**T1/2 [s]**	**Yield [1/s]**	**Err Yield [1/s]**	**Norm.Yield [1/s]**	**Err. Norm. [1/s]**
121	122,00	8,76E+03	8,31E+02	1,99E+03	1,89E+02
122	222,00	9,19E+04	1,00E+04	2,08E+04	2,27E+03
123	356,40	8,33E+04	1,41E+04	1,89E+04	3,20E+03
124	30,80	2,55E+05	2,20E+04	5,78E+04	4,98E+03
125	2700,00	6,51E+05	6,47E+04	1,48E+05	1,47E+04
126	98,40	7,52E+05	6,41E+04	1,70E+05	1,45E+04
127	22500,00	3,76E+06	3,62E+05	8,52E+05	8,20E+04
128	219,60	8,73E+05	7,42E+04	1,98E+05	1,68E+04
129	1,15E+05	7,64E+06	8,81E+05	1,73E+06	2,00E+05
130	207,60	8,94E+05	8,26E+04	2,03E+05	1,87E+04
132	5,60E+05	1,22E+07	5,00E+06	2,76E+06	1,13E+06
138	174,60	9,09E+05	8,30E+04	2,06E+05	1,88E+04
139	556,20	2,37E+06	2,33E+05	5,38E+05	5,28E+04
140	63,70	1,38E+06	1,24E+05	3,13E+05	2,80E+04
141	24,94	1,88E+06	2,07E+05	4,27E+05	4,69E+04
142	1,70	3,62E+05	3,17E+04	8,21E+04	7,20E+03
143	1,78	3,12E+05	2,71E+04	7,07E+04	6,15E+03
144	1,01	4,25E+04	3,77E+03	9,64E+03	8,54E+02
145	0,59	2,05E+04	3,10E+03	4,66E+03	7,03E+02

Cesium at T=1800°C			HDP		
A	**T1/2 [s]**	**Yield [1/s]**	**Err Yield [1/s]**	**Norm.Yield [1/s]**	**Err. Norm. [1/s]**
139	556,20	7,74E+05	7,75E+04	1,76E+05	1,76E+04
140	63,70	4,67E+05	4,21E+04	1,06E+05	9,54E+03
141	24,94	3,19E+06	3,49E+05	7,23E+05	7,90E+04
142	1,70	1,76E+05	1,53E+04	3,98E+04	3,47E+03
143	1,78	1,65E+05	1,41E+04	3,75E+04	3,19E+03
144	1,01	2,26E+04	1,98E+03	5,12E+03	4,48E+02
145	0,59	1,12E+04	1,92E+03	2,55E+03	4,35E+02